Evaluation of Flesh Material Model Implementation on GHBMC Kinematic Predictions for 50th Percentile Male and Female Occupants in Frontal Impacts in Reclined Postures

Rachel Newman, Adrian Caudillo, Jeesoo Shin, Matthew B. Panzer, Bronislaw D. Gepner

Abstract Until recently, human flesh tissue data covering a range of strains and strain-rates applicable to impact simulations did not exist. The goal of this research was to implement newly developed Ogden rubber flesh constitutive models into the Global Human Body Models Consortium (GHBMC) soft tissue parts (skin, adipose, muscle) and assess the biofidelity of these tissue formulations for whole body reclined frontal impact post-mortem human subject (PMHS) sled tests. Stock simplified rubber and Ogden flesh materials were analyzed for detailed (-O) and simplified (-OS) 50th percentile male (M50) and female (F50) GHBMC human body models (HBMs). Head, T1, T8, T11, L1, L3, and pelvis kinematics were compared across simulations and against PMHS corridors. Detailed HBMs performed closer to PMHS responses than simplified HBMs. Generally, Ogden flesh material implementation pushed HBM trajectories closer to PMHS responses. Ogden materials elicited larger improvements in response for detailed HBMs. Ogden flesh material implementation improved HBM prediction of forward and downward displacement and elicited a stiffer response of the HBMs, except for the F50-O. Ogden soft tissue material models showed promise in improving GHBMC kinematic predictions. This study identified differences in F50-O and M50-O pelvis construction and spine performance, which should be investigated further.

Keywords Biofidelity, flesh material models, GHBMC, Recline

I. INTRODUCTION

Human body models (HBMs) and virtual tools are becoming more important for the assessment of occupant safety in vehicle environments and will soon become a necessary step in regulatory procedures [1–3]. While HBMs offer an attractive alternative to physical surrogates for a wide range of motor vehicle crash scenarios, the results obtained from HBMs in different loading scenarios are only meaningful if the HBMs have been validated in comparable scenarios for which they are used.

Since current vehicle seats already allow occupants to sit in reclined postures [4] and we anticipate these postures to become more popular amongst occupants seated in highly autonomous vehicles [5], it will be critical that HBMs are validated for reclined occupants. There exists one biofidelity assessment of the Global Human Body Model Consortium (GHBMC) 5th percentile female HBM in recline [6], which measured agreement between the excursions, accelerations, and forces of the GHBMC and PMHS data, although submarining outcomes differed between the unmodified GHBMC and PMHS reference tests. To our knowledge, no biofidelity evaluations have been conducted for 50th percentile female (F50) HBMs in recline, although experimental PMHS reference data does exist for this anthropometry [7–9].

Biofidelity assessments of the 50th percentile male (M50) HBMs in recline have given mixed results. For both low [10] and high [11] speed frontal impact pulses, M50 HBMs were able to engage with the lap belt and properly differentiate between non-submarining and submarining events relative to PMHS outcomes. Additionally, for these validation assessments [10, 11], quantitatively, the HBMs have generated *good* and *reasonable* CORA and BioRank scores. However, qualitatively, the M50 HBMs overpredicted occupant downward displacement, lumbar spine flexion, and pelvis posterior rotation [11].

Some of the shortcomings in HBM biofidelity could be attributed to overly stiff HBM flesh material models that do not capture the nonlinear and viscoelastic properties of human flesh in shear [12]. Until recently, human flesh tissue data covering a range of strains and strain-rates applicable to impact simulations did not exist [13].

R. Newman (e-mail: rmn8ba@virginia.edu; tel: +1-434-297-8036) is a PhD student in Mechanical and Aerospace Engineering, A. Caudillo is a Research Specialist, J. Shin is a Research Engineer, M. Panzer is a Professor, B. Gepner is a Research Assistant Professor, all at the University of Virginia Center for Applied Biomechanics, Charlottesville, Virginia, USA.

This newly available human flesh tissue characterization data [14–17] has been used to develop Ogden rubber material models for the GHBMC soft tissues (skin, adipose, muscle) [13]. Initial evaluations of the implementation of these Ogden rubber skin, adipose, and muscle material formulations into the GHBMC M50 detailed occupant model have shown promise for improving HBM biofidelity at both the component and whole-body levels [13].

There remains room for improvement of M50 HBM biofidelity in recline, while there is a lack of biofidelity assessments for F50 HBMs in recline. Initial investigations suggest that Ogden soft tissue material models could be a viable source for improvement to HBM biofidelity. Therefore, the goal of this research was to implement newly developed Ogden rubber soft tissue constitutive models into the GHBMC 50th percentile male and female HBM flesh parts (skin, adipose, muscle) and assess the biofidelity of the HBMs with and without these tissue formulations for whole body reclined frontal impact post-mortem human subject (PMHS) sled tests.

II. METHODS

Software and Hardware Used

All simulations in this study were performed using LS-DYNA (R14) Massively Parallel Processing (MPP) single-precision, explicit finite element (FE) solver. The simulations were performed on a high-performance computational cluster (Intel Xeon64/sse2). All jobs were run on the same number of cores.

Reference Experimental Data

CAE environments were developed to replicate experimental environments of the tests run on midsize male [18] and female [7, 8] post-mortem human subjects (PMHS) in recline subjected to a 30 g, 50 km/h frontal impact pulse. PMHS were seated in a semi-rigid seat, which consisted of a seat pan and anti-submarining ramp and was designed to reproduce the behavior of a real front passenger seat [19]. The reference test restraint environments included a three-point belt equipped with dual lap belt pretensioners, a crash locking tongue (CLT), a shoulder belt pretensioner, and a shoulder belt load limiter set to 3.5 kN. The D-ring was positioned to mimic the position of a seat-integrated D-ring with the shoulder belt takeoff angle approximately 12° in the sagittal plane, relative to the horizontal. The PMHS feet were constrained to a toe pan.

CAE Environment

This study used four GHBMC HBMs for evaluation: GHBMC F50-O v6.0.1; GHBMC F50-OS v2.3.2, GHBMC M50-O v6.1; GHBMC M50-OS v2.3. The GHBMC F50-O and F50-OS were used for comparison against the midsize female reference tests [7–9]. The GHBMC M50-O and M50-OS were used for comparison against the midsize male reference tests [18].

The CAE environment included an FE model of the semi-rigid seat that has been previously validated against experimental semi-rigid seat moment-rotation responses [11, 20] and a toe pan. The restraint system used in the CAE environment matched that of the experimental studies and has been used and validated in previous computational studies assessing 50th male HBMs and FE-ATD models [11, 20, 21]. When used with the 50th female HBMs, anchorage points of the belt were adjusted accordingly to match experimental boundary conditions [7]

Soft Tissue Materials

This computational study explored the use of two different constitutive model formulations for the soft tissues of the GHBMC HBMs. For the purposes of this study, "soft tissues" will refer to skin, adipose, and muscle. The two different constitutive material models investigated were *MAT_SIMPLIFIED_RUBBER (181) and *MAT_OGDEN_RUBBER (077) material cards. Skin, adipose, and muscle each had separately developed constitutive models.

The *MAT_SIMPLIFIED_RUBBER (181) material cards were developed by the GHBMC and implemented into all commercially available versions of these HBMs. The *MAT_SIMPLIFIED_RUBBER (181) material cards will be referred to as the "stock" soft tissue material models throughout the remainder of the paper. Evaluation of the stock soft tissue material models meant assessment of the GHBMC HBMs as they were provided. Implementation of stock soft tissue materials required no modification to the HBMs.

The *MAT_OGDEN_RUBBER (077) material cards were previously developed to define Ogden hyperelastic flesh constitutive models with quasi-linear viscoelastic formulations (Table I) [13]. The *MAT_OGDEN_RUBBER (077) material cards will be referred to as the "Ogden" soft tissue material models throughout the remainder of the paper. To evaluate the performance of the Ogden soft tissue models, the skin, adipose, and muscle

*MAT_OGDEN_RUBBER (077) material IDs were implemented into all GHBMC HBM skin, adipose, and muscle parts, respectively, for each of the HBMs under investigation. Implementation of the Ogden soft tissue materials replaced any cross references to the default (stock) GHBMC soft tissue materials. For all HBMs, the head, neck, and foot flesh parts were not updated to reference the Ogden soft tissue materials. For the F50-O only, the shoulder fat pad materials were not updated to reference the Ogden soft tissue materials because these parts, when defined by Ogden materials, were unstable.

Robustness evaluations of the Ogden materials were performed previously by Panzer et al. [13] for abdomen and thorax rigidized impactor simulations. For the previously performed rigid impactor tests, replacement of the stock materials with Ogden materials reduced internal energies but did not significantly change hourglass energies. Despite the internal energy attenuation, behavior of the Ogden materials was cautiously deemed sufficient for the GHBMC HBMs since the rigid impactor simulations produced GHBMC HBM force-displacement responses of similar magnitudes to biological data. For the rigid impactor tests, implementation of the Ogden materials had a negligible effect on execution time and resulted in no error terminations. As mentioned, application of the Ogden materials to the shoulder fat caused instabilities in the reclined pulse for only the F50-O HBM. Once the F50-O shoulder fat materials were returned to their original simplified rubber material definition, errors due to numerical instabilities were not observed for reclined simulations.

TABLE I
OGDEN HYPERELASTIC MATERIAL PARAMETERS FOR VARIOUS FLESH MATERIALS

Material	μ_1 α_1	μ_2 α_2	μ_3 α_3	G_1 β_1	G_2 β_2	G_3 β_3	G_4 β_4	G_5 β_5
Skin	24.1e-3 2.830	-51.0e-3 2.002	55.55e-3 0.613	0.043 1e-4	0.314 1e-3	0.240 1e-2	0.277 1e-1	0.000
Adipose	1.467e-3 3.36e-2	7.201e-9 16.40	-1.89e-4 0.258	0.045 1e-4	0.585 1e-2	0.290 1e-1	0.290	0.000
Muscle	1.25e-7 8.000	-2.50e-7 -4.000		0.055 1e-4	0.098 1e-3	0.041 1e-2	0.557 1e-1	0.232 1e-0

Note: μ terms have units of GPa, β terms have units of ms^{-1}, and α and G terms are unitless.

Positioning

For each HBM, first, the H-Point of the HBM was positioned so that it matched that of the PMHS average. Then, the orientation of the HBM pelvis was adjusted to align with the average PMHS anatomical pelvis landmarks. The HBM pelvises were rotated to visually align with the reconstructed PMHS pelvis CT scans transformed into the global sled coordinate system. Since the pelvis is one of the most variable bone shapes of the human body, orientation alignments were not trivial and visual alignment served as the best method to align the HBM pelvis' relative to the average orientation of the PMHS. Following pelvis positioning of the HBM, pelvis translation and rotation were constrained and the position and orientation of L3, L1, T11, T8, T1, and the head were adjusted to match PMHS averages. Finally, the upper and lower extremities were adjusted to match PMHS surface landmark averages at the knee, ankle, elbow, and shoulder. HBM positioning procedures matched those of previous computational studies [11].

Positioning for each HBM was carried out in the Oasys (Arup, London, England) PRIMER HBM positioning module using a displacement-based cable approach. Two positioning simulations were performed per HBM. The first positioning simulation was performed on the HBM with its stock soft tissue materials implemented. The second positioning simulation was performed on the HBM with Ogden rubber soft tissue materials implemented.

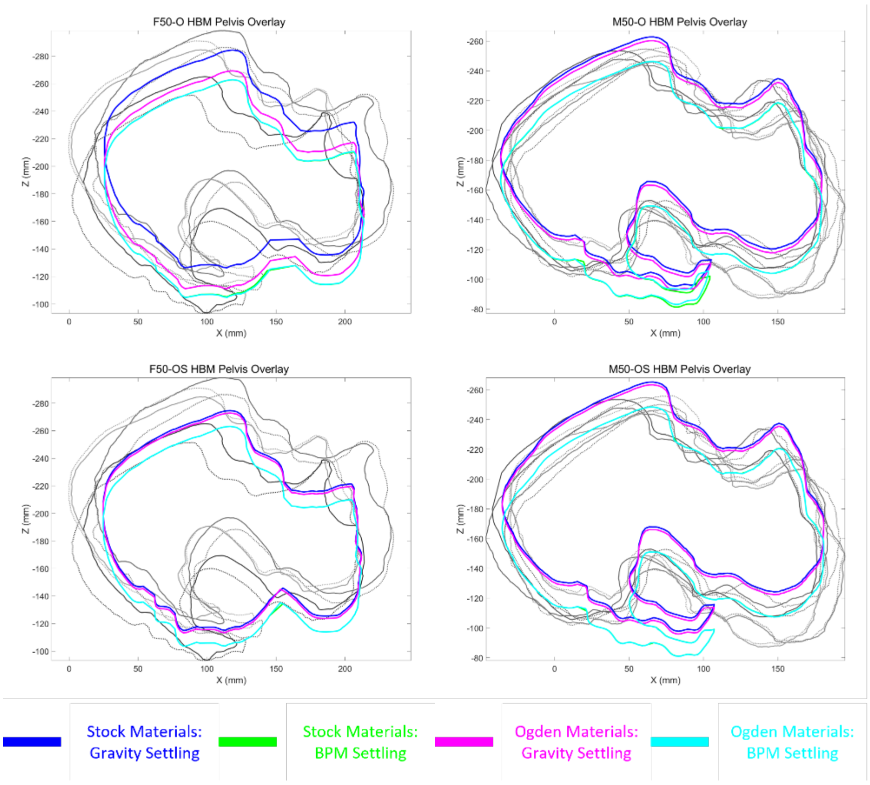

Fig. 1. Settled height of each HBM pelvis transformed to the experimental global CS for each FE settling method relative to the reference PMHS pelvis computed tomography (CT) scans.

Settling

All semi-rigid seat parts were constrained in translation and rotation during settling simulations. Nodes and rigid body parts of the skeletal structure of each HBM were constrained in X, Y, RX, RY, and RZ. At t=0, the HBMs were positioned 50 mm above their positioning targets. Two settling procedures, gravity settling and boundary prescribed motion (BPM) settling, were used for this study.

The gravity settling method settled the HBM into the seat under only the force of gravity. Gravity settling simulations were performed to determine the naturally settled height of the HBMs. Gravity settled HBM pelvises sat higher than the reference male PMHS pelvises and within the range of female PMHS pelvis seated heights.

The BPM settling method leveraged a BPM in Z to force the pelvis deeper into the semi-rigid seat. The BPM was applied such that the HBM pelvis seated height roughly matched that of the PMHS that sat the deepest in the semi-rigid seat.

During settling simulations, rate dependencies were ignored through use of a *CONTROL_IMPLICIT_DYNAMICS card with IRATE variable set to 2. Each settling simulation was run for 300 ms and nodal displacements were evaluated to confirm steady state. Initial stresses and strains were not maintained after settling. Only nodal coordinates were referenced for impact simulations. The two settling methods were applied twice per HBM, once per each soft tissue material type, resulting in four settling simulations per HBM.

Implementation of Ogden rubber soft tissue materials influenced the gravity settled height of the F50-O HBM but had minimal effect on the settled height of the F50-OS, M50-O, or M50-OS HBM pelvises (Fig. 1, TABLE A-I). Compared to the stock soft tissue materials, implementation of the Ogden rubber soft tissue materials allowed the F50-O pelvis to settle approximately 15 mm deeper into the semi-rigid seat, when using gravity settling methods. Also, during gravity settling, the F50-OS settled deeper into the semi-rigid seat, regardless of soft tissue material type, when compared to the F50-O (TABLE A-I). There was minimal difference in the gravity settled pelvis height between the M50-O and M50-OS. For each HBM, pelvis height due to BPM settling remained consistent regardless of the soft tissue materials (TABLE A-I).

Belt-Routing

Belt-routing was performed using the semi-automatic belt fitting tool in Oasys PRIMER. Belt routing was performed four times per HBM, once for each soft tissue material implementation at each settled height.

Frontal Impact Simulations

HBMs were subjected to a 30 g, 50 km/h frontal impact sled pulse that matched that of the PMHS reference tests [7, 8, 18]. The calcanei of the HBMs were constrained to the toe pan to replicate foot constraints implemented in PMHS testing. Contacts were in place between the HBM and toe pan, HBM and belt, HBM and CLT, and HBM and semi-rigid seat. In total, 16 frontal impact simulations were performed, 4 for each HBM (TABLE II). Frontal impact simulations were run for 150 ms.

TABLE II
TEST MATRIX

MODEL	SOFT TISSUE MATERIAL	SETTLING METHOD	TOTAL IMPACT SIMULATIONS PER HBM
F50-O	Stock	Gravity	4
		BPM	
	Ogden	Gravity	
		BPM	
F50-OS	Stock	Gravity	4
		BPM	
	Ogden	Gravity	
		BPM	
M50-O	Stock	Gravity	4
		BPM	
	Ogden	Gravity	
		BPM	
M50-OS	Stock	Gravity	4
		BPM	
	Ogden	Gravity	
		BPM	

Data Analysis

HBM kinematics at the head, T1, T8, T11, L1, L3, and pelvis matched PMHS instrumentation and were deemed to be the most relevant for biofidelity evaluation. Kinematic and biofidelity comparisons were made across the different settling methods and soft tissue materials used by each HBM. Additionally, kinematic and biofidelity comparisons were made between detailed (-O) and simplified (-OS) HBMs and between the F50 and M50 HBMs. These comparisons allowed us to assess not only the biofidelity of the HBMs but also the effect of settling method (gravity vs. BPM), soft tissue material properties (stock vs. Ogden), and HBM detail (detailed vs. simplified) on HBM performance in recline. Comparisons were performed leveraging a combination of qualitative and quantitative methods.

Responses were compared qualitatively by plotting HBM bone X and Z displacement and RY rotation displacement time histories against PMHS averages and corridors [7–9, 18]. Similarly, HBM trajectory responses were plotted against PMHS trajectories [7, 8, 18] for visual comparisons. Trajectory and time history plots and simulation still frames were also used to compare HBMs across settling methods, soft tissue material properties, and HBM detail. The responses were compared quantitatively using the CORrelation and Analysis method CORA [22]. The total CORA score was calculated with equal weights assigned to corridor score and cross-correlation score. The cross-correlation score was calculated with contributions of 25% from phase and size scores and 50% from progression (shape) score. A complete list of CORA parameter values is provided in TABLE D-I.

III. RESULTS

Frontal Impact Simulation Outcomes

For each HBM (F50-O, F50-OS, M50-O, M50-OS), a simulation was performed for each soft tissue material implementation and for each settling method (gravity vs. BPM), resulting in 16 final simulations (TABLE II). All HBM impact simulations were initiated targeting a termination time of 150 ms and all simulations reached normal termination.

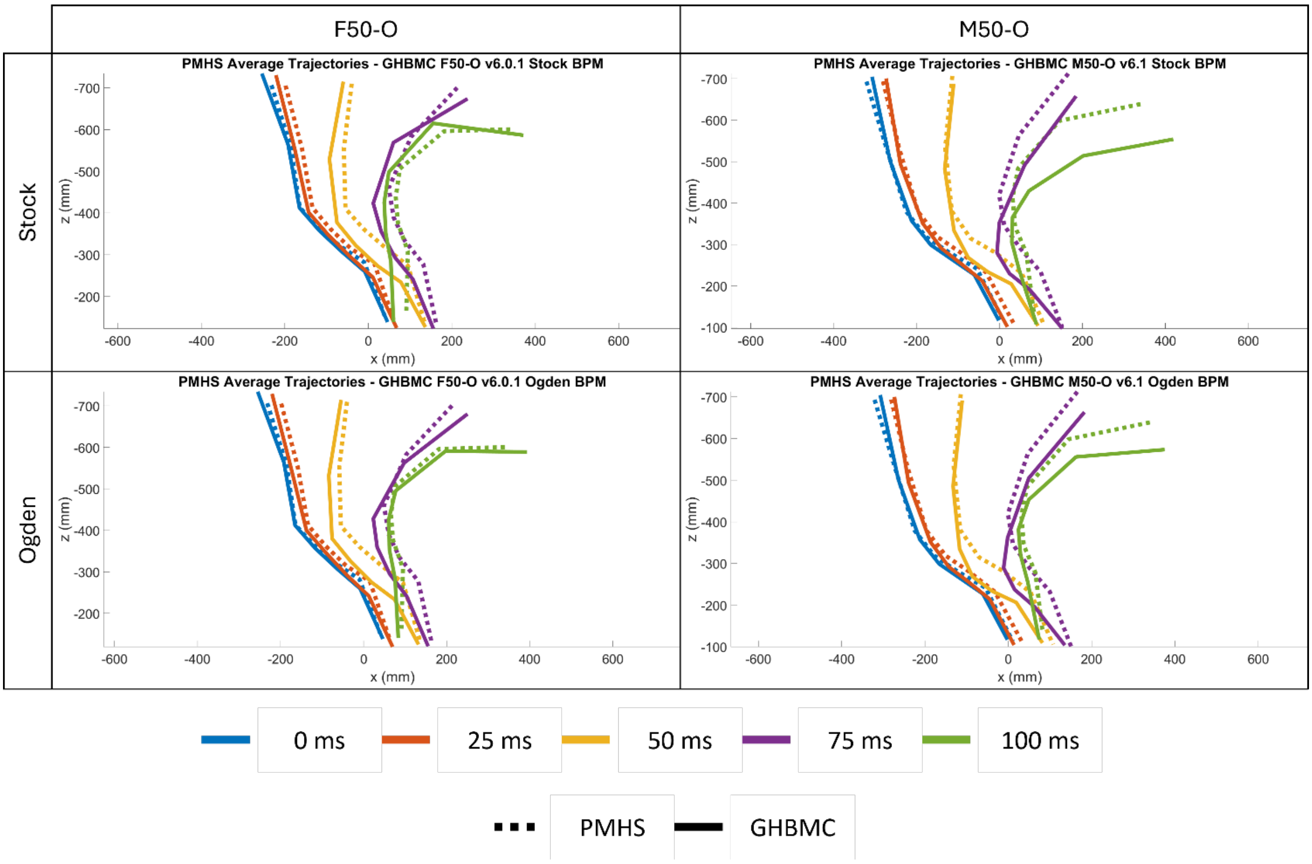

Fig. 2. Comparison of the average PMHS XZ trajectories of the head T1, T8, T11, L1, L3, and pelvis (PSIS) with XZ trajectories of the detailed HBMs following settling with the BPM method.

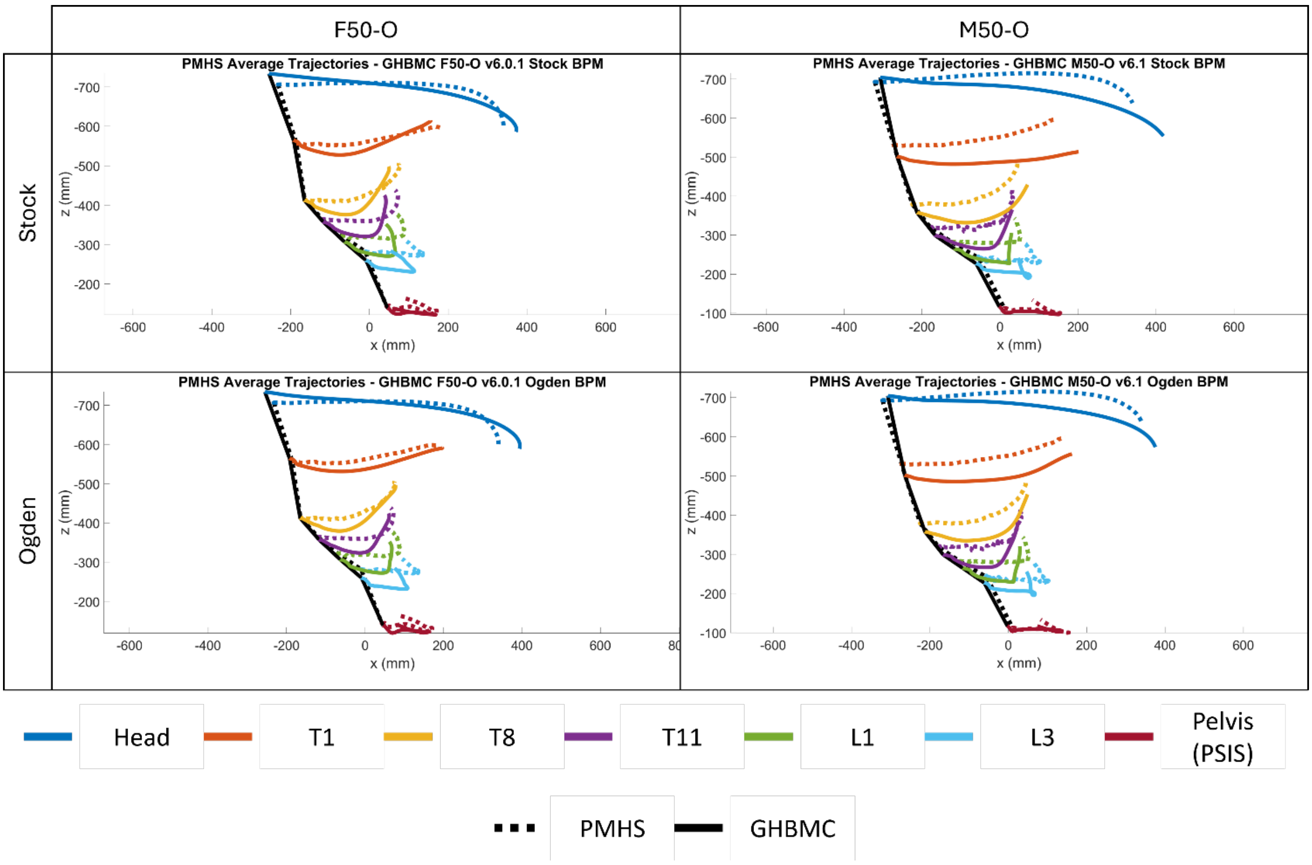

Fig. 3. Comparison of the average PMHS intersegmental XZ trajectories of the head T1, T8, T11, L1, L3, and

pelvis (PSIS) with XZ trajectories of the detailed HBMs following settling with the BPM method.

HBM Kinematics

Similar to the experimental PMHS reference tests, each HBM was restrained by the lap and shoulder belt, and no submarining was observed for the 16 impact simulations performed. With the pelvis restrained by the lap belt in simulation, each HBM experienced considerable torso flexion prior to rebound.

HBM kinematics at the Head, T1, T8, T11, L1, L3, and the pelvis for each soft tissue material implementation and settling method were evaluated with respect to PMHS time history corridors (APPENDIX C) and average PMHS trajectories reconstructed in the XZ plane (Fig. 2, Fig. 3, APPENDIX B). HBMs were closer to PMHS corridors when predicting forward excursions while consistently overpredicting downward excursions of the bony anatomy.

HBM Kinematics for Gravity vs. BPM Settling Methods

Impact simulations with the BPM settled height of the HBM reduced downward excursion overpredictions of the bony anatomy (APPENDIX C). This was true for simulations with both stock and Ogden soft tissue material implementations and for both the detailed and simplified HBMs. The choice in settling method had less influence over forward excursion of the head, neck, and upper spine (APPENDIX C). Impact simulations performed with a BPM settled HBM measured less forward displacement of the lower spine and pelvis (APPENDIX C). BPM settling positions showed the largest reductions to forward excursions for the M50 HBMs, both detailed and simplified, and for HBMs utilizing stock soft tissue materials.

HBM Kinematics for Stock vs. Ogden Soft Tissue Materials

For the simplified HBMs, the HBMs utilizing Ogden rubber soft tissue materials exhibited a stiffer response in all but the head and T1 locations. For the spine (T8 and inferior) and pelvis, implementation of the Ogden soft tissue materials reduced forward and downward displacement of the simplified HBMs (Fig. B3-B8, Fig. C8-C14). Reductions in forward excursions due to the utilization of Ogden materials could be seen throughout the simulation but were most noticeable starting at peak forward excursion of each respective bone (T8, T11, L1, L3, pelvis) and remained throughout the rest of the simulation. Similarly, for the M50-OS, reductions in downward displacements due to the utilization of Ogden materials became most prominent starting at peak downward excursion of each respective bone (T8, T11, L1, L3, pelvis) and remained throughout the rest of the simulation. For the F50-OS, reductions in downward displacement due to the utilization of Ogden materials were mostly evident during rebound of each respective bone (T8, T11, L1, L3, pelvis).

For the detailed models, utilization of the Ogden soft tissue materials reduced downward displacement overpredictions of the bony anatomy (Fig. 2-5, Fig B1-B2, Fig. C1-7). The largest differences in downward excursions between HBMs with stock compared to Ogden flesh materials were seen when comparing simulations performed with gravity settled positions of the HBM, since gravity settled HBMs allowed for different initial HBM seated heights (Fig. 1) and inferior pelvis flesh deformations. Since BPM settling allowed for identical seated heights (Fig. 1) and similar deformations of the inferior pelvis flesh, reductions in downward excursions caused by the implementation of Ogden flesh materials were less pronounced for impact simulations using BPM settled positions.

For the M50-O, impact simulations utilizing Ogden materials experienced less forward displacement of the tracked bones (Fig. 5, Fig. C1-C7). The same was not true for the F50-O. Impact simulations utilizing Ogden materials for the F50-O saw greater forward excursion of the head and thoracic spine (Fig. 4, Fig. C1-C7). For F50-O simulations utilizing Ogden soft tissue materials, until the time of maximum forward displacement, forward excursions of L1, L3, and the pelvis were typically less than that of F50-O simulations utilizing stock soft tissue materials. For the F50-O, L1, L3, and the pelvis all saw less rearwards displacement during rebound when implemented with Ogden materials.

Ogden material implementation had opposite effects on the F50-O and M50-O when comparing the forward rotation calculated for the T1 and T8 vertebral bodies. For the F50-O, utilization of Ogden materials increased the forward rotation observed for T1 and T8; whereas, for the M50-O, utilization of Ogden materials reduced the forward rotation observed for T1 and T8. Implementation of Ogden soft tissue materials reduced rearward rotations observed at the pelvis for all HBMs. For the remaining bones with kinematic tracking, soft tissue material properties had less consistent effects on bone rotation (RY) in the sagittal plane.

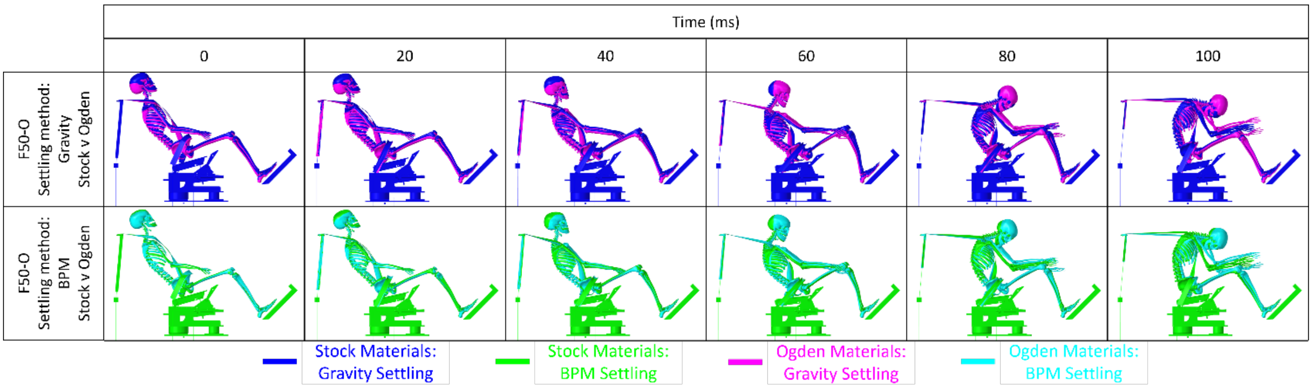

Fig. 4. Comparison of F50-O kinematics when using stock vs. Ogden soft tissue materials for both settling methods.

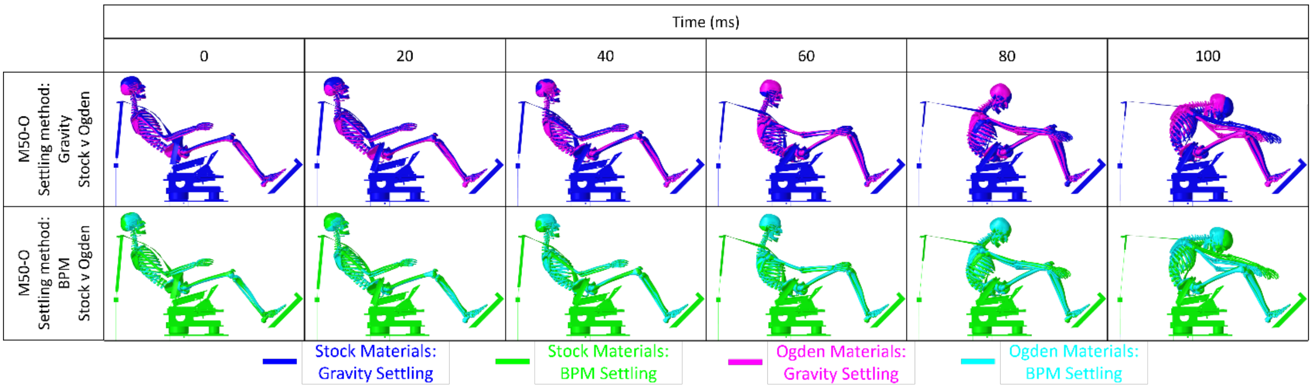

Fig. 5. Comparison of M50-O kinematics when using stock vs. Ogden soft tissue materials for both settling methods.

HBM Kinematics for Detailed vs. Simplified HBMs

Detailed models experienced less forward excursion of the head and thoracic spine than simplified models (Fig. 6-7, Fig. B9-B10, Fig. C15-C18, Fig. C22-25). For the head and thoracic spine, maximum forward displacements measured by the F50-OS were well above those measured by the F50-O and PMHS reference corridors (Fig. C15-C18, Fig. C22-25). Head and thoracic spine forward displacements measured by the M50-OS were better matched to the M50-O and PMHS reference corridors (Fig. C15-C18, Fig. C22-25). Forward displacements of L1, L3, and the pelvis are better matched between detailed and simplified HBMs, with simplified HBMs generally maintaining greater forward excursions throughout the time history plots. (Fig. 6-7, Fig. B9-B10, Fig. C19-C21, Fig. C26-28).

When using Ogden soft tissue material implementations, the M50-OS generally measured larger maximum downward displacements than the M50-O (Fig. C22-C28). Compared to Ogden material implementations, detailed and simplified models with stock soft tissue material implementations measured more comparable maximum downward displacements for the M50 HBMs (Fig. C15-C21). Stock soft tissue material implementation for the F50 models allowed for greater maximum downward displacements of F50-O when compared to the F50-OS except for at the head, L3, and pelvis (Fig. C15-C21). The opposite was true for Ogden soft tissue material implementation for the F50 models, where less maximum downward displacements were observed in the F50-O when compared to the F50-OS (Fig. C22-C28).

For both the F50 and M50 HBMs, the detailed models predicted larger upwards displacements of the bones during rebound, which brought the measured Z displacements closer to PMHS corridors for the final stages of simulations (Fig. 6-7, Fig. B9-B10, Fig. C15-C28). For T1 in particular, the simplified HBMS were unable to achieve upwards displacement during rebound, allowing for large deviations between simplified HBM T1 kinematics and the reference PMHS corridors (Fig. C16, Fig. C23).

Regardless of soft tissue material properties, the F50-OS predicted substantially more forward rotation in the spine than the F50-O. For Ogden soft tissue materials, the M50-OS also predicted substantially more forward rotation in the spine than the M50-O. Differences in forward rotation of the vertebral bodies were less apparent when using stock soft tissue materials for the M50 HBMs.

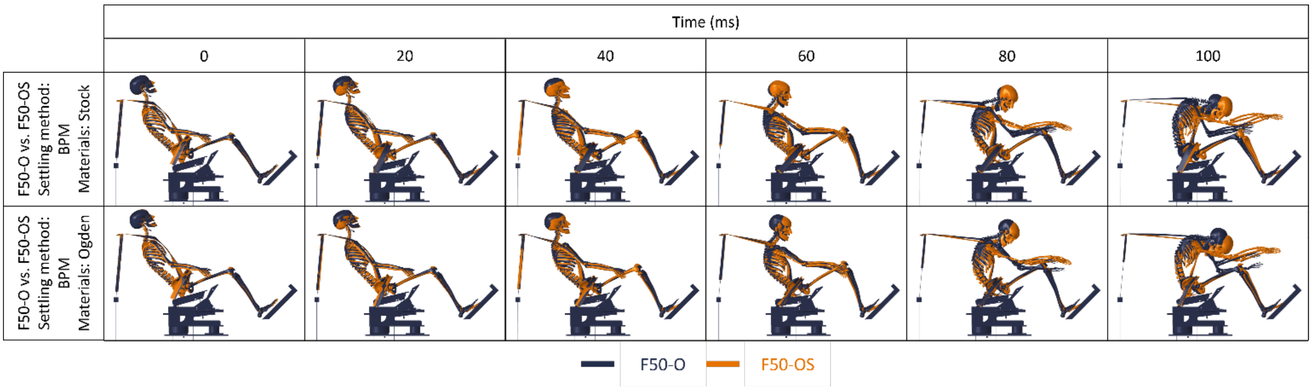

Fig. 6. Comparison of F50-O and F50-OS kinematics when using the BPM settling methods for both stock and Ogden soft tissue materials.

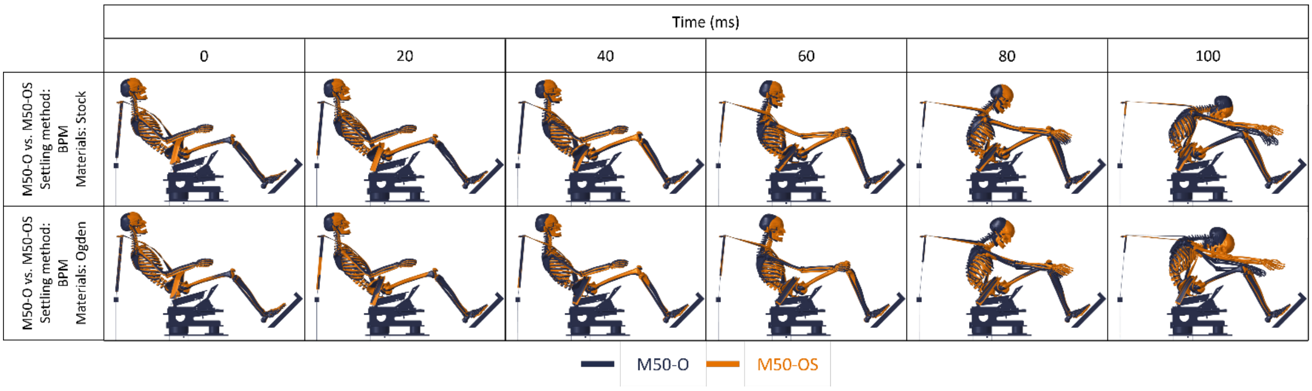

Fig. 7. Comparison of M50-O and M50-OS kinematics when using the BPM settling methods for both stock and Ogden soft tissue materials.

CORA ANALYSIS

Individual signal (X displacement, Z displacement, RY displacement) CORA scores were analyzed for the Head, T1, T8, T11, L1, L3, and pelvis for each settling method and soft tissue material implementation of each of the four HBMs evaluated in this study (APPENDIX D). Average CORA scores (TABLE D-II - D-V) were grouped by HBM, divided into three categories, X Avg., Z Avg., RY Avg, and calculated for each of the four impact simulations performed per HBM (TABLE II). The three categories, X Avg., Z Avg., RY Avg, included the average CORA scores for the Head, T1, T8, T11, L1, L3, and pelvis displacement time histories.

For matched settling methods, implementation of the Ogden rubber soft tissue materials improved the X Avg. total CORA scores for all four of the HBMs under investigation. Except for gravity settling with the F50-O, for matched settling methods, implementation of the Ogden rubber soft tissue materials also improved the Z Avg. total CORA scores for all four of the HBMs under investigation. For each of the four HBMs, X Avg. CORA scores were higher than Z Avg. CORA scores.

For matched soft tissue material implementations, X Avg. CORA scores decreased with BPM settling methods for all four HBMs. In contrast, for matched soft tissue material implementations, Z Avg. CORA scores increased with BPM settling methods for all four HBMs.

When soft tissue material properties are held equal, CORA scores associated with RY Avg. measurements increased for BPM settling methods. When settling methods were held equal, CORA scores associated with RY Avg. measurements decreased with the implementation of Ogden soft tissue materials, with the exception of the M50-O HBM.

IV. DISCUSSION

This study allowed us to evaluate the effects of seated height, soft tissue materials, and detailed and simplified

HBMs on kinematics of the head, T1, T8, T11, L1, L3, and the pelvis for GHBMC 50th percentile HBMs seated in recline on a semi-rigid seat and subjected to a 50 km/h frontal impact sled pulse. Initial stresses and strains incurred during positioning and settling procedures were not considered. Consequently, all stresses and strains were equal to zero at t=0 of the impact simulations. The kinematic response of the four GHBMC HBMs under evaluation were compared to PMHS corridors and used to assess HBM biofidelity.

While the CORA analysis gave a quantitative comparison across the different HBMs, settled heights, and soft tissue material implementations, these scores are best used when comparing the kinematics responses to one another and these CORA scores alone do not give definitive conclusions about the applicability of these HBMs for recline frontal impact tests [11].

Seated Height Prior To Impact

Gravity settling methods resulted in the pelvises of the M50-O and M50-OS sitting higher than those of the midsize male PMHS. This relationship agrees with previous 50th percentile male HBM validation work [11] using the same PMHS reference data and is likely a consequence of the semi-rigid seat, which does not deform under settling, localizing all deformation during settling to the HBM flesh [18]. In contrast, gravity settling methods allowed the F50-O and F50-OS pelvises to settle within the range of seated heights observed in the female PMHS (Fig. 1). The female HBMs likely aligned better because the female PMHS generally had more soft tissue below the pelvis, causing them to sit higher on the semi-rigid seat [7].

When controlling for rate effects in constitutive models, compared with stock soft tissue materials, Ogden rubber materials had a slightly softer quasi-static response [13], allowing the F50-OS, M50-O, and M50-OS to settle 1-3 mm deeper into the semi-rigid seat during gravity settling (Fig. 1, TABLE A-1). Compared with stock soft tissue materials, Ogden rubber materials allowed the F50-O to settle 15 mm deeper into the semi-rigid seat (Fig. 1, TABLE A-1). Differences in the distribution and connectivity of the soft tissue around the pelvis allowed the F50-O to respond differently than the other HBMs during gravity settling.

For each HBM, the pelvis flesh is comprised of hexahedral and tetrahedral elements. The pelvis tetrahedral flesh has shared nodes with the pelvis bone and hexahedral pelvis flesh elements, effectively connecting the bones and flesh and tying their response to one another. For the F50-OS, M50-O, and M50-OS, the volume ratio of tetrahedral to hexahedral elements is 0.66, 0.48, and 0.70, respectively, and the tetrahedral elements are well spread along the width of the pelvis. However, for the F50-O this ratio is 0.15 and the tetrahedral elements are concentrated at midline.

For the simplified HBMs, the pelvis flesh and skin are the only soft tissue parts that reside below the pelvis and undergo deformation under settling, with their deformation dictating the pelvis settled height. For the detailed HBMs, in addition to the pelvis flesh and skin, the gluteus also resides below the pelvis. In the M50-O, the gluteus muscle is connected to the pelvis flesh hexahedral and tetrahedral elements through shared nodes. The connectivity between the gluteus and flesh elements in the M50-O adds a boundary condition to the shape of the flesh elements, limiting the deformation of the flesh elements underneath the pelvis during settling. In the F50-O, the gluteus muscle is connected by shared nodes to the tetrahedral pelvis flesh elements but not to the hexahedral pelvis flesh elements. The absence of connectivity of the gluteus to the pelvis hexahedral flesh elements combined with the F50-O tetrahedral flesh distribution allows for gaps between the gluteus and hexahedral flesh elements. During settling, the gluteus elements fill these gaps and achieve greater levels of deformation, explaining why the F50-O was able to experience large changes in deformation during gravity settling.

Forcing the HBMs deeper into the seat with BPM settling was the most effective parameter for reducing downward displacement of the HBMs during impact simulations, although the BPM seated posture was still not enough to bring HBM downward displacements to within PMHS corridors. BPM seated heights allowing for reductions in downward displacement was expected, since the HBMs in BPM seated postures had a shorter distance to travel before engaging with stiffer and undeformable structures of the semi-rigid seat. Also in the BPM seated postures, the soft tissues elements started off in more deformed states, reducing the amount of soft tissue deformation possible during impact simulations.

Effect of Stock vs. Ogden Soft Tissue Materials

Ogden materials showed clear signs of improvement to the XZ displacements and trajectories of all four HBMs, bringing HBM responses closer to that of the PMHS (Fig. B1-B10, Fig. C1-C28). Aside from the head and neck, where soft tissue materials were excluded from Ogden material replacement, implementation of the Ogden materials generated a stiffer whole-body response, reducing X-displacement, Z-displacement, and forward flexion of the upper torso, highlighting the fact that the current GHBMC 50th HBMs are overpredicting forward displacement and flexion of the spine. This relationship held true for all but the F50-O, for which the stock materials underpredicted flexion of the thoracic spine (Fig. 2-3, Fig. B1-B2) and implementation of Ogden soft tissue materials increased the forward displacement and flexion at T1, T8, and T11. While the F50-O performs differently from the other HBMs at the spine, relative to PMHS corridors, the underprediction of spinal flexion appears to be less severe than the overprediction of spinal flexion observed in the F50-OS, M50-O, and M50-OS, as shown by the stick figure trajectories (Fig. 2-3, Fig. B1-B6) and RY CORA scores for T1, T8, T11, L1, and L3 (TABLE D-VI – D-XXI).

The relationships and HBM constraints that allow for underprediction of spinal flexion appear to be specific to the F50-O, since this relationship was not captured by neither its detailed male (M50-O) nor simplified female (F50-OS) counterparts. When subjected to the frontal impact pulse, the M50-O had elongation of the posterior spinal ligaments and pinching anteriorly at the intervertebral discs. Whereas the F50-O saw minimal stretching of the posterior spinal ligaments and bulging of the intervertebral discs, resulting in the internal energies of the posterior spinal ligaments being three orders of magnitude smaller in the F50-O than M50-O. The F50-O behavior suggests that some other parts of the F50-O are carrying the energy of the torso motion since material properties and stiffnesses between the spinal ligaments are nearly identical between the M50-O and F50-O. Furthermore, it remains unclear why the implementation of Ogden soft tissue materials elicited a more relaxed response in forward displacement of the F50-O thoracic spine and a stiffer response at L1, L3, and the pelvis of the F50-O and for all regions of the body, aside from the head, for all other HBMs. This suggests that there are attributes specific to the F50-O thoracic spine region that are not only different from the other GHBMC HBMs but also alter the impact of the Ogden materials. Ideally, there should not be differences in the response at the spine across the different HBMs, since experimental tests in recline suggest that the kinematic patterns and relative vertebral body rotations for males and females should be similar [8].

These results suggest further investigation of the cause for F50-O and M50-O differences in response at the spine is warranted. Refinements of the spine of the GHBMC HBMs might be necessary to not only better align the performance of the spine across HBMs, but to improve the performance of the spine in general, as this region serves as a limitation for HBM biofidelity in reclined postures [11, 23].

One of the biggest challenges for improving the biofidelity of the HBMs under evaluation was reducing the downward motion of the body. For each of the four HBMs under evaluation, the Ogden soft tissue materials were able to help reduce this motion, although more improvement is needed for the HBMs to fall within PMHS corridors. Since the Ogden materials reduced pelvis rearward rotation, their implementation also reduced downward displacement at the pelvis (measured at the PSIS), which had a chain effect and helped reduce downward displacement of the thoracolumbar vertebral bodies. Additionally, the Ogden constitutive model for skin is stiffer than that of the stock skin material [13], providing more tension on the posterior side. Added posterior tension helped reduce downward bending, and consequently downward displacement of the spine.

Previous implementation of the Ogden materials into the GHBMC M50-O [13] was performed for whole-body simulations of shoulder impact, abdomen bar impact, abdomen oblique impact, frontal chest hub impact, gravity settling, and frontal crash impacts with reclined seating. The current study was performed to address the lack of HBM, particularly 50th female, biofidelity assessments and look to find improvements of the current state of biofidelity of HBMs in reclined postures [10, 11]. While Ogden materials have shown improved performance for both the whole-body simulations performed in Panzer et al. [13] and the recline simulations performed in the current study, to the authors' knowledge, these materials have yet to be implemented into HBMs subjected to frontal impacts in upright postures. Further validation of these material models for upright configurations is warranted.

Effect of Detailed vs. Simplified Models

Implementation of Ogden materials in detailed HBMs brings HBM responses closer to PMHS corridors than implementation of Ogden materials in simplified HBMs. Specifically, implementation of Ogden materials in detailed HBMs did well to push the X-displacement time histories for the head, T1, T8, and T11 closer to PMHS corridors. The M50-O and M50-OS, which were well matched in response when using stock soft tissue materials, had their X-displacement time histories become less aligned with the implementation of Ogden rubber soft tissue models. Conversely, the F50-O and F50-OS, which predicted varied magnitudes of forward excursions when using stock soft tissue materials, had their X-displacement time histories become more aligned with the implementation of Ogden rubber soft tissue models. The X-displacement time history of T1, T8, and T11 measured by the F50-O and F50-OS, when implemented with stock soft tissue materials, resided on opposite ends of the PMHS corridors (Fig. C15-C21). Once again, it seems that there is something unique in the makeup of the F50-O thoracic spine region that is not captured by the other HBMs. It would serve the community well to invest more research into the performance of the F50-O and F50-OS, to (1) better understand the causes for thoracic spine performance in the F50-O and (2) better align the responses between the detailed and simplified F50 HBMS. The results of this study suggest that replacement of the stock soft tissue material models with Ogden soft tissue material models is one solution to better aligning F50-O and F50-OS responses.

V. CONCLUSION

Overall, all four HBMs did better in matching the forward displacement of the PMHS, while consistently overpredicting downward displacement relative to the PMHS. For all 16 simulations, each HBM pelvis engaged the lap belt throughout pelvis forward excursion and no HBM submarining was observed. Restraint of the pelvis by the lap belt and absence of submarining matches what was observed in the PMHS reference tests, for which only one midsized male PMHS experienced partial submarining. Forcing the pelvis deeper into the semi-rigid seat using BPM settling methods reduced but did not correct for overpredictions in downward displacement.

Detailed HBMs predicted kinematic displacement and trajectory responses closer to those of the PMHS than did the simplified HBMs. Furthermore, Ogden materials were more effective in improving the response of the detailed HBMs, doing well to push the X-displacement time histories for the head, T1, T8, and T11 closer to PMHS corridors. Although more effective for the detailed models, implementation of the Ogden materials showed clear signs of improvement to the XZ displacements and trajectories of all four HBMs. Generally, implementation of the Ogden materials stiffened up the whole-body response, except for at the spine of the F50-O, for which the Ogden materials increased F50-O thoracic spine forward displacement and spinal flexion. Furthermore, responses at T1, T8, and T11 are not comparable between the detailed and simplified F50 models, with X-displacements of the two residing on opposite sides of PMHS corridors.

The results of this study identified that the F50-O was unique in its pelvis construction and spine performance. Spine performance discrepancies do not appear to be due to spinal ligament construction differences but rather suggest that a structure other than the spinal ligaments is withstanding the load caused by the forward motion of the torso. Further investigation of the F50-O should be carried out to understand the causes of its underprediction in flexion and lack of recruitment of the posterior spinal ligaments. These answers will be critical for improving the biofidelity of the thoracic and lumbar spine for all HBMs, as this region is still a limitation in terms of HBM biofidelity for reclined occupants.

Although the implementation of Ogden soft tissue materials improved the ability of HBMs to match the kinematic response of reclined PMHS in frontal impact sled tests, the results of this study suggest further refinement of the HBMs is still necessary for these HBMs to be perfect in matching PMHS responses in reclined postures. Most notably, the downward motion of the HBMs is still far, in magnitude, from aligning with PMHS measurements.

VI. ACKNOWLEDGEMENTS

This research was supported by the Global Human Body Models Consortium (GHBMC).

VII. REFERENCES

[1] Van Gils, S. (n.d.). *Final report on dissemination of the EU-funded project VIRTUAL* (Deliverable D7.5)

[2] Euro NCAP. (2023). *Euro NCAP Roadmap 2030: Vision Zero for Road Safety*Euro NCAP

[3] Klug, C.; Schachner, M.; Eggers, A.; Galazka, J.; Jimenez, C.; Kirch, J.; Levallois, I.; Lobenwein, U.; Meissner, N.; Pardede, V.; Pipkorn, B.; Ellway, J.; van Ratingen, M. (2023). EURO NCAP VIRTUAL TESTING - CRASHWORTHINESS, *27th International Technical Conference on the Enhanced Safety of Vehicles (ESV)*Presented at the Conference on the Enhanced Safety of Vehicles (ESV)

[4] Dissanaike, S.; Kaufman, R.; Mack, C. D.; Mock, C.; Bulger, E. (2008). The Effect of Reclined Seats on Mortality in Motor Vehicle Collisions, *Journal of Trauma and Acute Care Surgery*, Vol. 64, No. 3, 614. doi:10.1097/TA.0b013e318164d071

[5] Jorlöv, S.; Bohman, K.; Larsson, A. (2017). Seating Positions and Activities in Highly Automated Cars – A Qualitative Study of Future Automated Driving Scenarios, *Proceedings of the International Research Conference on the Biomechanics of Impact*Presented at the IRCOBI, , Antwerp, Belgium, 13–22

[6] Umale, S.; Khandelwal, P.; Humm, J.; Pintar, F.; Yoganandan, N. (2022). Comparison of small female occupant model responses with experimental data in a reclined posture, *Traffic Injury Prevention*, Vol. 23, No. sup1, S211–S213. doi:10.1080/15389588.2022.2125237

[7] Shin, J.; Donlon, J. P.; Richardson, R.; Espelien, C.; Gallaher, M.; Luong, V.; Gepner, B.; Forman, J.; Östling, M.; Kerrigan, J. (2023). Comparison of Pelvis Kinematics and Injuries in Reclined Frontal Impact Sled Tests Between Mid-Size Adult Male and Female PMHS, *Proceedings of the International Research Conference on the Biomechanics of Impact*Presented at the IRCOBI, , Cambridge, United Kingdom, 266–284

[8] Shin, J.; Donlon, J. P.; Richardson, R.; Espelien, C.; Sochor, S.; Gallaher, M.; Luong, V.; Gepner, B.; Forman, J.; Östling, M.; Kerrigan, J. (2023). Comparison of thoracolumbar spine kinematics and injuries in reclined frontal impact sled tests between mid-size adult female and male PMHS, *Accident Analysis & Prevention*, Vol. 193, 107334. doi:10.1016/j.aap.2023.107334

[9] Shin, J.; Kerrigan, J.; Östling, M. (2025). Using anthropometry-based scaling to predict responses across sex in reclined frontal impact sled tests, *Traffic Injury Prevention*, Vol. 26, No. 5, 577–586. doi:10.1080/15389588.2024.2430584

[10] Investigation of the Biofidelity of Human Body Models and ATD Models in Sled Test Conditions. (2023)Presented at the 27th International Technical Conference on the Enhanced Safety of Vehicles (ESV)National Highway Traffic Safety Administration

[11] Gepner, B.; Perez-Rapela, D.; Forman, J. L.; Östling, M.; Pipkorn, B.; Kerrigan, J. R. (2022). Evaluation of GHBMC, THUMS and SAFER Human Body Models in Frontal Impacts in Reclined Postures, *Proceedings of the International Research Conference on the Biomechanics of Impact*Presented at the IRCOBI, , Porto, Portugal, 116–143

[12] Gepner, B.; Joodaki, H.; Sun, Z.; Jayathirtha, M.; Kim, T.; Forman, J. L.; Kerrigan, J. R. (2018). Performance of the Obese GHBMC Models in the Sled and Belt Pull Test Conditions, *Proceedings of the International Research Conference on the Biomechanics of Impact*Presented at the IRCOBI, , Athens, Greece, 355–368

[13] Panzer, M. B.; Caudillo, A.; Gepner, B. (2024). Developing and Implementing New Flesh Materials based on Human Tissue Data for GHBMC M50-O, *Proceedings of the International Research Conference on the Biomechanics of Impact*Presented at the IRCOBI, , Stockholm, Sweden, 734–735

[14] Kong, K. S. Y. (2020, December 3). *Development of a Computational Model of Skin Damage under Blunt Impact to Investigate Skin Failure Threshold* (Doctoral Dissertation)University of VirginiaRetrieved from https://libraetd.lib.virginia.edu/public_view/kh04dq423

[15] Sun, Z.; Gepner, B. D.; Lee, S.-H.; Rigby, J.; Cottler, P. S.; Hallman, J. J.; Kerrigan, J. R. (2021). Multidirectional mechanical properties and constitutive modeling of human adipose tissue under dynamic loading, *Acta Biomaterialia*, Vol. 129, 188–198. doi:10.1016/j.actbio.2021.05.021

[16] Van Loocke, M.; Lyons, C. G.; Simms, C. K. (2008). Viscoelastic properties of passive skeletal muscle in compression: Stress-relaxation behaviour and constitutive modelling, *Journal of Biomechanics*, Vol. 41, No. 7, 1555–1566. doi:10.1016/j.jbiomech.2008.02.007

[17] Takaza, M.; Cooney, G. M.; McManus, G.; Stafford, P.; Simms, C. K. (2014). Assessing the microstructural response to applied deformation in porcine passive skeletal muscle, *Journal of the Mechanical Behavior of Biomedical Materials*, Vol. 40, 115–126. doi:10.1016/j.jmbbm.2014.08.019

[18] Richardson, R.; Donlon, J.-P.; Jayathirtha, M.; Forman, J. L.; Shaw, G.; Gepner, B.; Kerrigan, J. R.; Östling, M.; Mroz, K.; Pipkorn, B. (2020). Kinematic and Injury Response of Reclined PMHS in Frontal Impacts, *Stapp Car Crash Journal*, Vol. 64. doi:10.4271/2020-22-0004

[19] Uriot, J.; Potier, P.; Baudrit, P.; Trosseille, X.; Petit, P.; Richard, O.; Compigne, S.; Masuda, M.; Douard, R. (2015). Reference PMHS Sled Tests to Assess Submarining, *Stapp Car Crash Journal*, Vol. 59, 203–223. doi:10.4271/2015-22-0008

[20] Gepner, B. D.; Draper, D.; Mroz, K.; Richardson, R.; Östling, M.; Pipkorn, B.; Forman, J. L.; Kerrigan, J. R. (2019). Comparison of Human Body Models in Frontal Crashes with Reclined Seatback, *Proceedings of the International Research Conference on the Biomechanics of Impact*Presented at the IRCOBI, , Florence, Italy

[21] Richardson, R. E.; Gepner, B.; Kerrigan, J. R.; Forman, J. L. (2024). Evaluation of lap belt-pelvis load transfer in frontal impact simulations using finite element occupant models, *Traffic Injury Prevention*, Vol. 25, No. 8, 1137–1145. doi:10.1080/15389588.2024.2381084

[22] Gehre, C.; Gades, H.; Wernicke, P. (2009). OBJECTIVE RATING OF SIGNALS USING TEST AND SIMULATION RESPONSES, *21st International Technical Conference on the Enhanced Safety of Vehicles Conference (ESV)*Presented at the Enhanced safety of vehicles conference (ESV), , 09–0407

[23] Tushak, S. K.; Gepner, B.; Pipkorn, B.; Kerrigan, J. R. (2022). Evaluation of the GHBMC Lumbar Spine in Sub-injurious and Injurious Loading, *Proceedings of the International Research Conference on the Biomechanics of Impact*Presented at the IRCOBI, , Porto, Portugal, 866–883

VIII. APPENDIX

Appendix A – Pre-Impact Positioning

TABLE A-I
PELVIS CG SETTLED LOCATION RELATIVE TO THE GLOBAL CS.

F50-O	Pelvis CG X-Coordinate (mm)	Pelvis CG Z-Coordinate (mm)
Stock – Gravity	117	-208
Stock -BPM	117	-187
Ogden -Gravity	117	-193
Ogden - BPM	117	-187
F50-OS	Pelvis CG X-Coordinate (mm)	Pelvis CG Z-Coordinate (mm)
Stock – Gravity	108	-193
Stock -BPM	108	-182
Ogden -Gravity	108	-192
Ogden - BPM	108	-182
M50-O	Pelvis CG X-Coordinate (mm)	Pelvis CG Z-Coordinate (mm)
Stock – Gravity	74	-181
Stock -BPM	74	-164
Ogden -Gravity	74	-178
Ogden - BPM	74	-164
M50-OS	Pelvis CG X-Coordinate (mm)	Pelvis CG Z-Coordinate (mm)
Stock – Gravity	64	-182
Stock -BPM	64	-165
Ogden -Gravity	64	-180
Ogden - BPM	64	-165

Appendix B – Trajectories

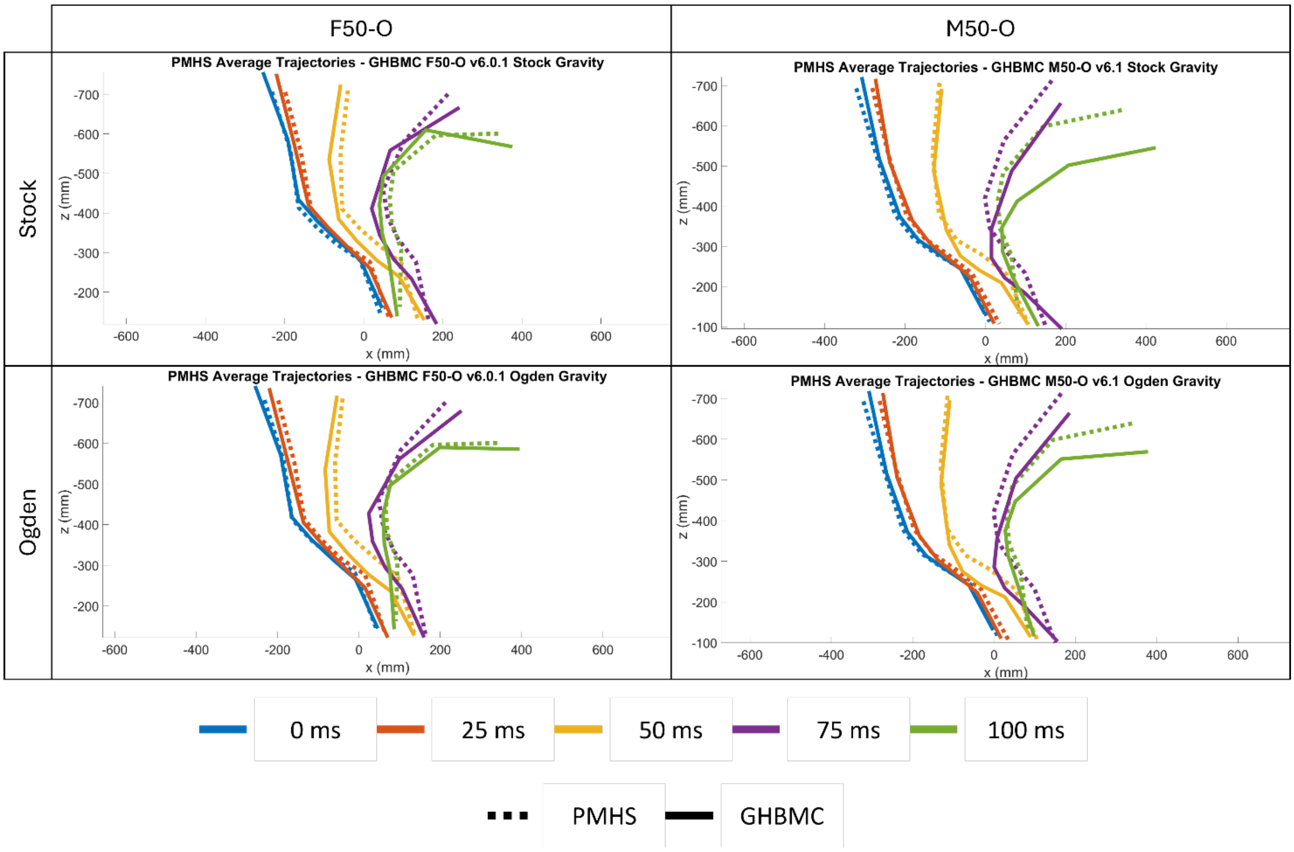

Fig. B1. Comparison of the average PMHS XZ trajectories of the head T1, T8, T11, L1, L3, and pelvis (PSIS) with XZ trajectories of the detailed HBMs following settling with the gravity method.

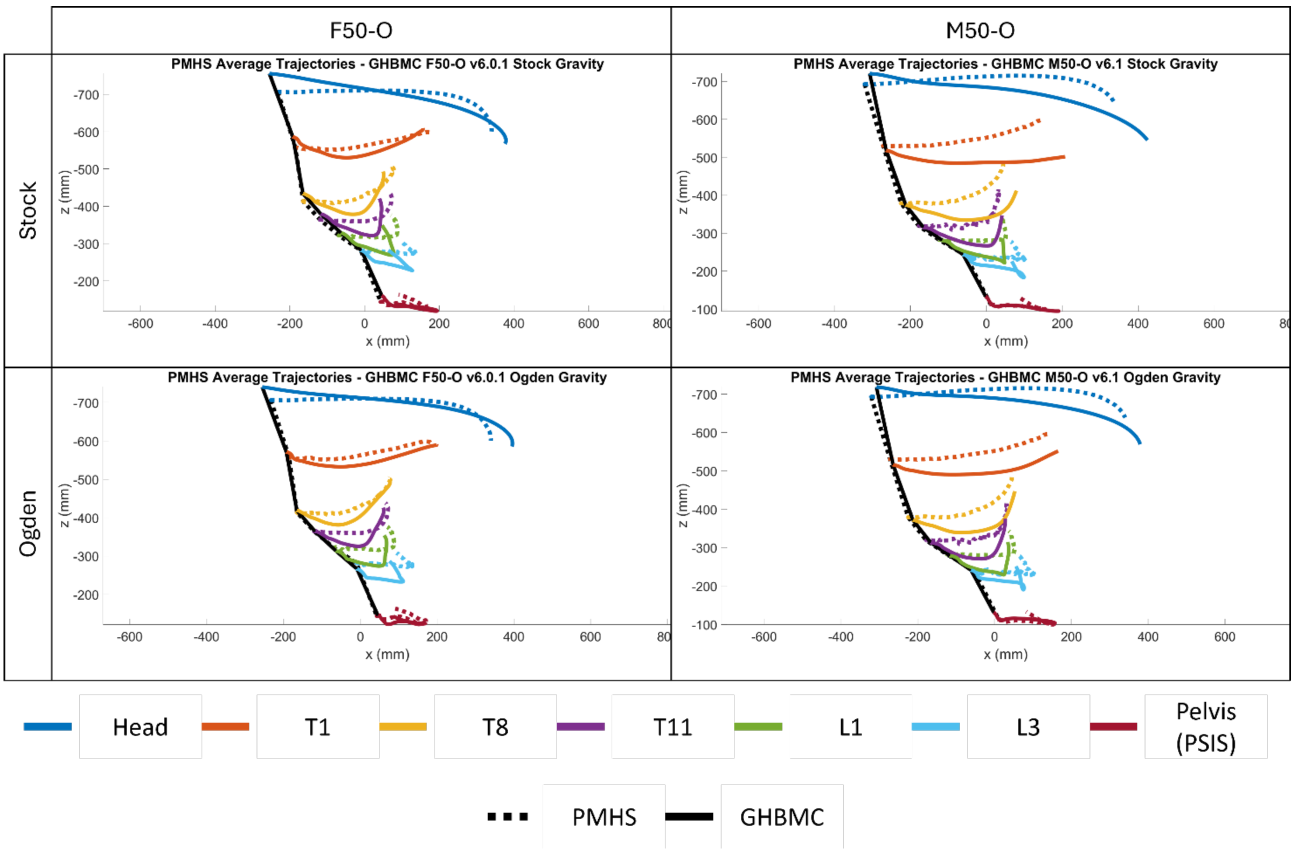

Fig. B2. Comparison of the average PMHS intersegmental XZ trajectories of the head T1, T8, T11, L1, L3, and pelvis (PSIS) with XZ trajectories of the detailed HBMs following settling with the gravity method.

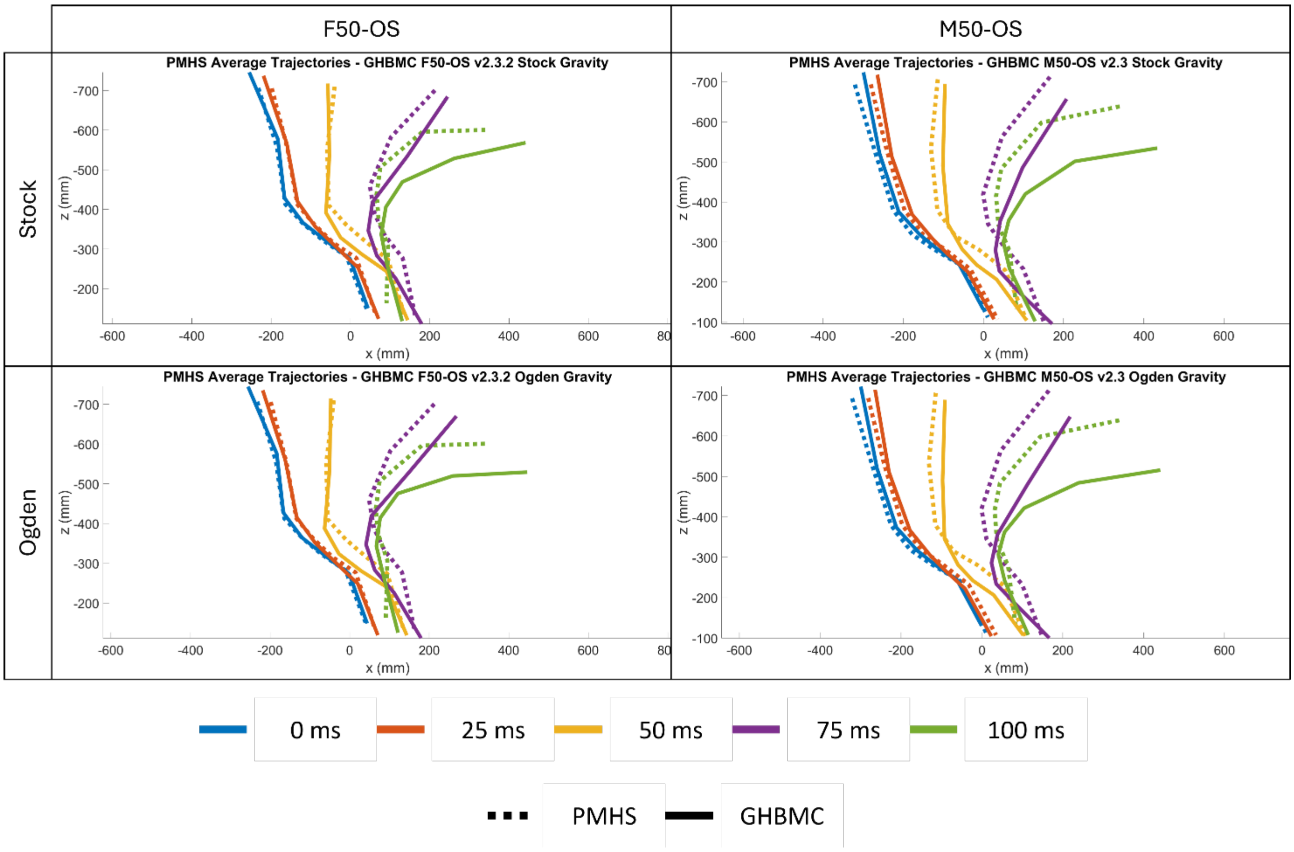

Fig. B3. Comparison of the average PMHS XZ trajectories of the head T1, T8, T11, L1, L3, and pelvis (PSIS) with XZ trajectories of the simplified HBMs following settling with the gravity method.

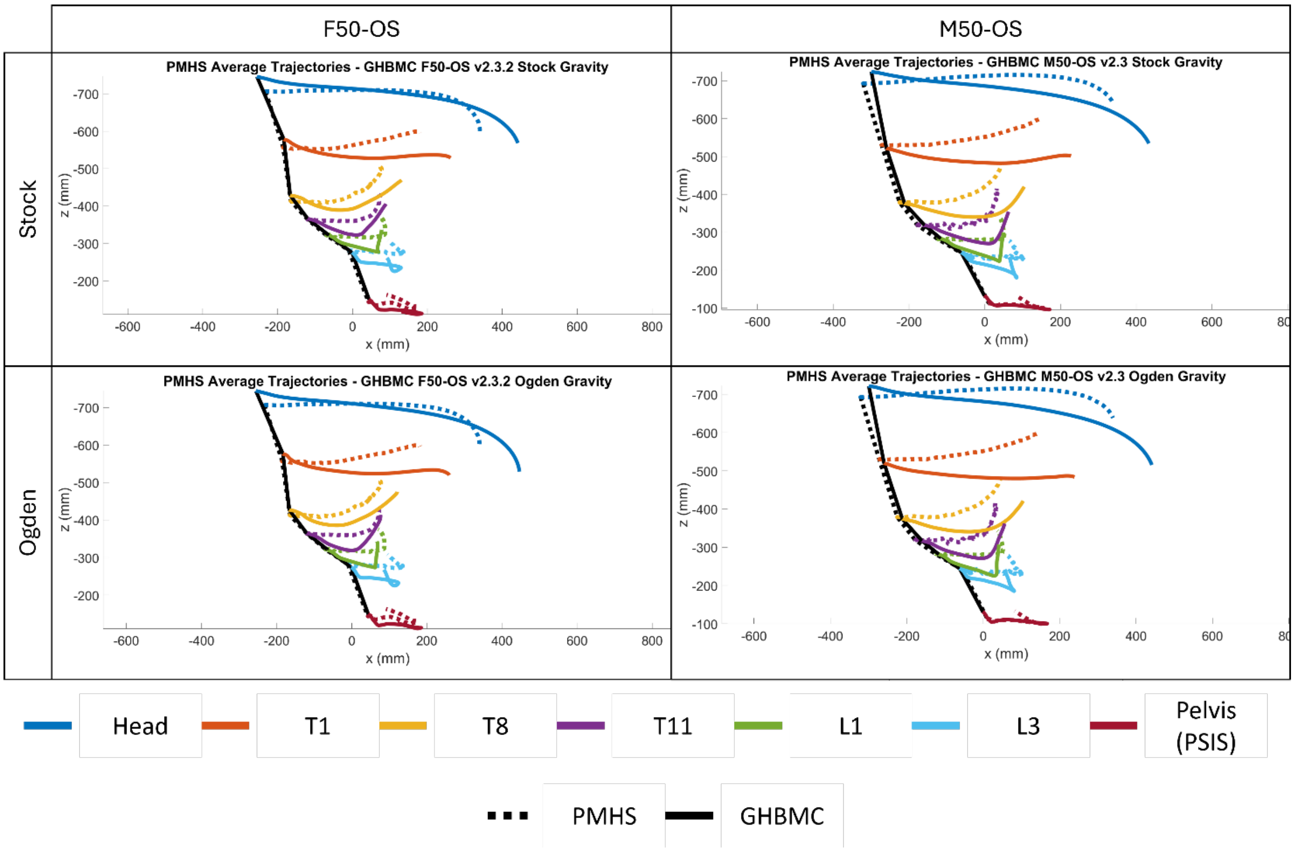

Fig. B4. Comparison of the average PMHS intersegmental XZ trajectories of the head T1, T8, T11, L1, L3, and pelvis (PSIS) with XZ trajectories of the simplified HBMs following settling with the gravity method.

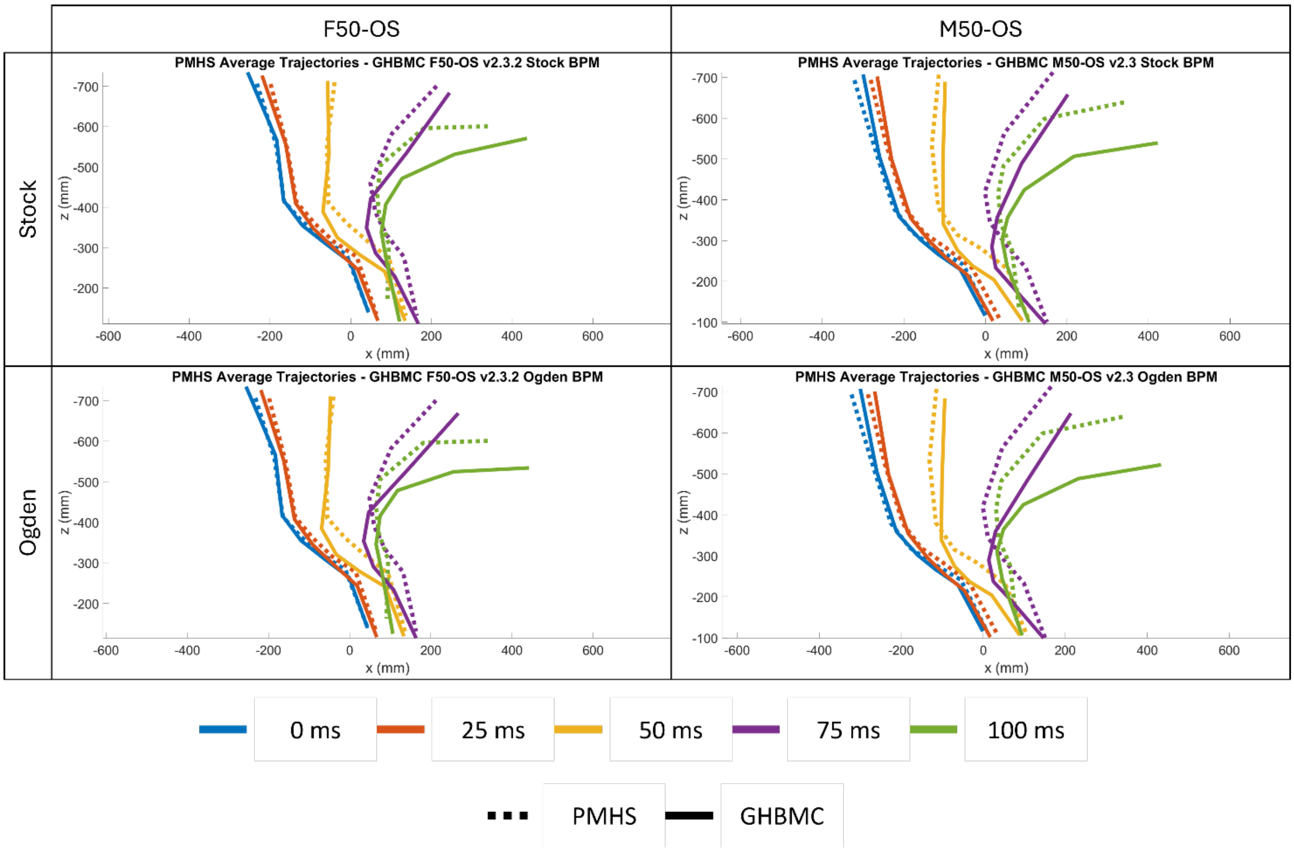

Fig. B5. Comparison of the average PMHS XZ trajectories of the head T1, T8, T11, L1, L3, and pelvis (PSIS) with XZ trajectories of the simplified HBMs following settling with the BPM method.

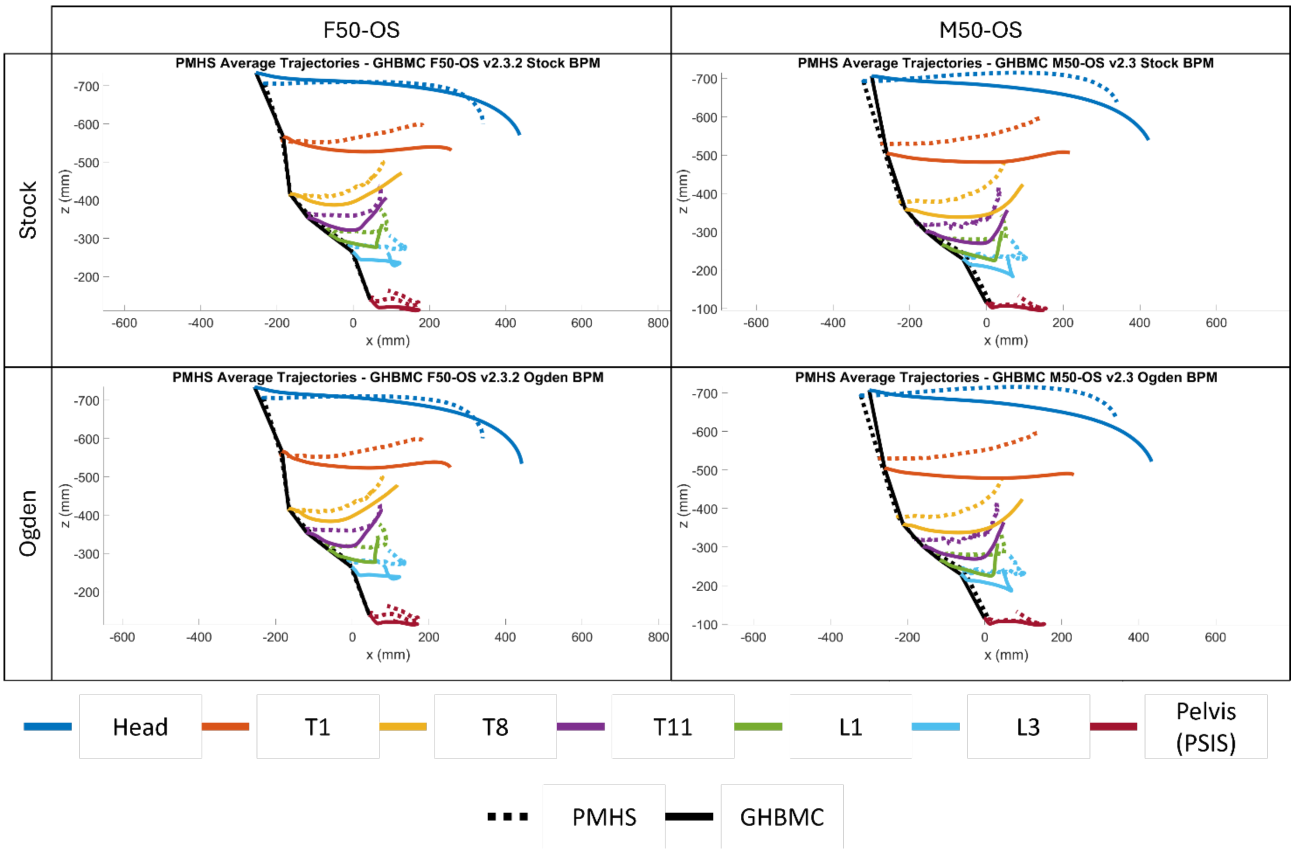

Fig. B6. Comparison of the average PMHS intersegmental XZ trajectories of the head T1, T8, T11, L1, L3, and pelvis (PSIS) with XZ trajectories of the simplified HBMs following settling with the BPM method.

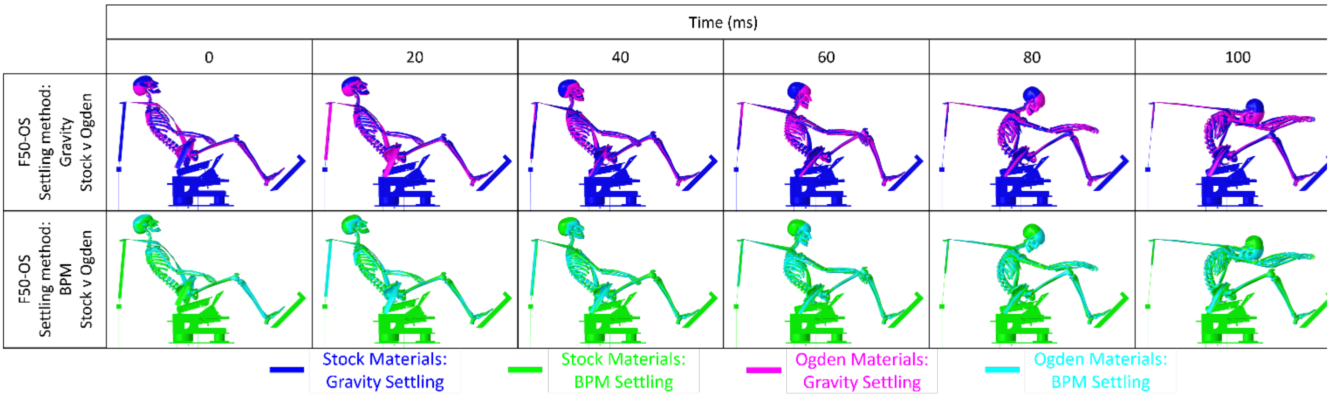

Fig. B7. Comparison of F50-OS kinematics when using stock vs. Ogden soft tissue materials for both settling methods.

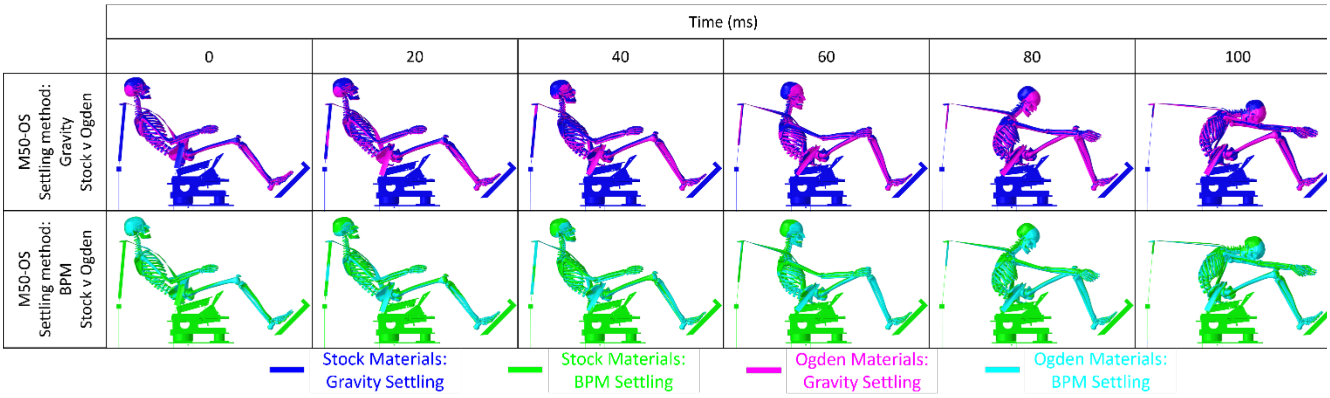

Fig. B8. Comparison of M50-OS kinematics when using stock vs. Ogden soft tissue materials for both settling methods.

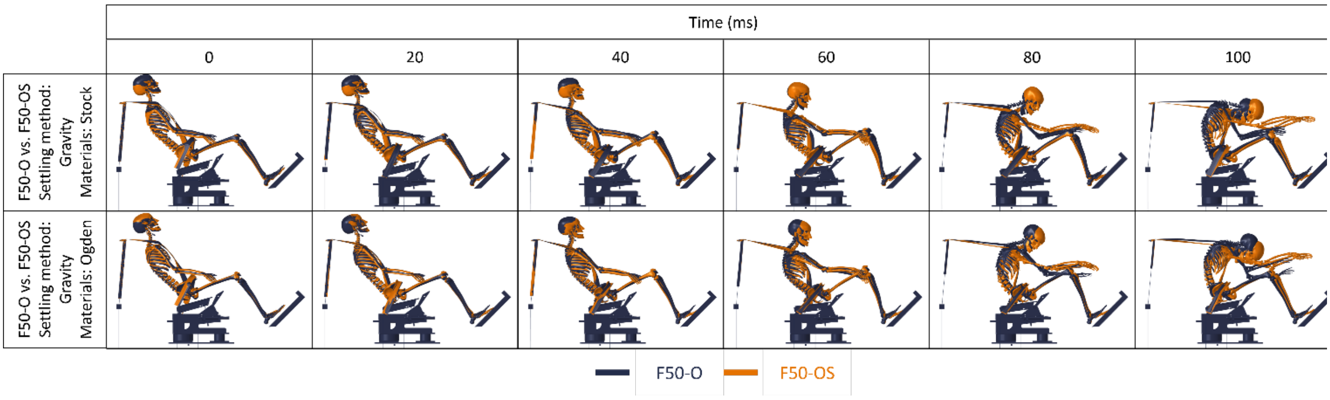

Fig. B9. Comparison of F50-O and F50-OS kinematics when using the gravity settling methods for both stock and Ogden soft tissue materials.

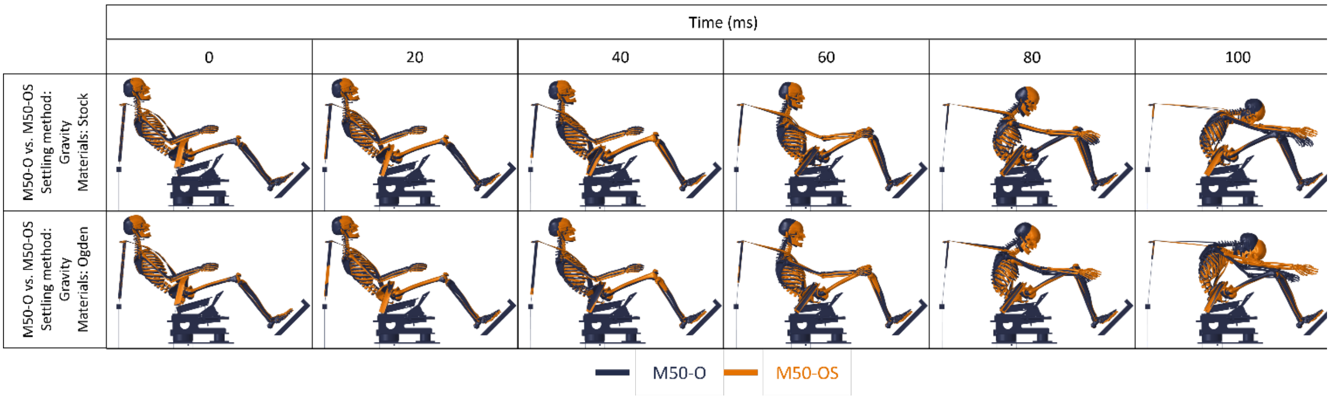

Fig. B10. Comparison of M50-O and M50-OS kinematics when using the gravity settling methods for both stock and Ogden soft tissue materials.

Appendix C – Time History Plots

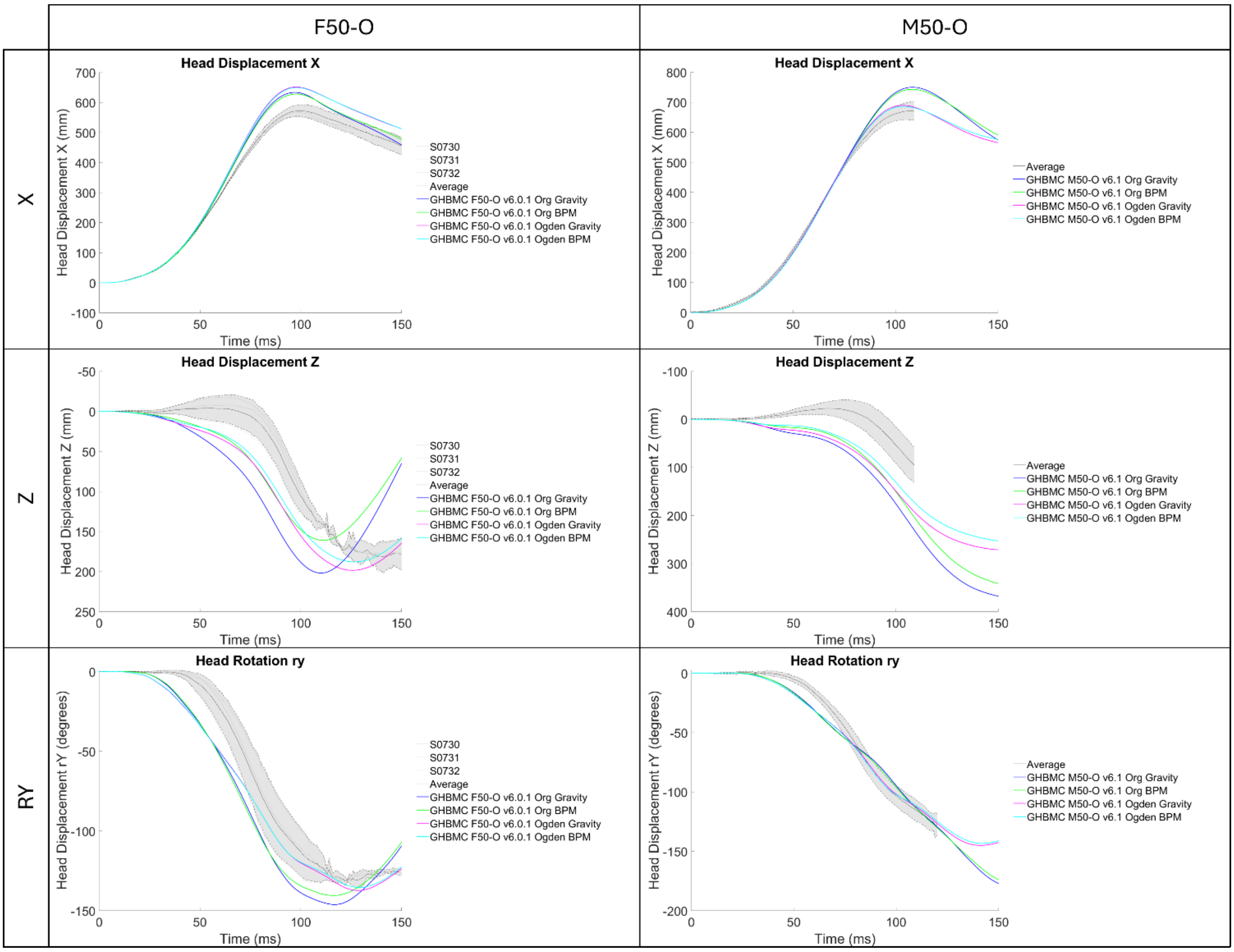

Fig. C1. Comparison of the average PMHS X, Z, RY time histories of the head with X, Z, RY time histories of the head for the detailed HBMs.

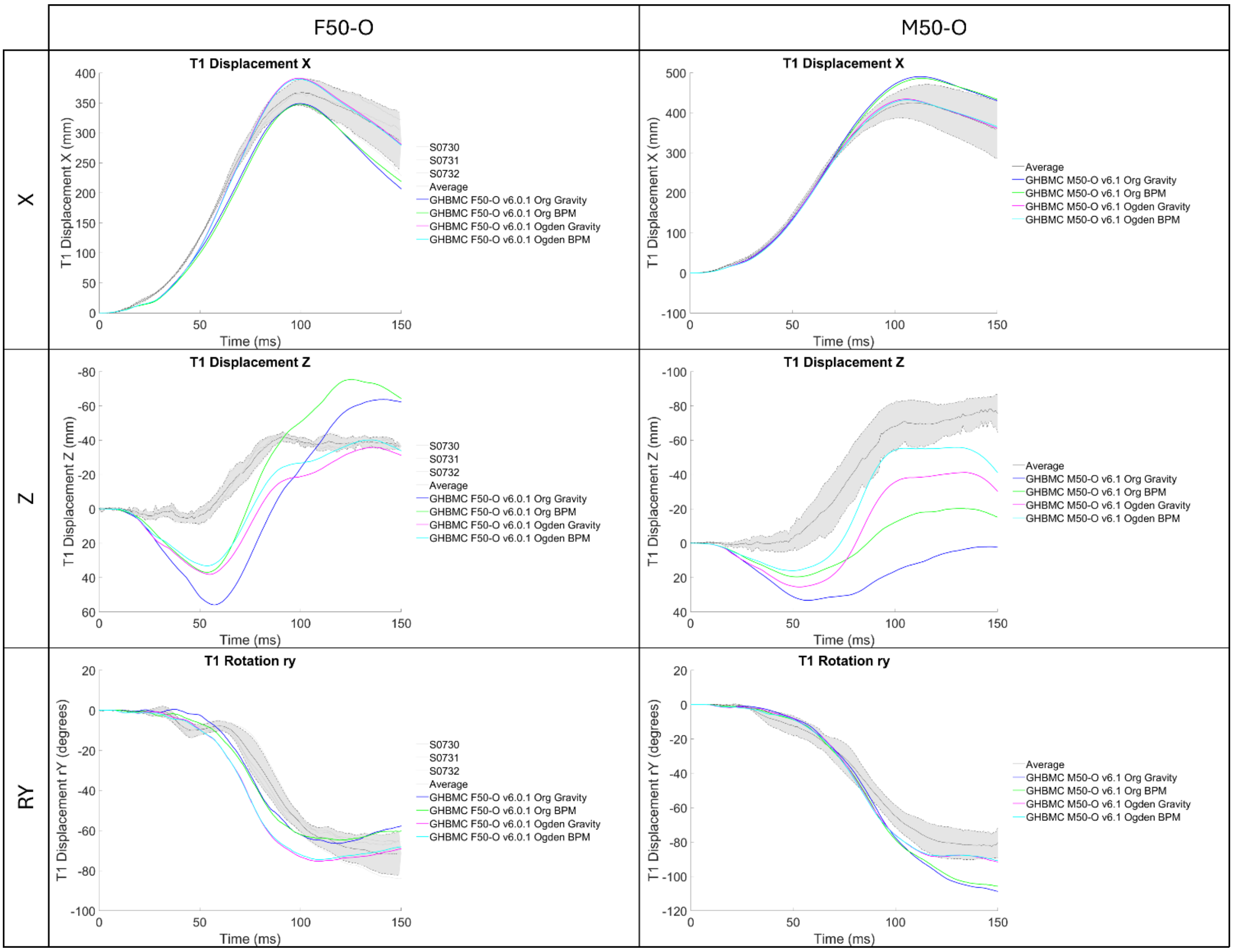

Fig. C2. Comparison of the average PMHS X, Z, RY time histories of T1 with X, Z, RY time histories of T1 for the detailed HBMs.

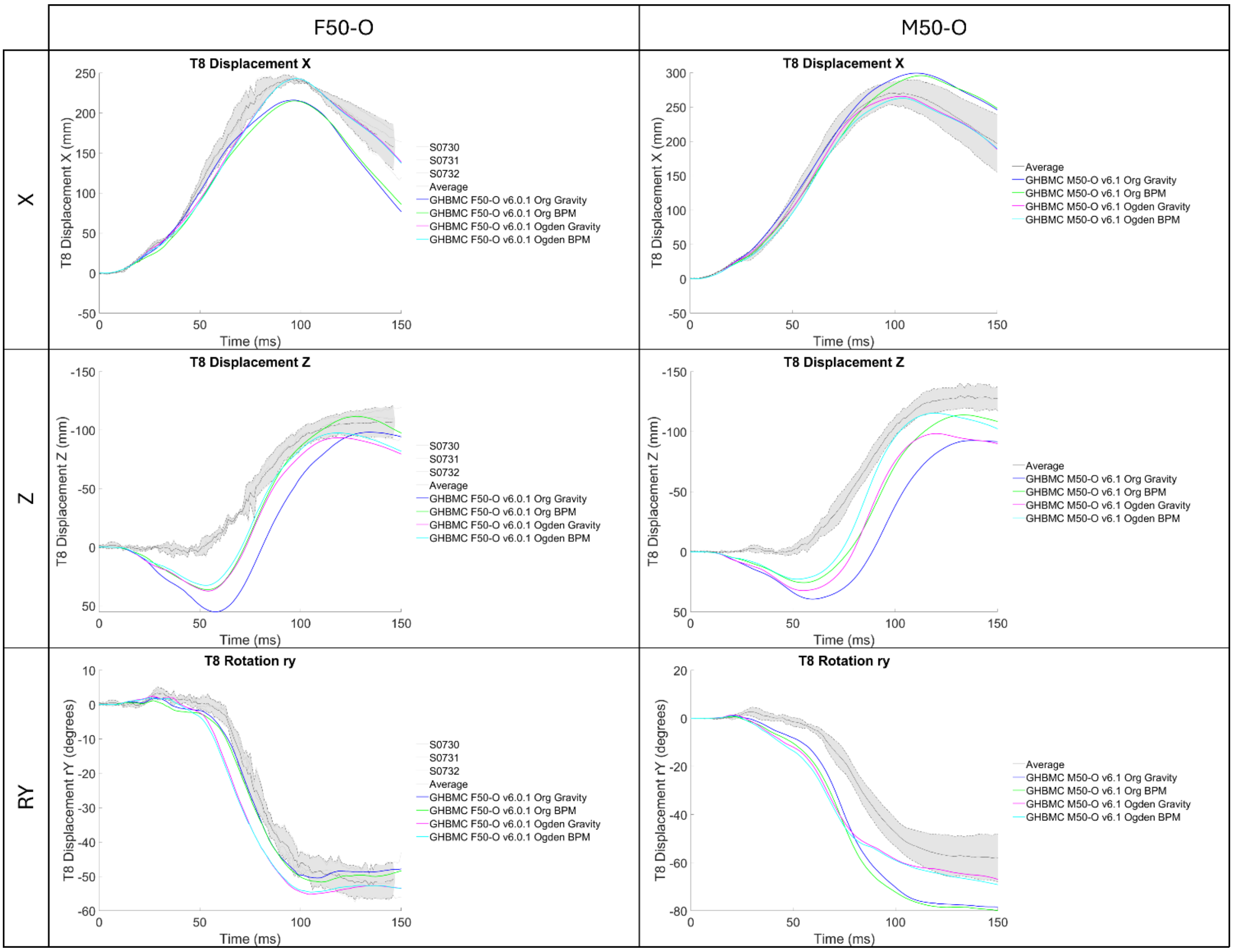

Fig. C3. Comparison of the average PMHS X, Z, RY time histories of T8 with X, Z, RY time histories of T8 for the detailed HBMs.

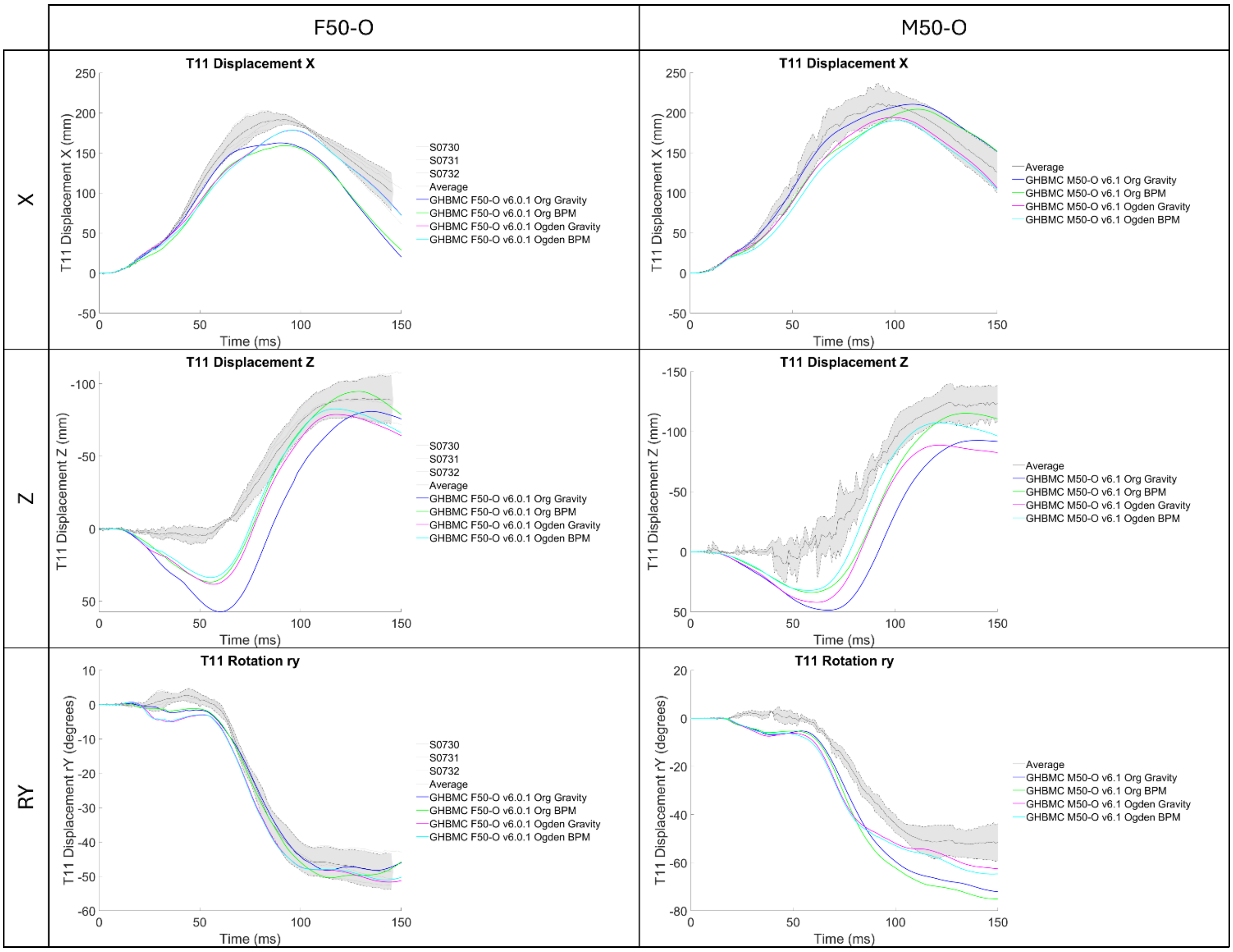

Fig. C4. Comparison of the average PMHS X, Z, RY time histories of T11 with X, Z, RY time histories of T11 for the detailed HBMs.

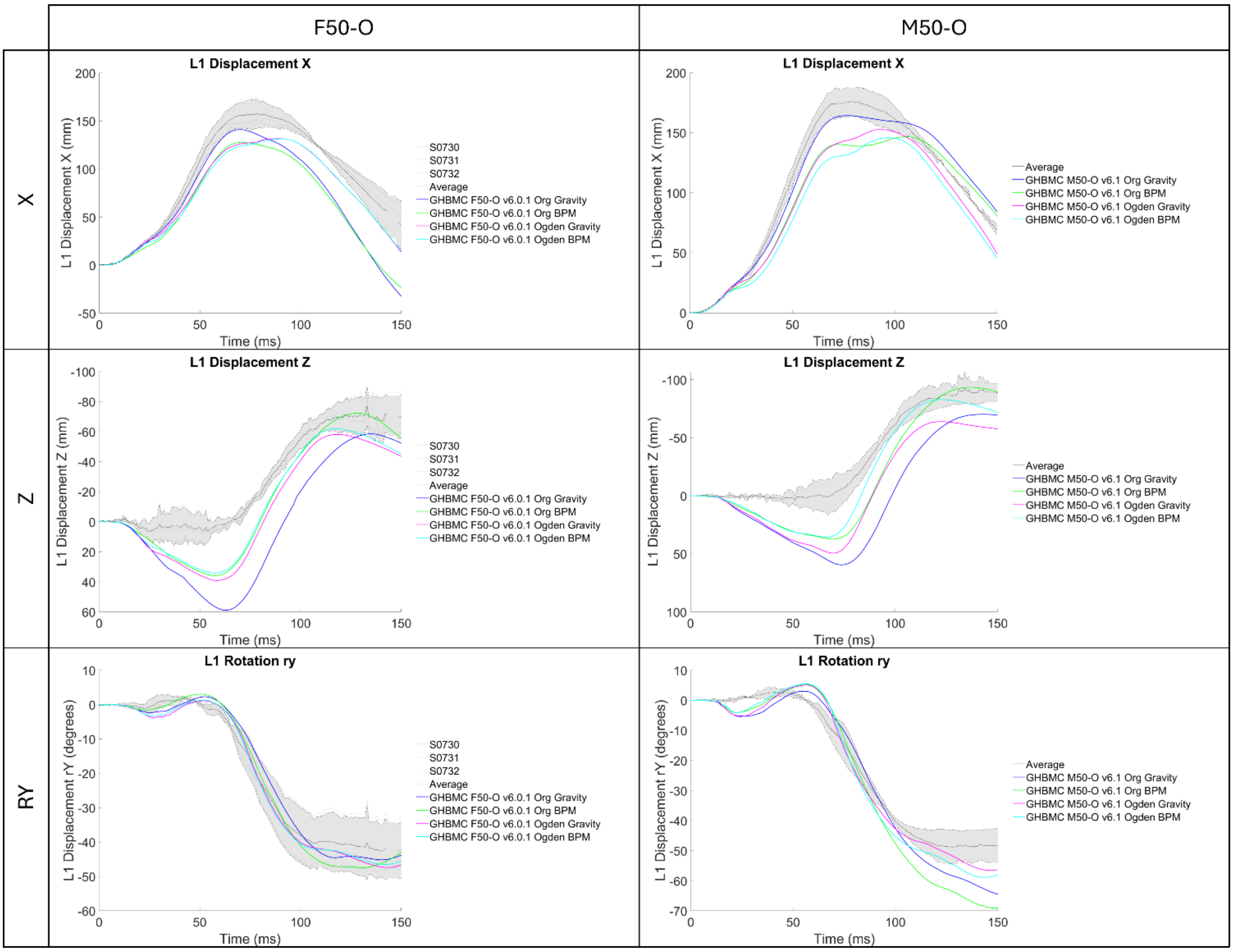

Fig. C5. Comparison of the average PMHS X, Z, RY time histories of L1 with X, Z, RY time histories of L1 for the detailed HBMs.

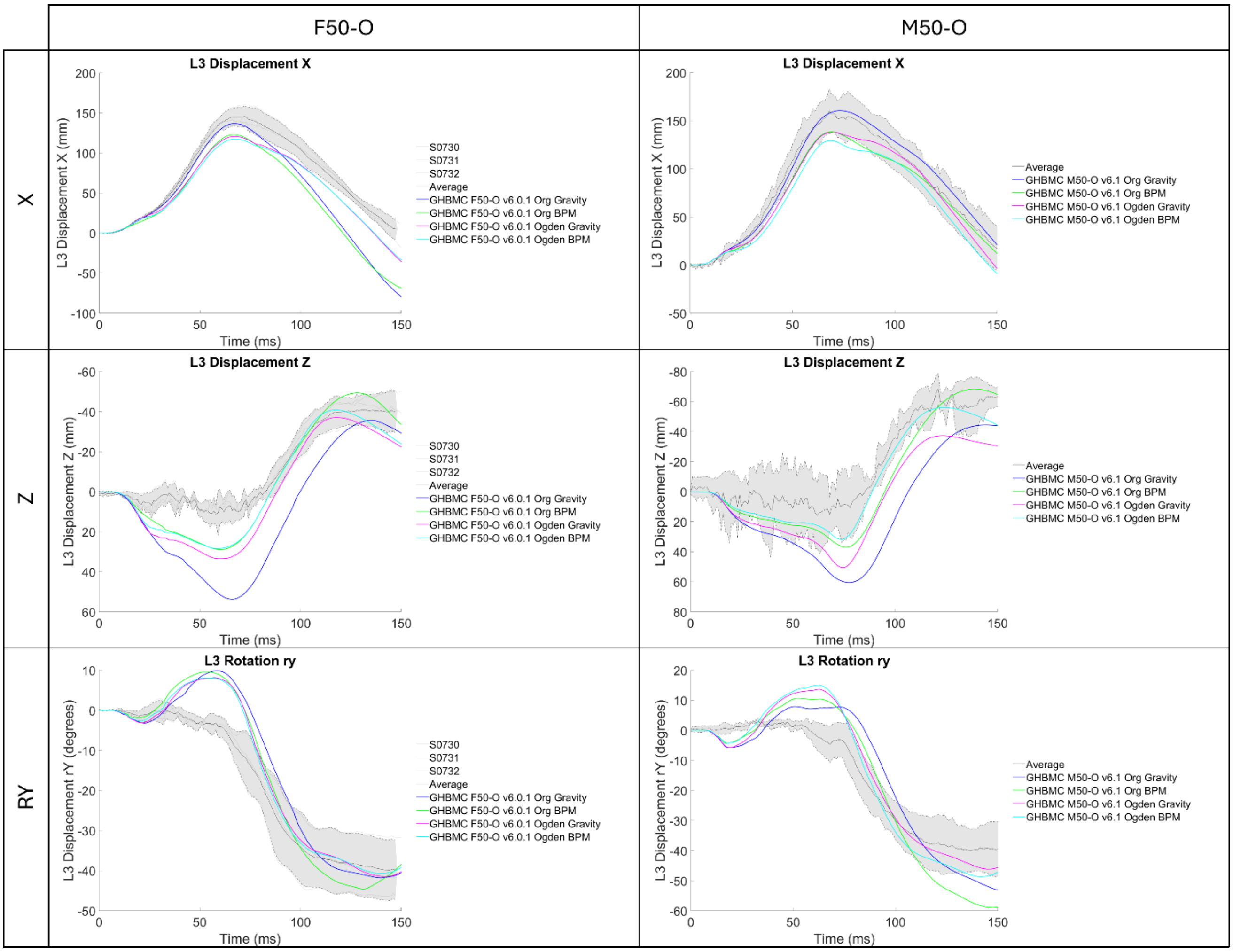

Fig. C6. Comparison of the average PMHS X, Z, RY time histories of L3 with X, Z, RY time histories of L3 for the detailed HBMs.

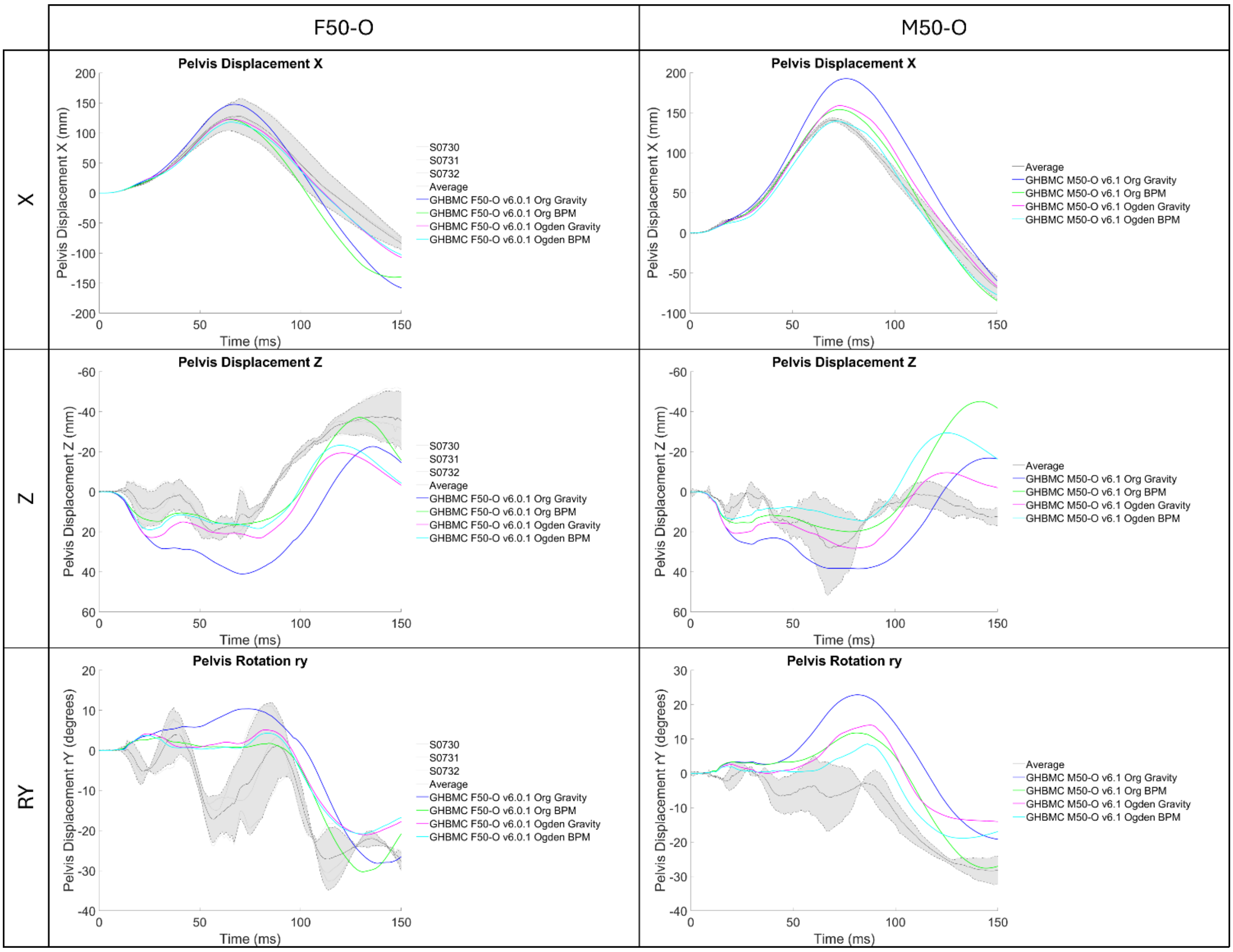

Fig. C7. Comparison of the average PMHS X, Z, RY time histories of the pelvis with X, Z, RY time histories of the pelvis for the detailed HBMs.

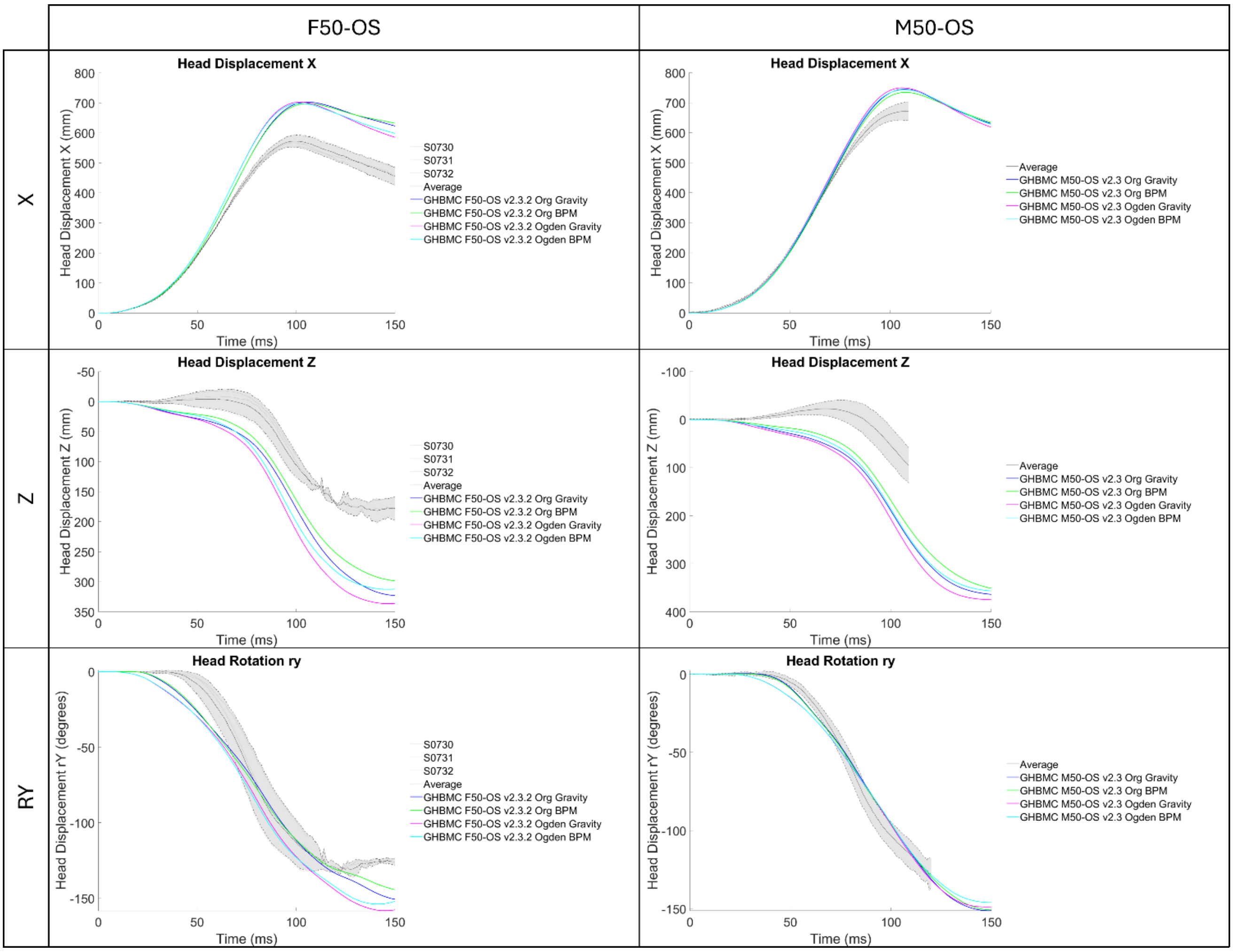

Fig. C8. Comparison of the average PMHS X, Z, RY time histories of the head with X, Z, RY time histories of the head for the simplified HBMs.

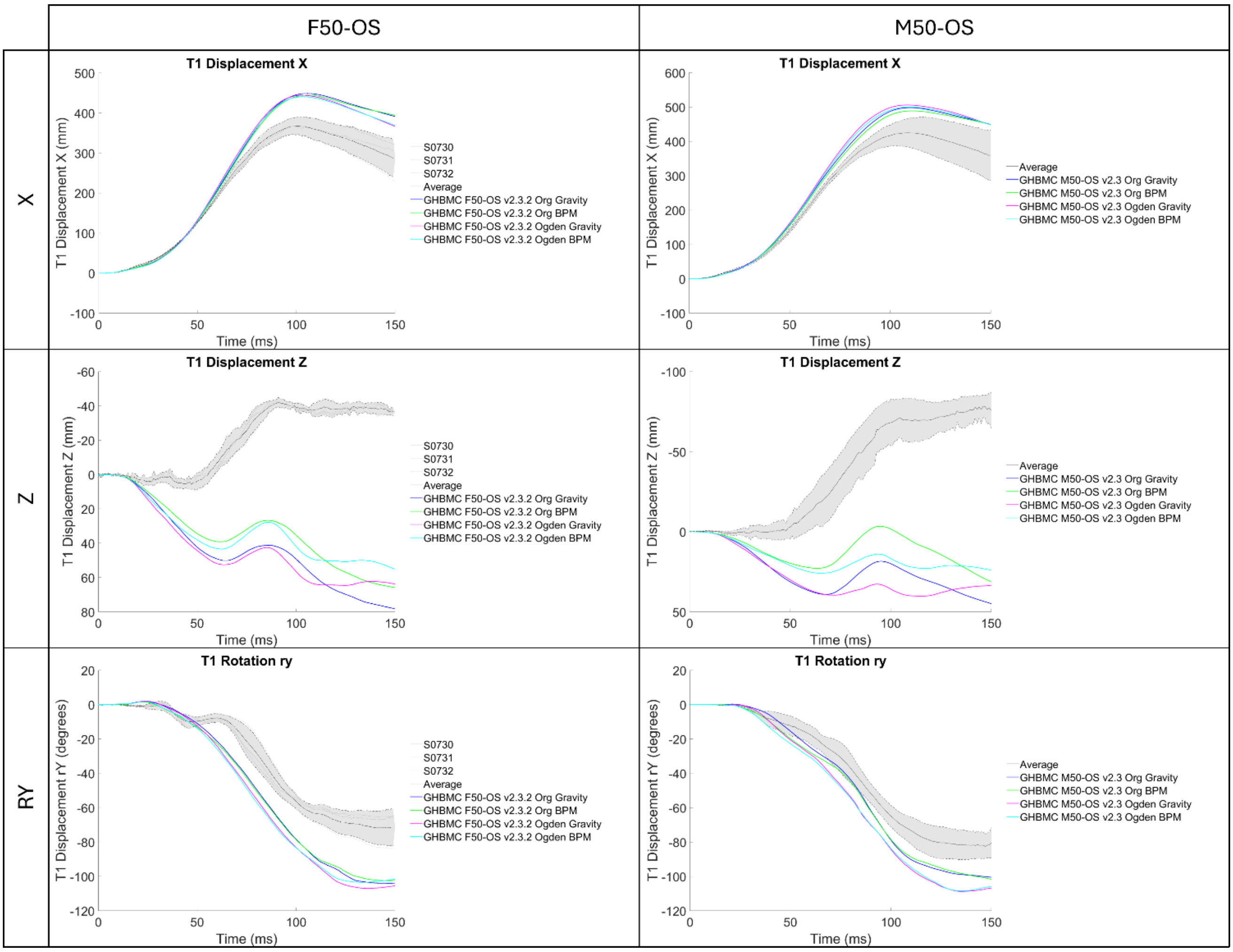

Fig. C9. Comparison of the average PMHS X, Z, RY time histories of T1 with X, Z, RY time histories of T1 for the simplified HBMs.

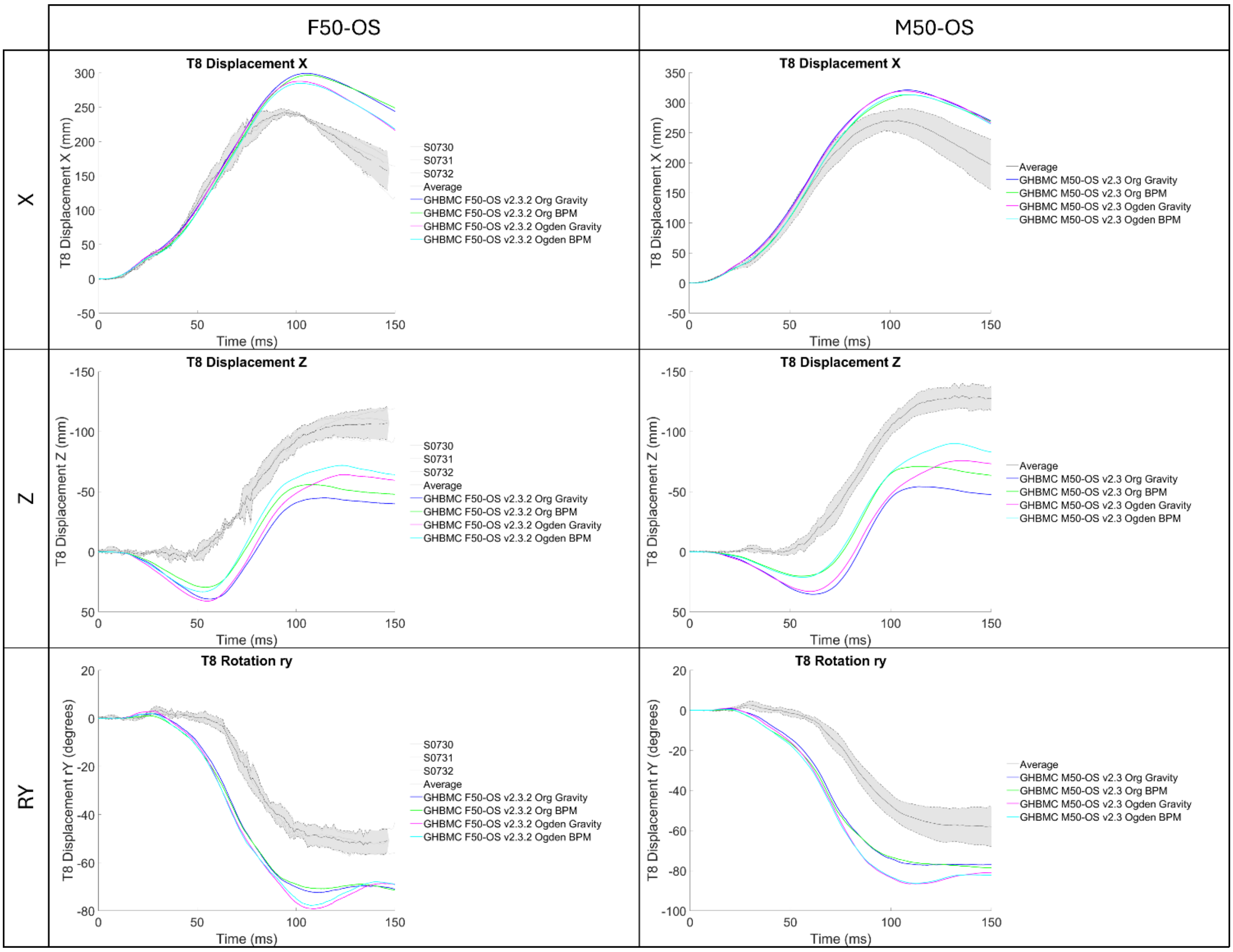

Fig. C10. Comparison of the average PMHS X, Z, RY time histories of T8 with X, Z, RY time histories of T8 for the simplified HBMs.

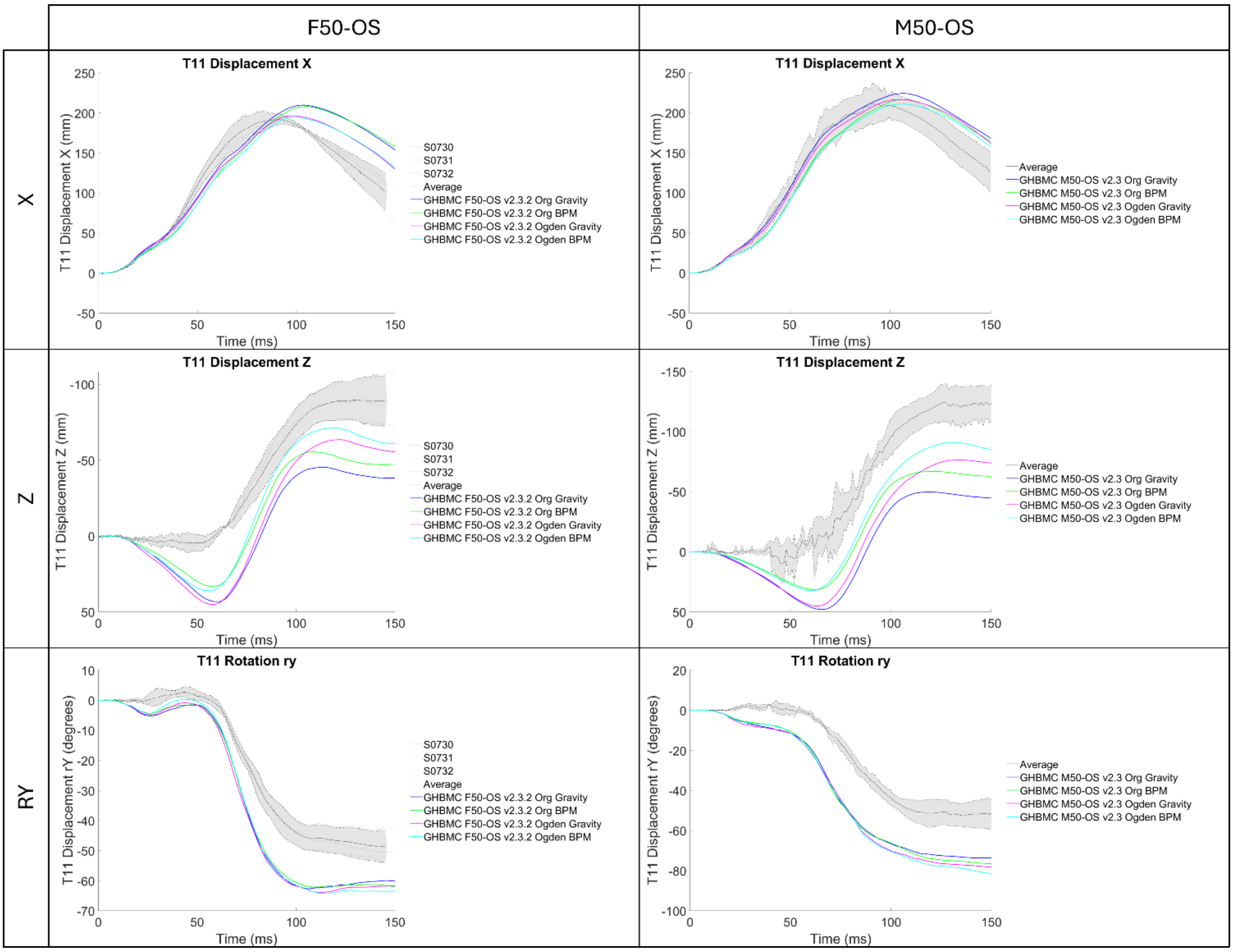

Fig. C11. Comparison of the average PMHS X, Z, RY time histories of T11 with X, Z, RY time histories of T11 for the simplified HBMs.

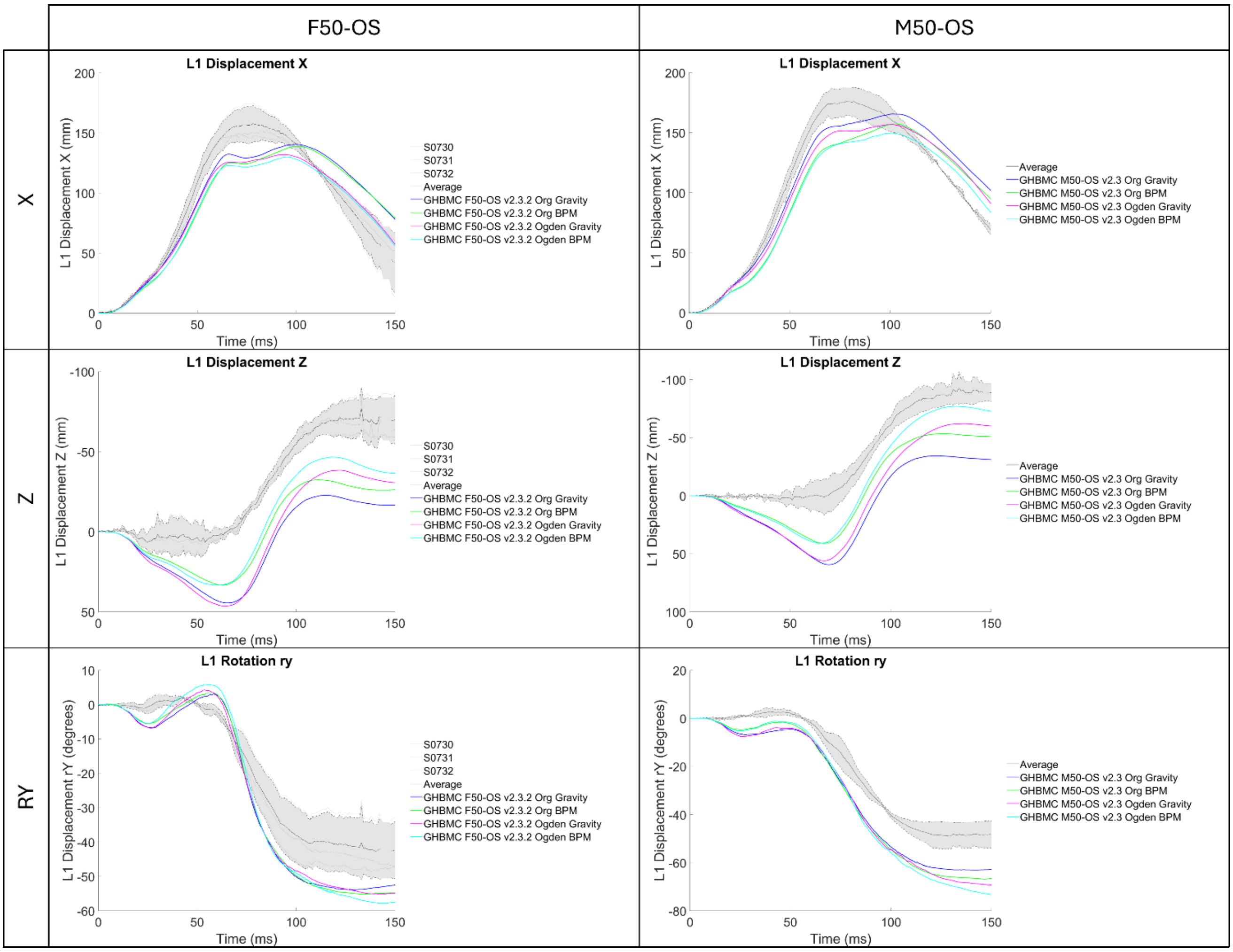

Fig. C12. Comparison of the average PMHS X, Z, RY time histories of L1 with X, Z, RY time histories of L1 for the simplified HBMs.

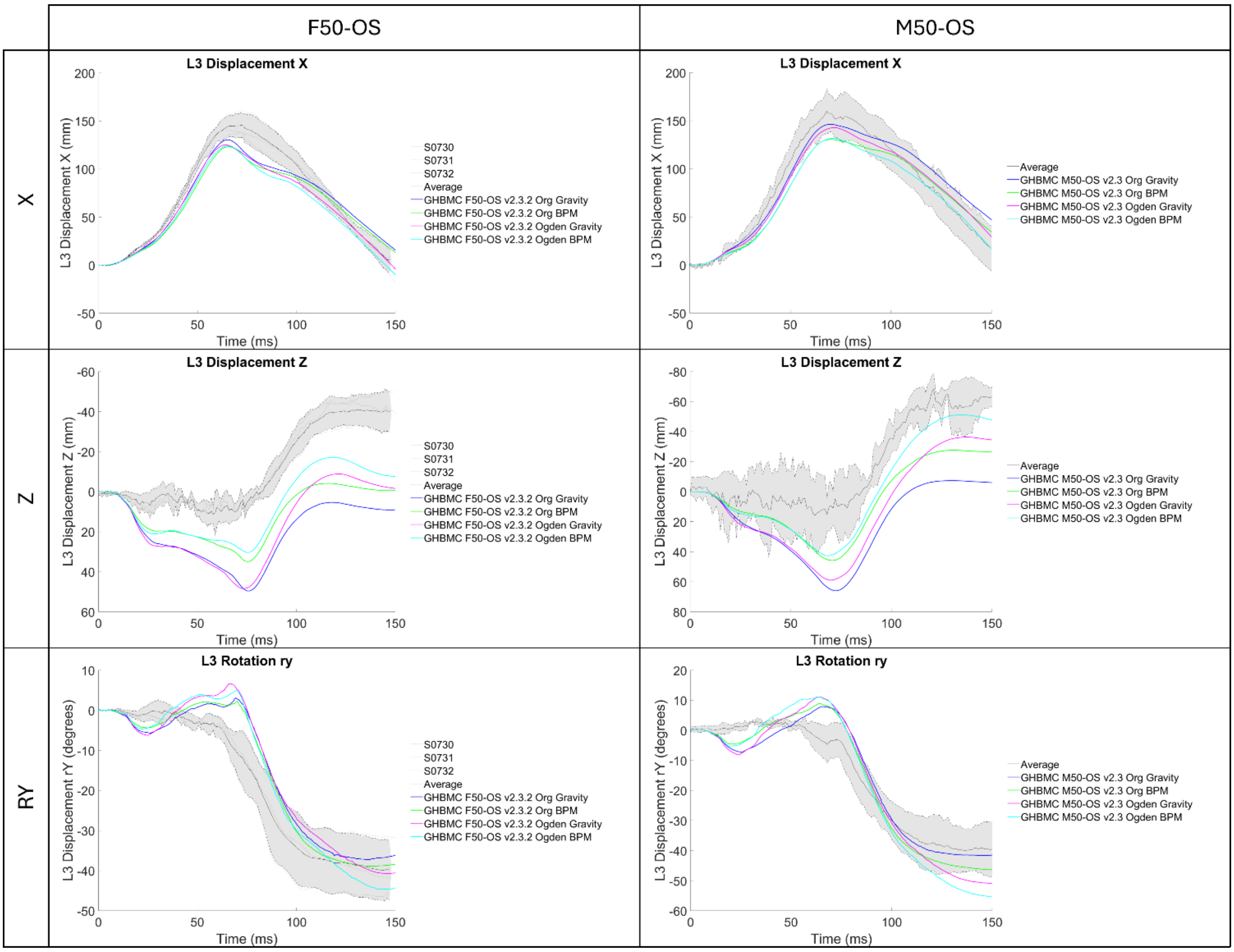

Fig. C13. Comparison of the average PMHS X, Z, RY time histories of L3 with X, Z, RY time histories of L3 for the simplified HBMs.

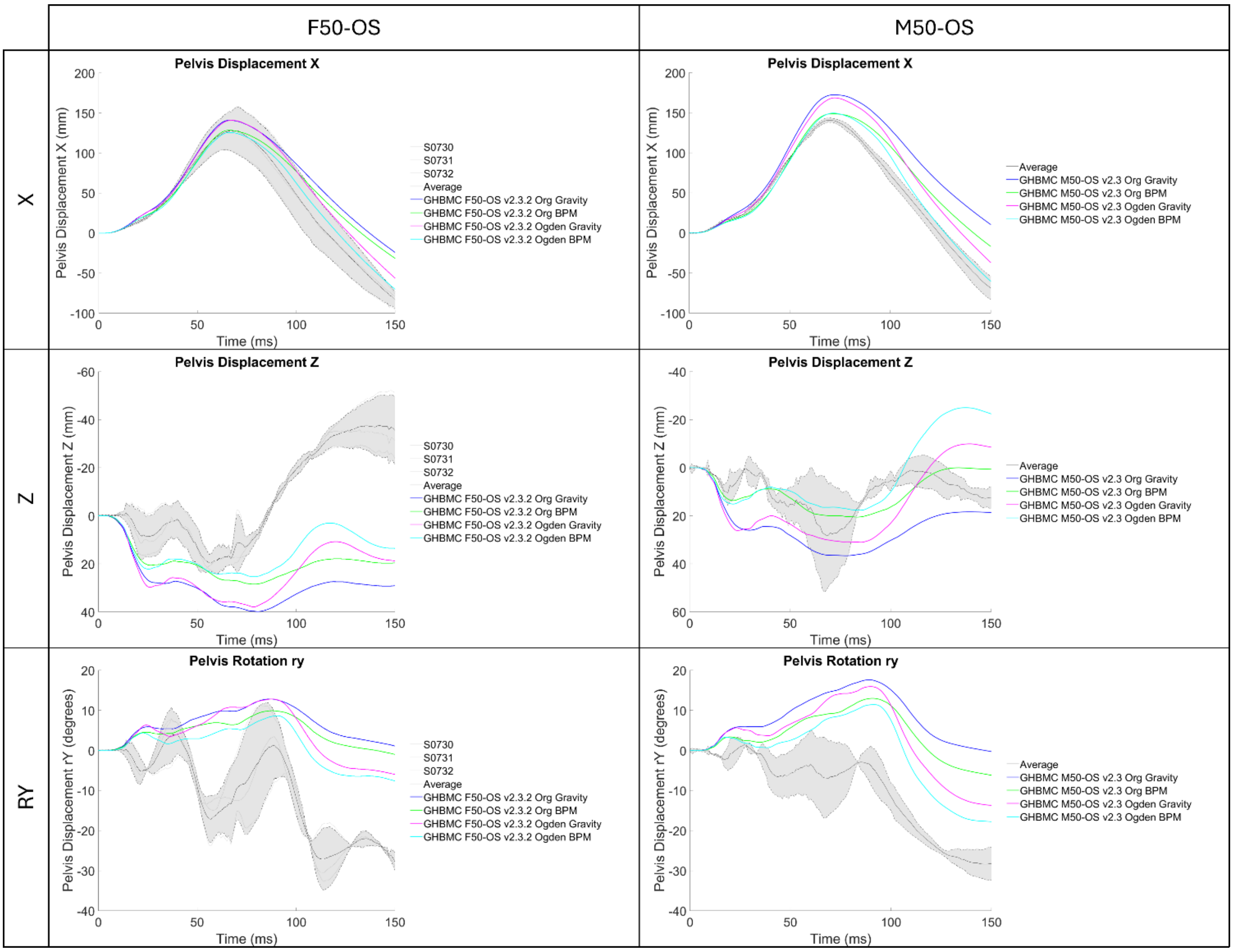

Fig. C14. Comparison of the average PMHS X, Z, RY time histories of the pelvis with X, Z, RY time histories of the pelvis for the simplified HBMs.

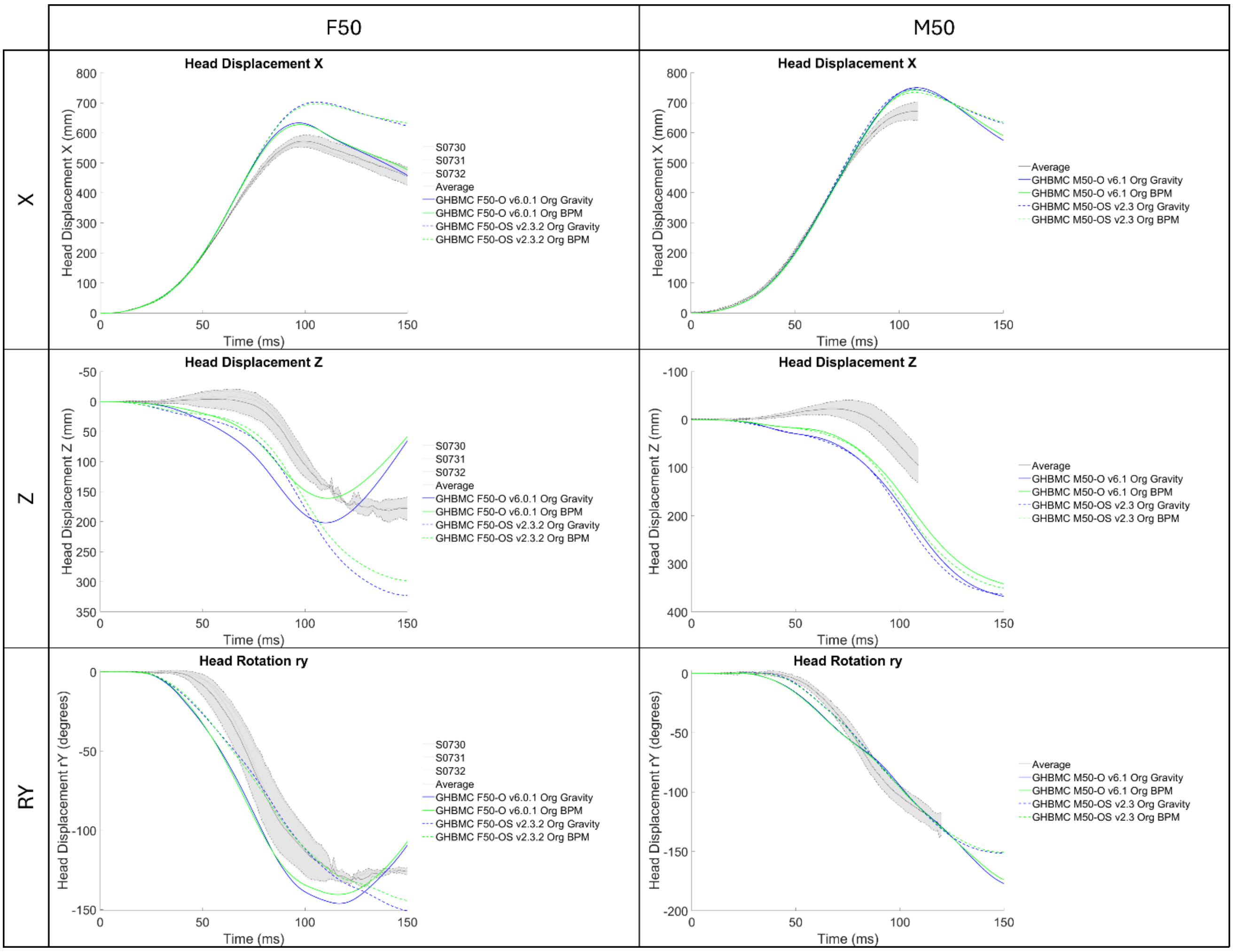

Fig. C15. Comparison of the average PMHS X, Z, RY time histories of the head with X, Z, RY time histories of the head for HBMs using stock soft tissue materials.

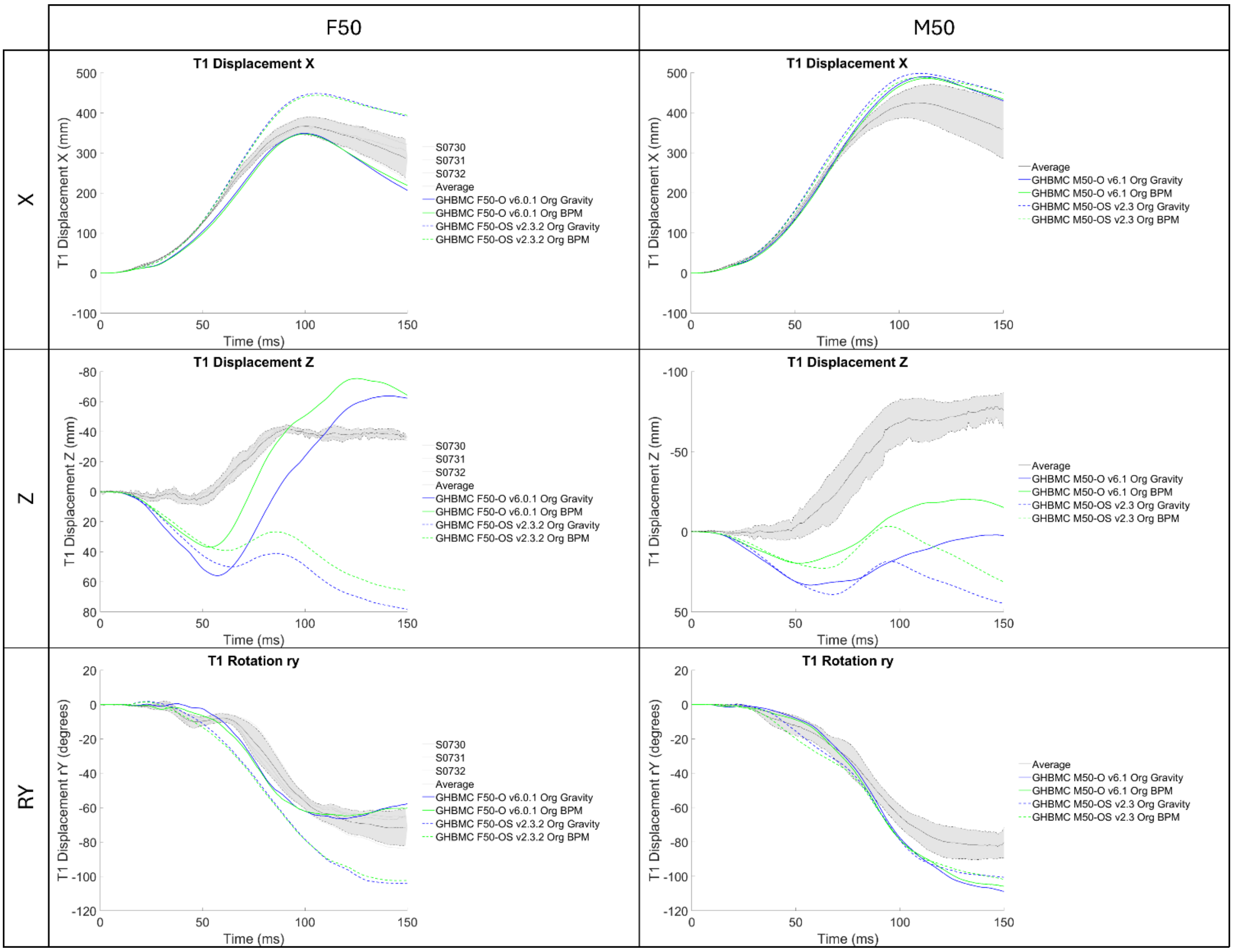

Fig. C16. Comparison of the average PMHS X, Z, RY time histories of T1 with X, Z, RY time histories of T1 for HBMs using stock soft tissue materials.

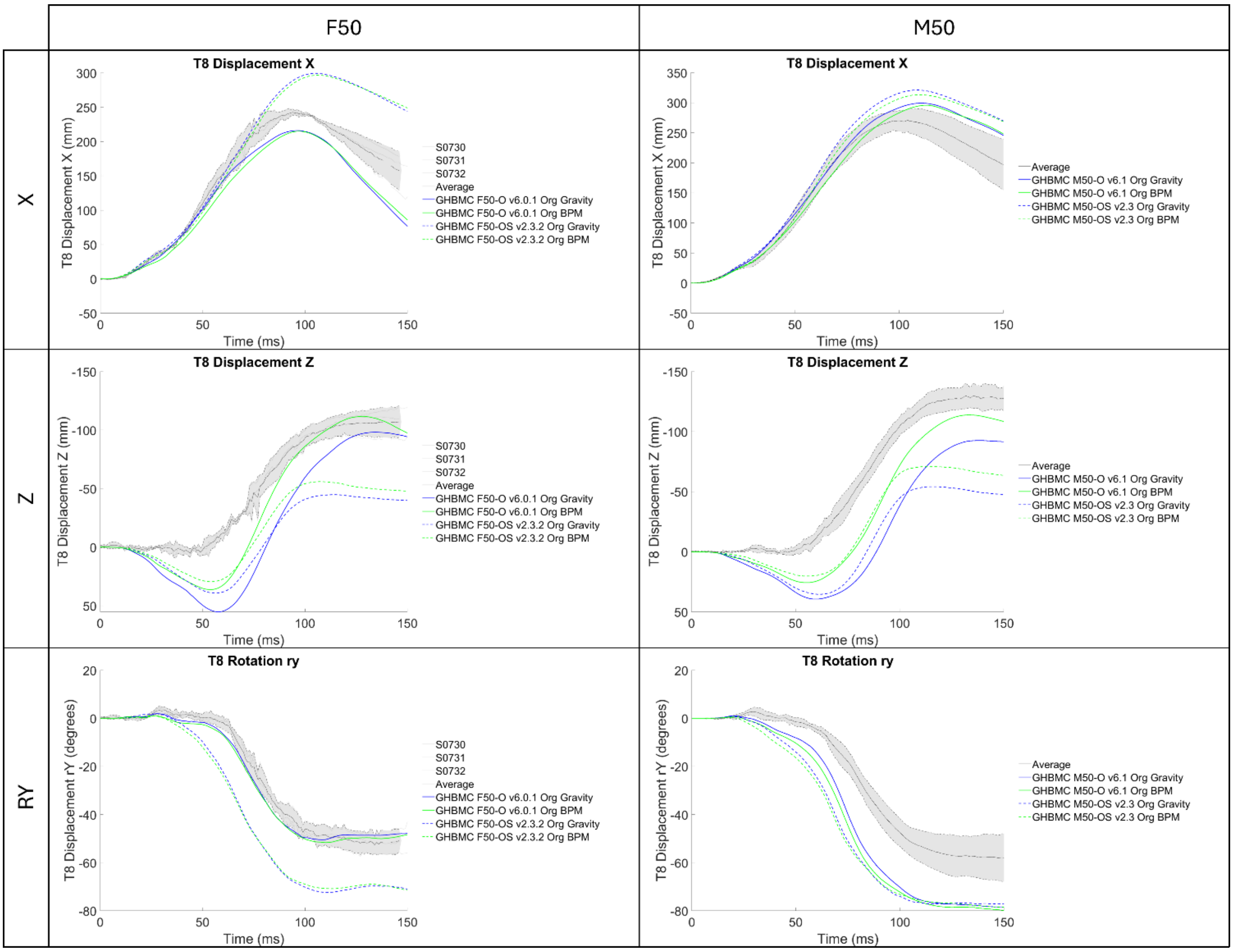

Fig. C17. Comparison of the average PMHS X, Z, RY time histories of T8 with X, Z, RY time histories of T8 for HBMs using stock soft tissue materials.

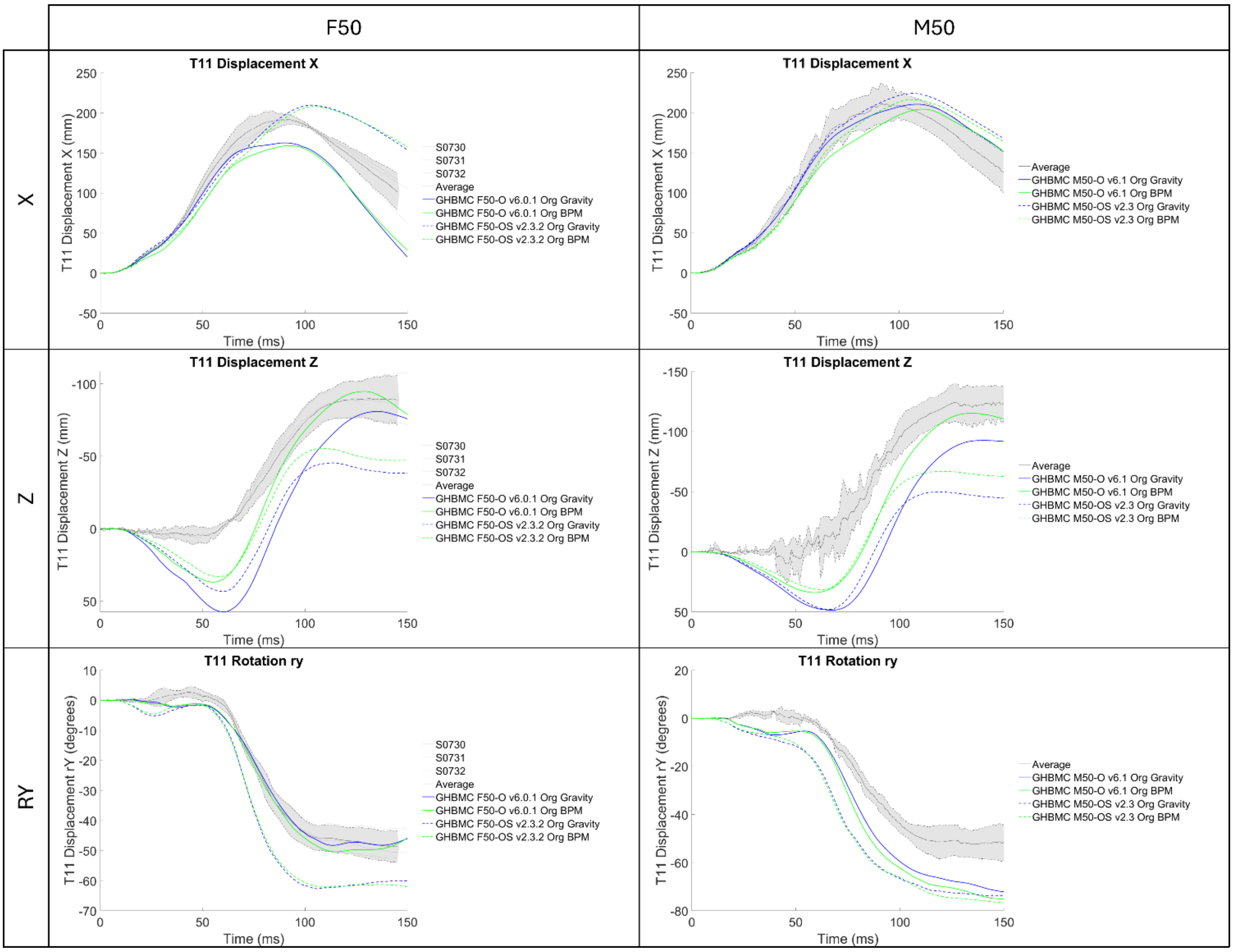

Fig. C18. Comparison of the average PMHS X, Z, RY time histories of T11 with X, Z, RY time histories of T11 for HBMs using stock soft tissue materials.

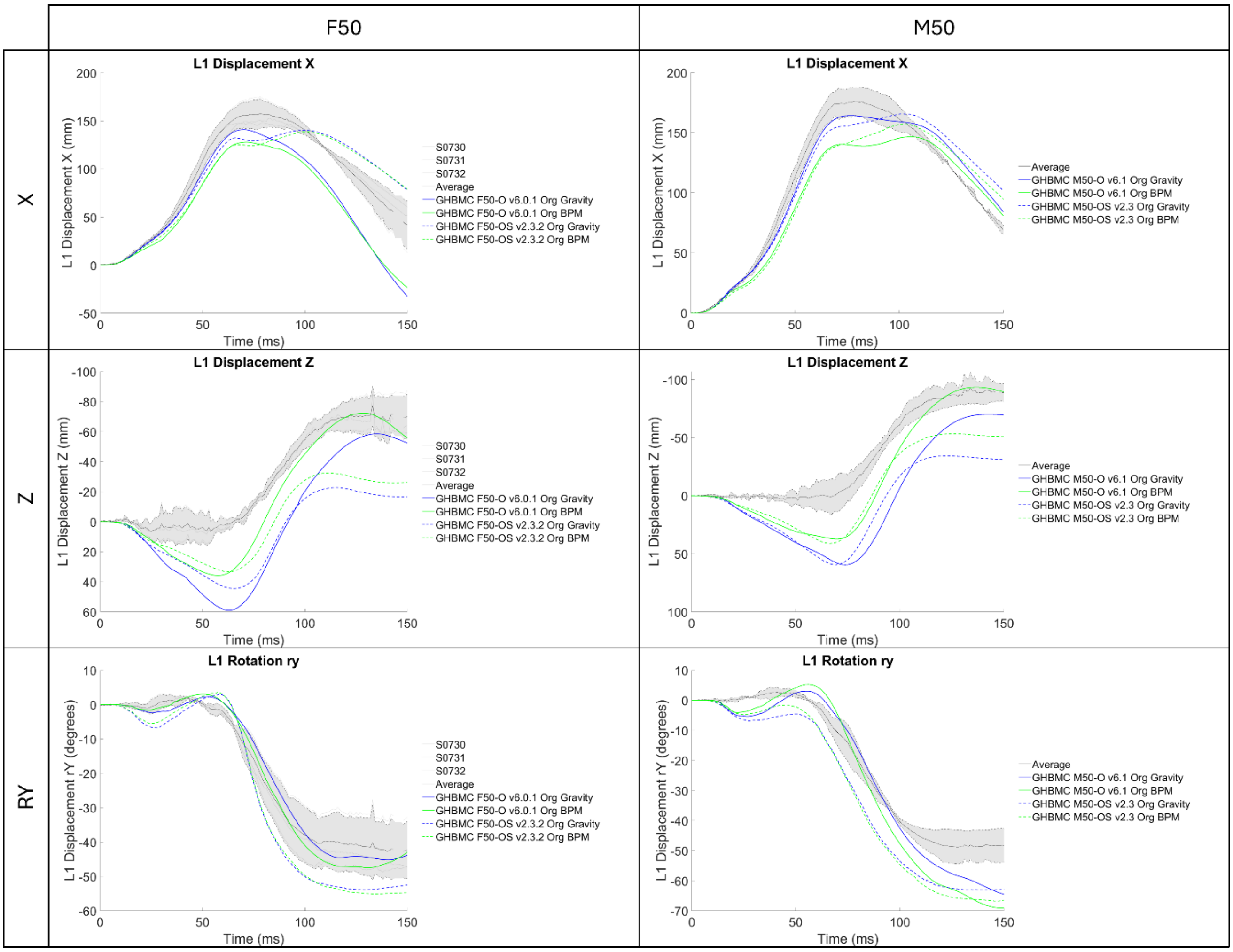

Fig. C19. Comparison of the average PMHS X, Z, RY time histories of L1 with X, Z, RY time histories of L1 for HBMs using stock soft tissue materials.

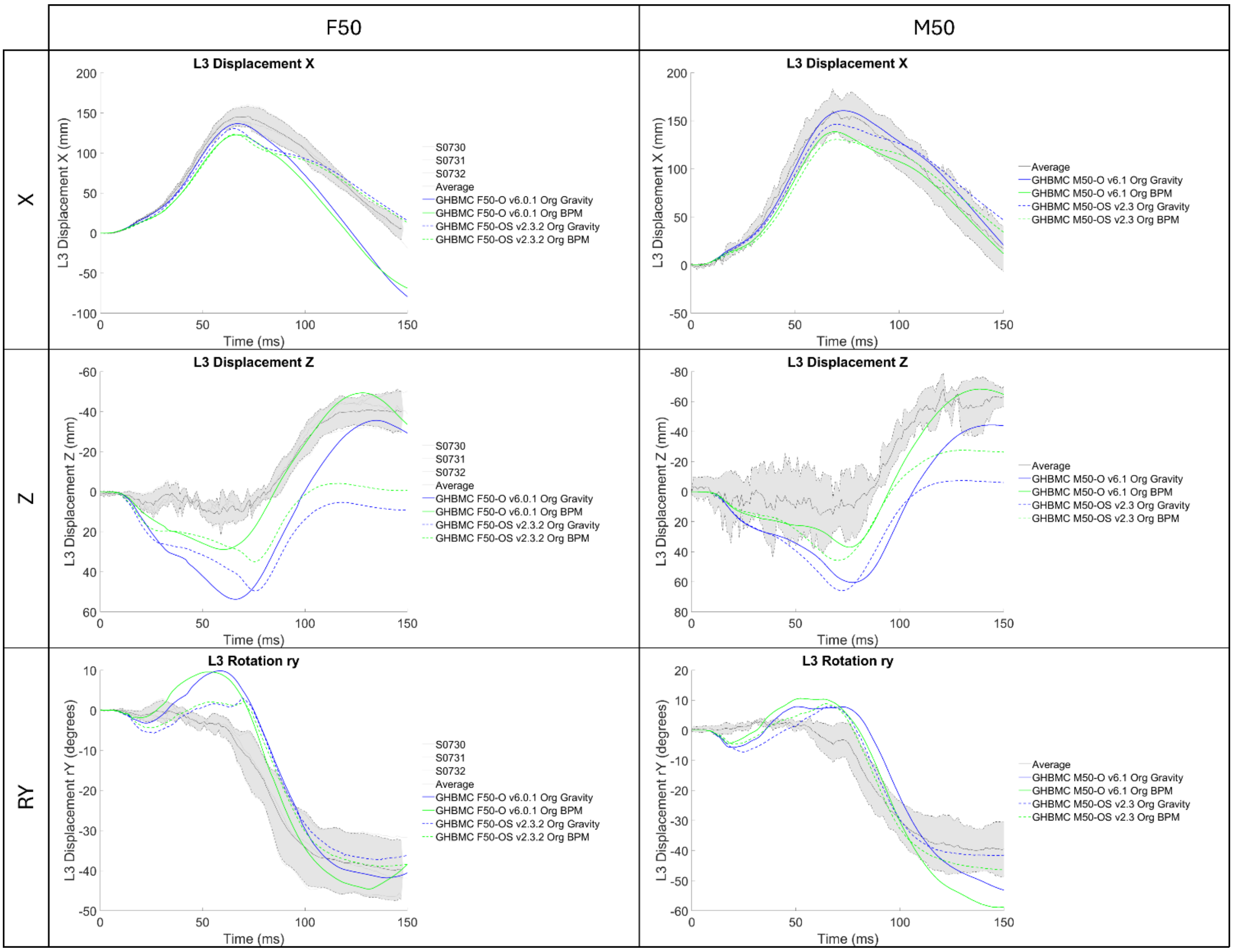

Fig. C20. Comparison of the average PMHS X, Z, RY time histories of L3 with X, Z, RY time histories of L3 for HBMs using stock soft tissue materials.

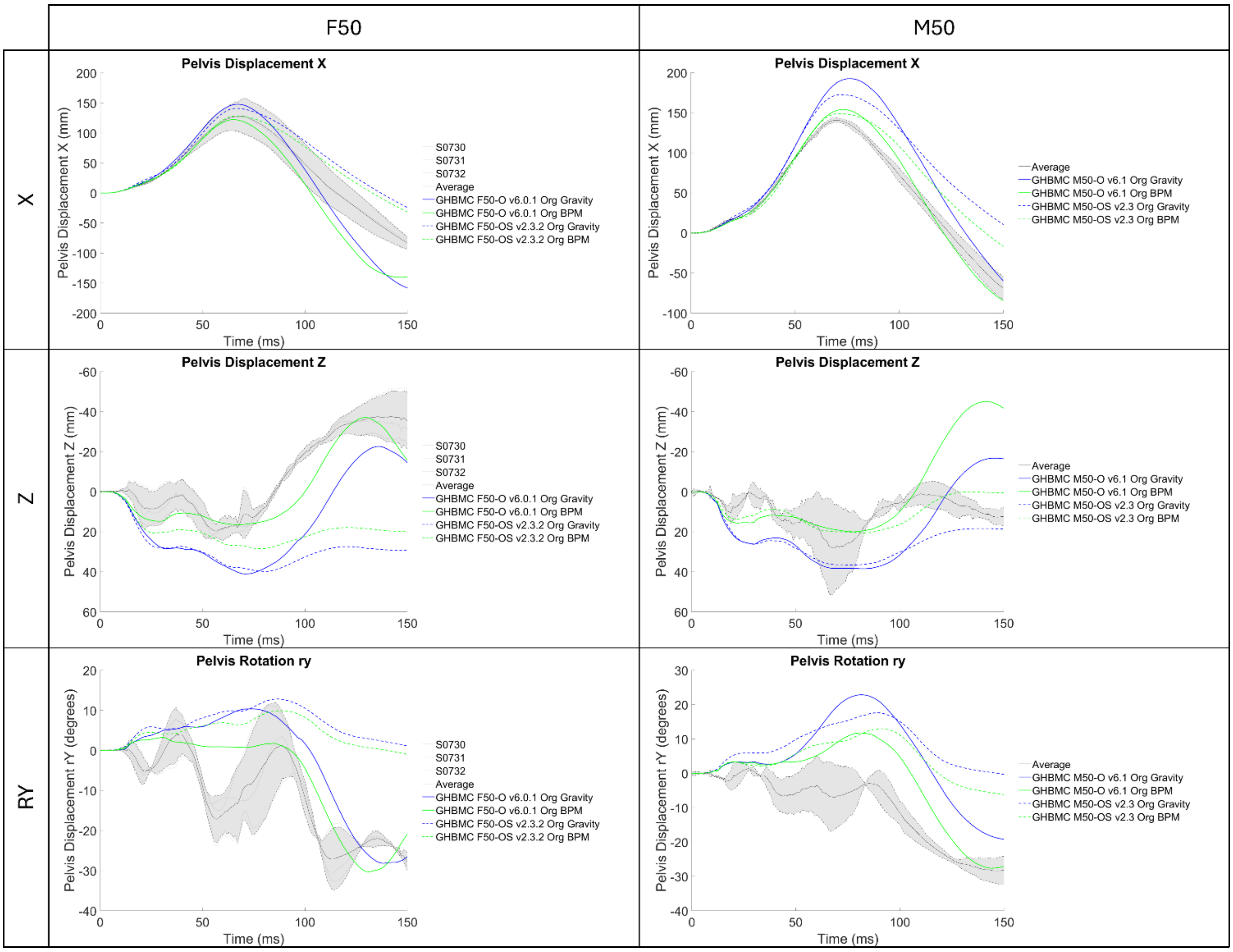

Fig. C21. Comparison of the average PMHS X, Z, RY time histories of the pelvis with X, Z, RY time histories of the pelvis for HBMs using stock soft tissue materials.

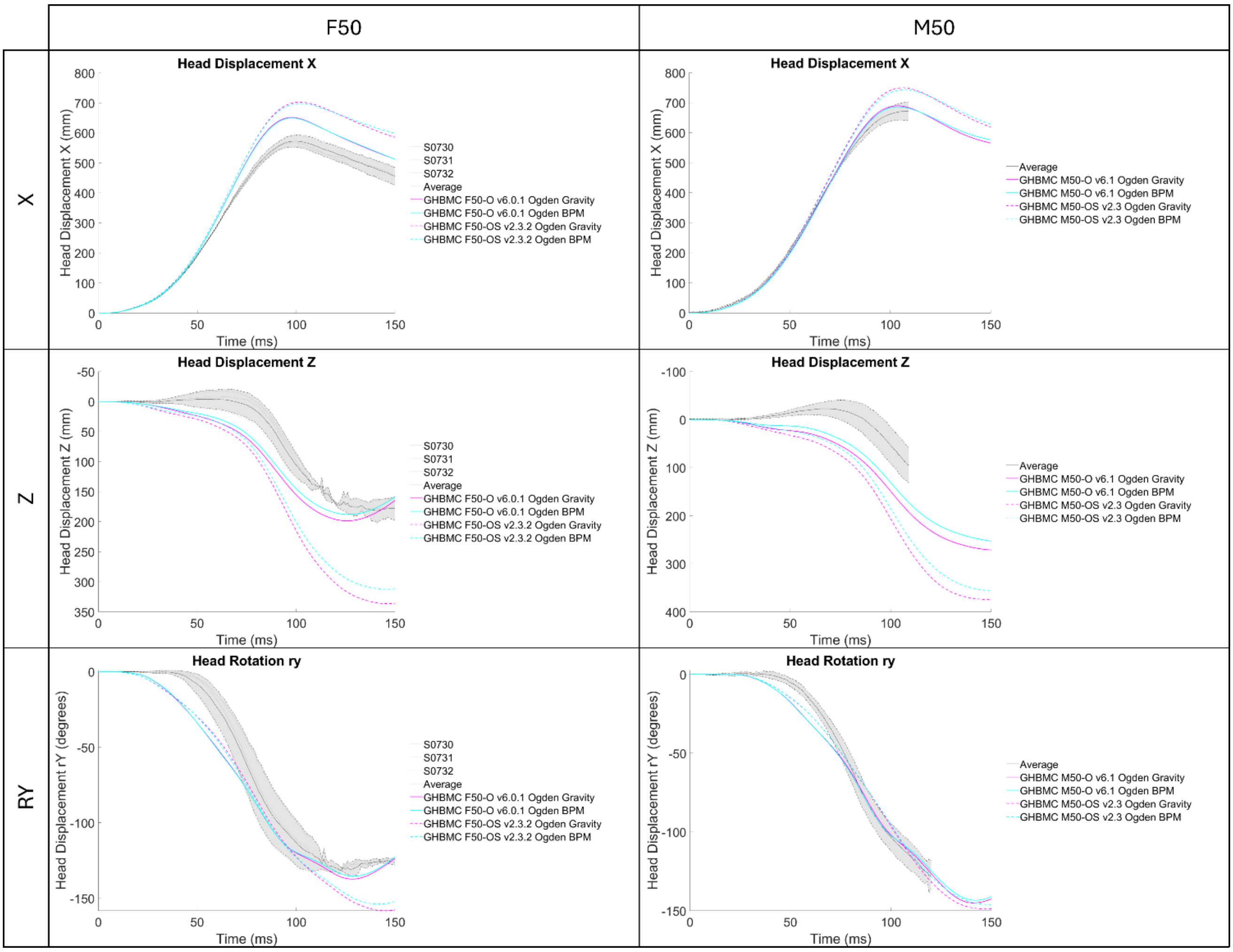

Fig. C22. Comparison of the average PMHS X, Z, RY time histories of the head with X, Z, RY time histories of the head for HBMs using Ogden soft tissue materials.

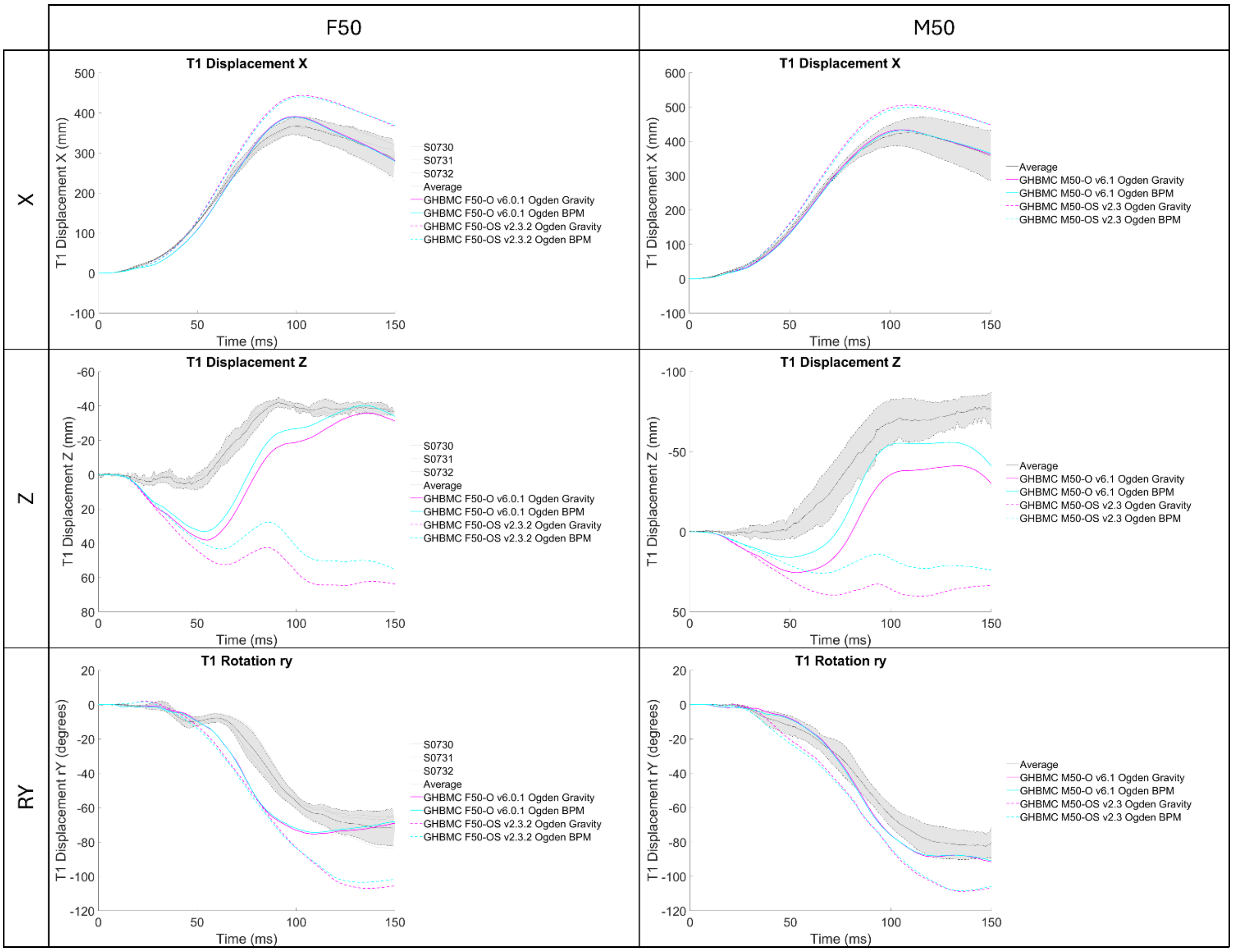

Fig. C23. Comparison of the average PMHS X, Z, RY time histories of T1 with X, Z, RY time histories of T1 for HBMs using Ogden soft tissue materials.

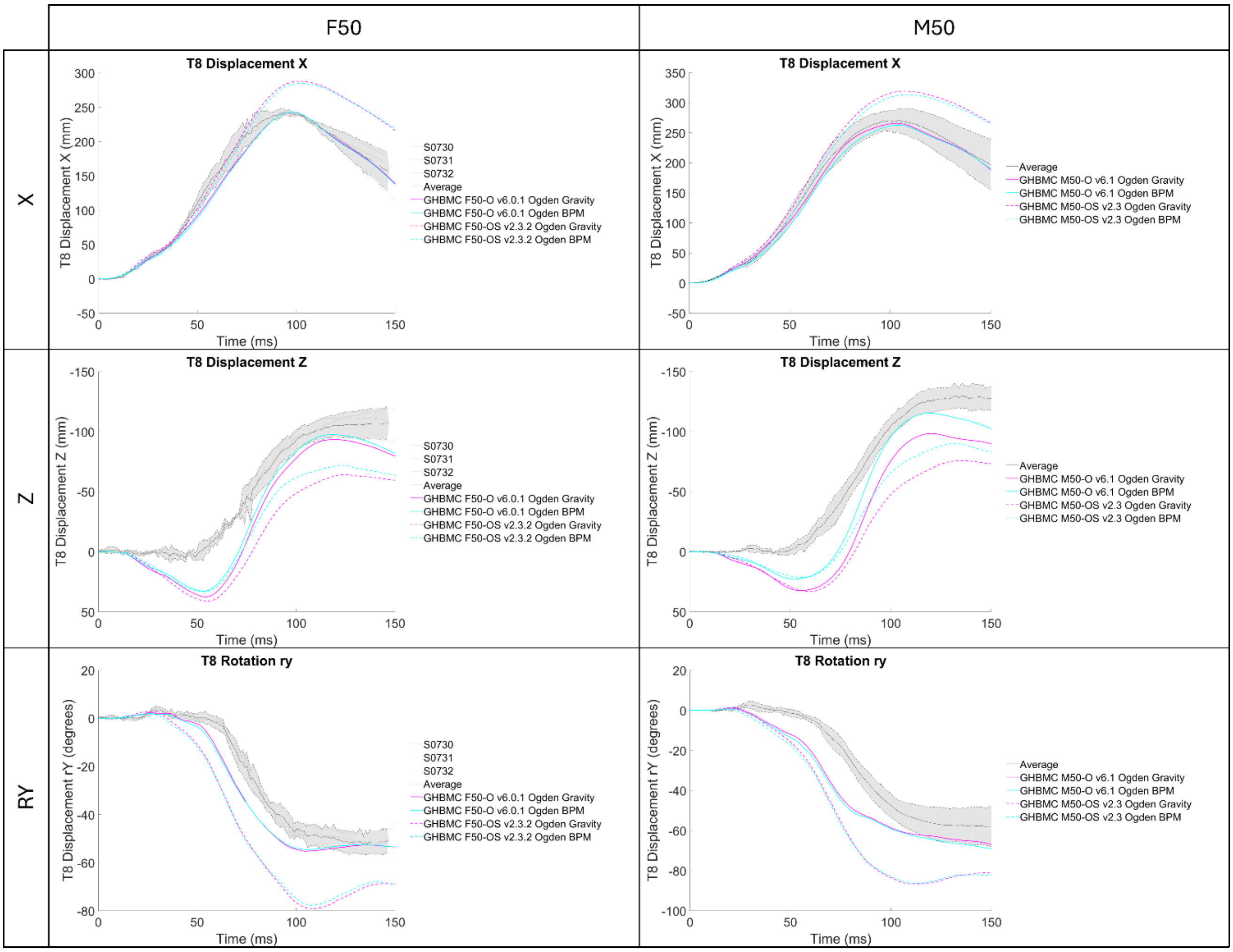

Fig. C24. Comparison of the average PMHS X, Z, RY time histories of T8 with X, Z, RY time histories of T8 for HBMs using Ogden soft tissue materials.

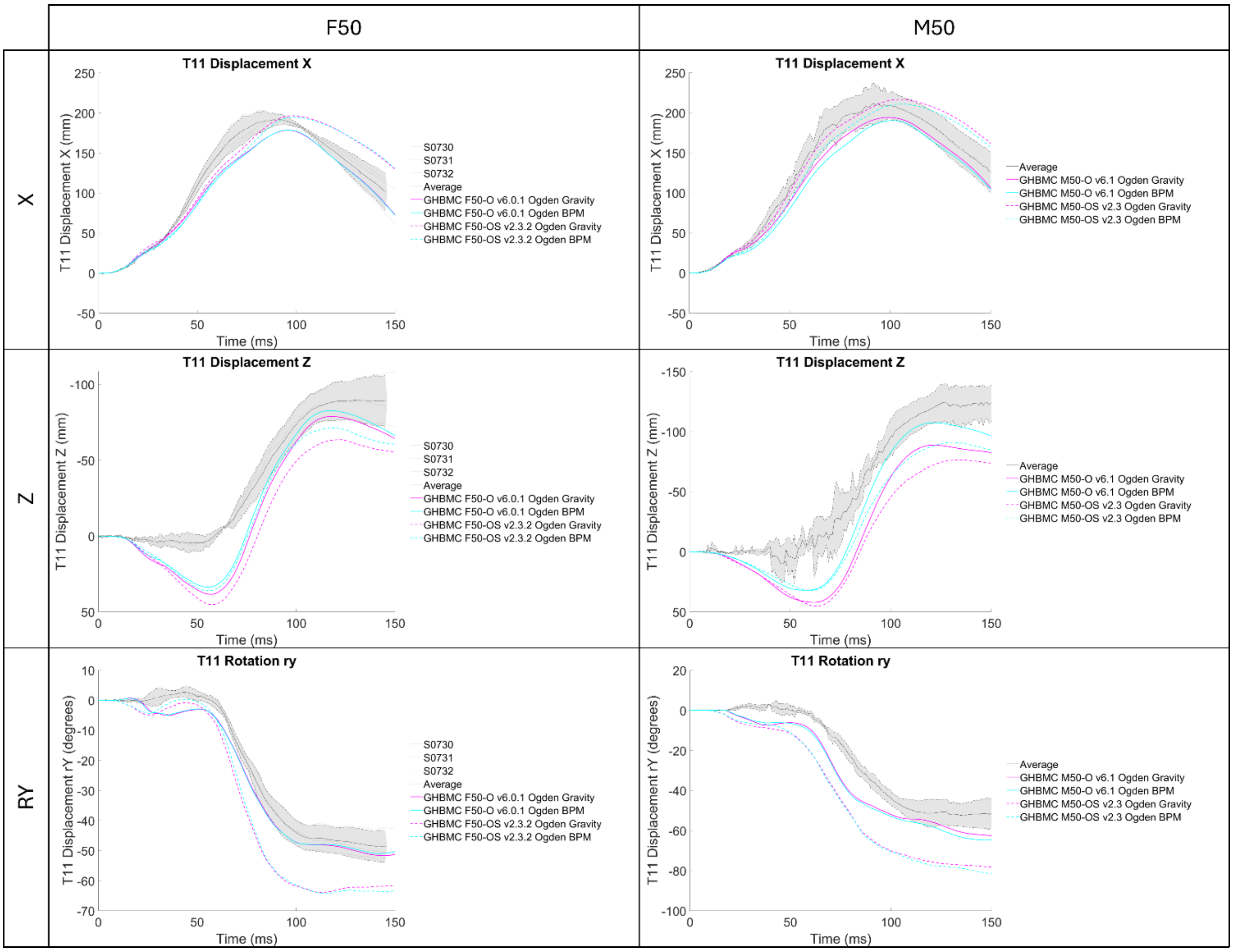

Fig. C25. Comparison of the average PMHS X, Z, RY time histories of T11 with X, Z, RY time histories of T11 for HBMs using Ogden soft tissue materials.

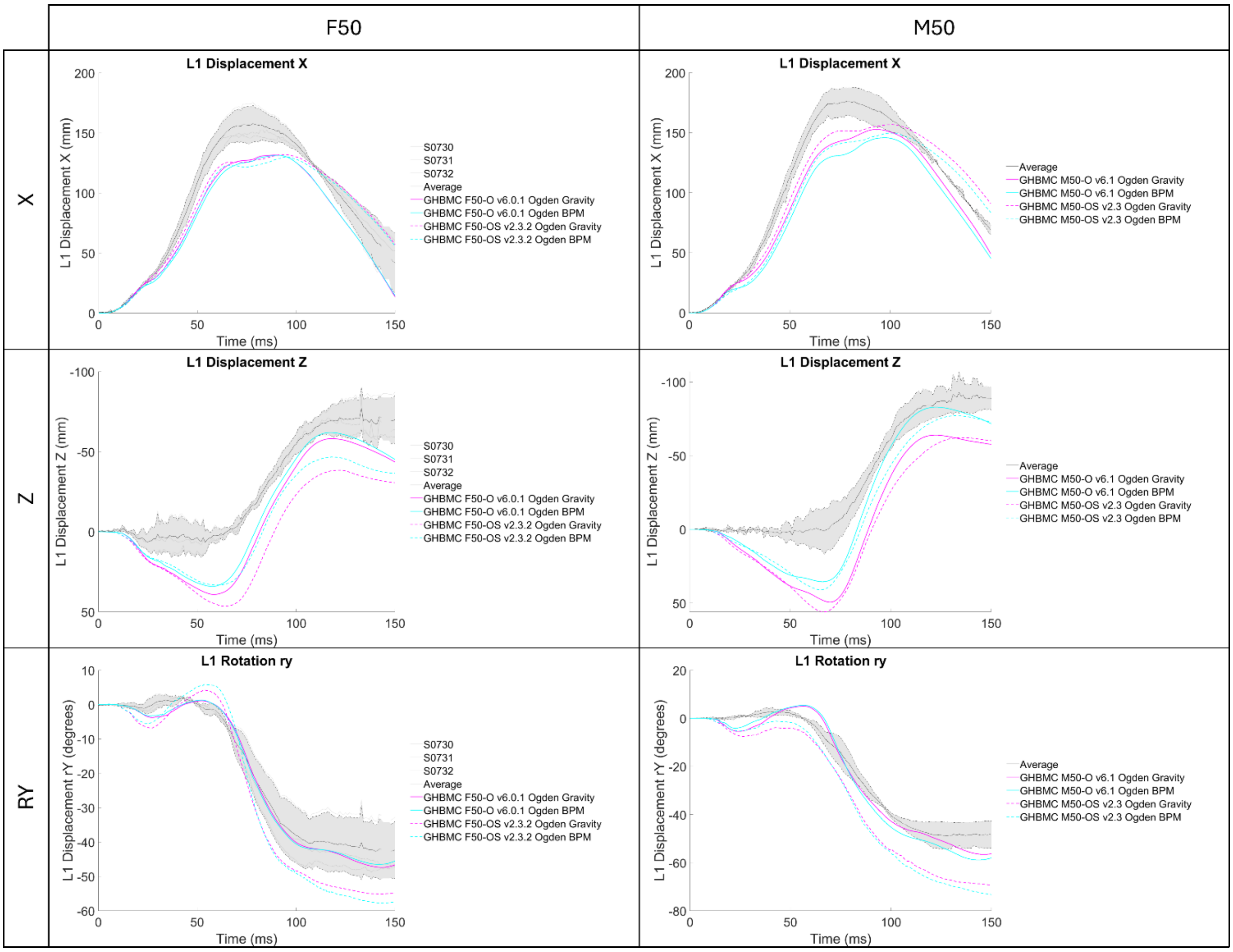

Fig. C26. Comparison of the average PMHS X, Z, RY time histories of L1 with X, Z, RY time histories of L1 for HBMs using Ogden soft tissue materials.

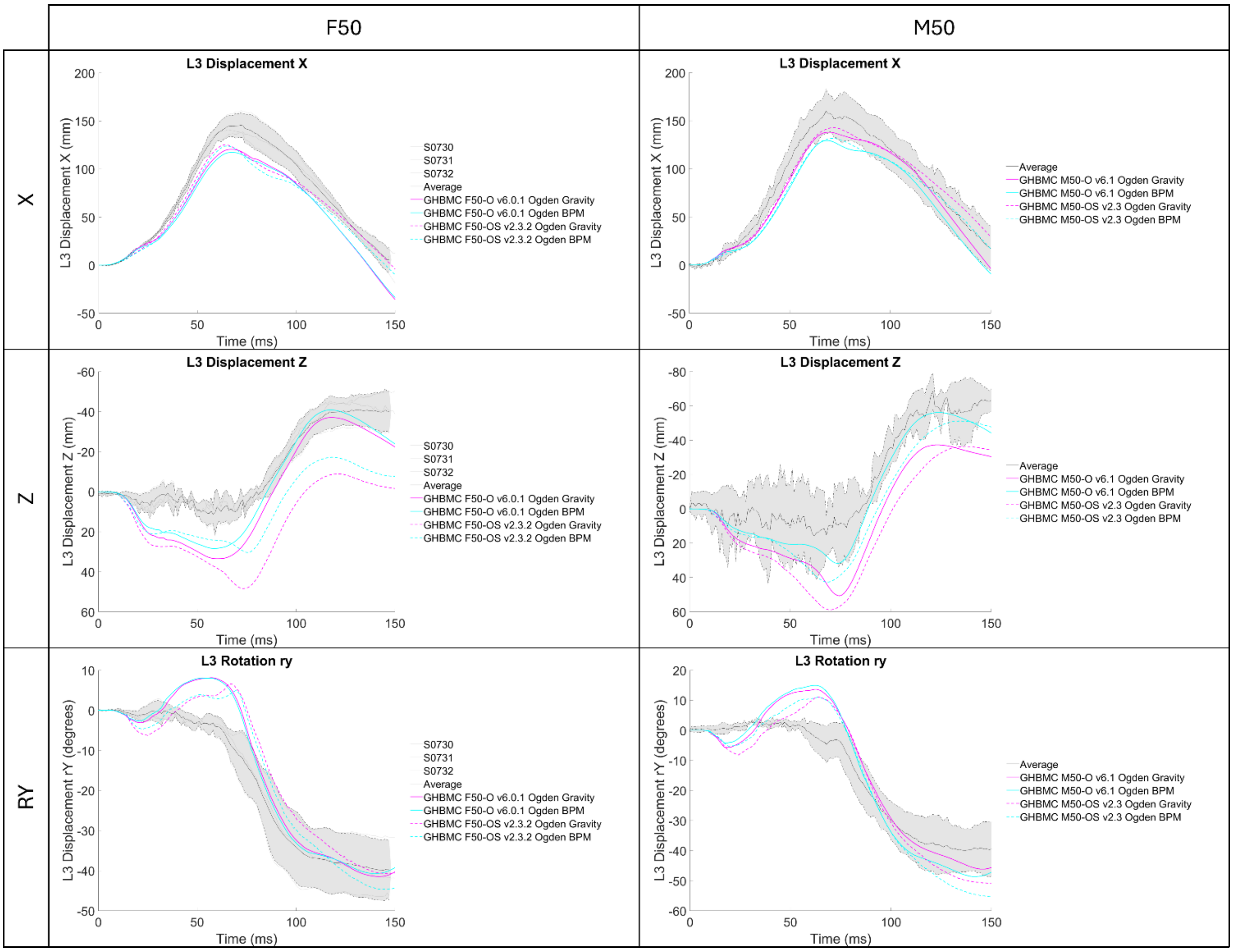

Fig. C27. Comparison of the average PMHS X, Z, RY time histories of L3 with X, Z, RY time histories of L3 for HBMs using Ogden soft tissue materials.

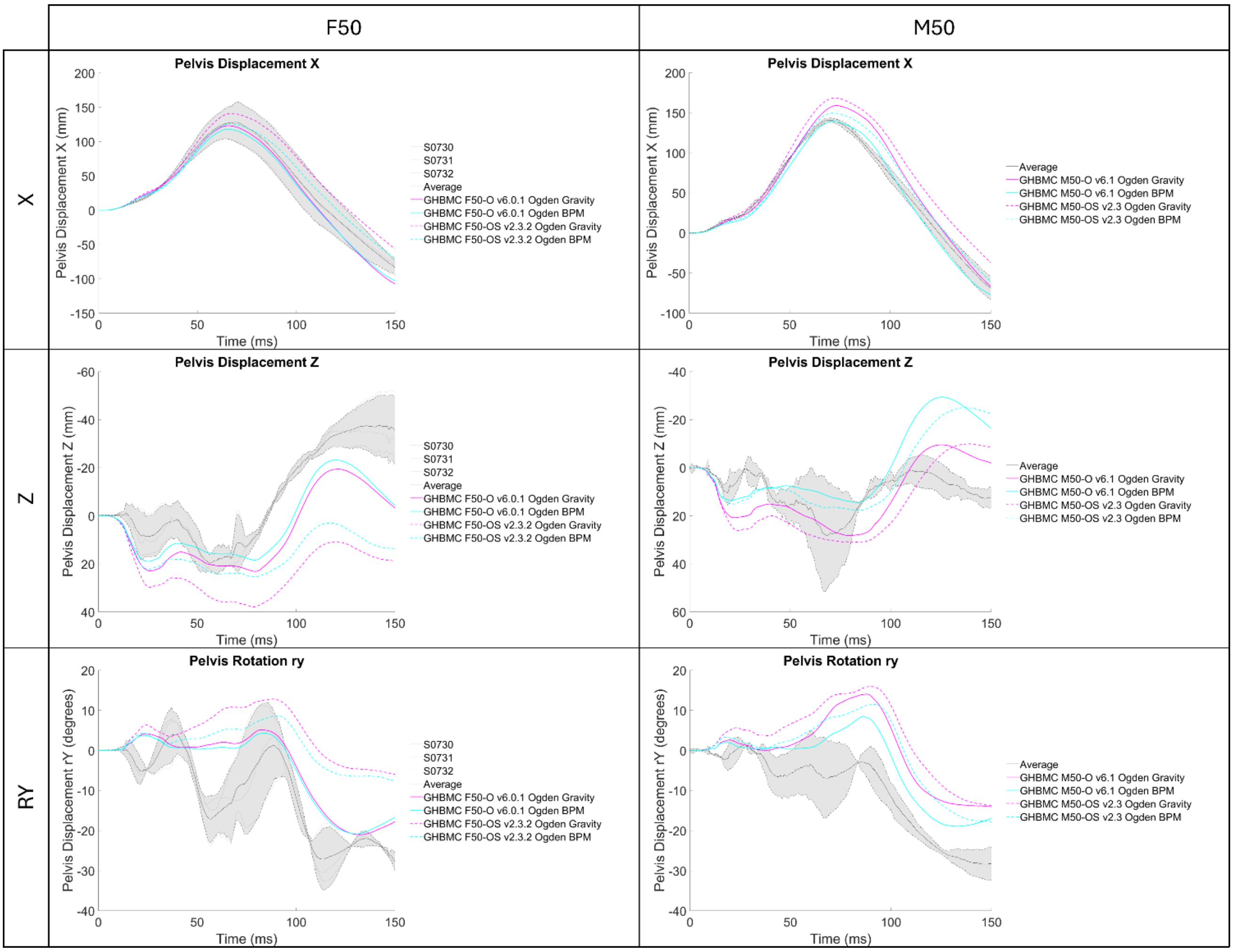

Fig. C28. Comparison of the average PMHS X, Z, RY time histories of the pelvis with X, Z, RY time histories of the pelvis for HBMs using Ogden soft tissue materials.

Appendix D – CORA Tables

TABLE D-I
CORA PARAMETERS USED FOR EVALUATION.

Parameter	**Setting/Value**
T_MIN	0
T_MAX	150
Automatic	NO
Corridor Method (standard deviation vs. constant)	Standard deviation
INT_min	0.8
a0	1
b0	2
Y_NORM	Extremum
K	2
K_V	10
K_P	1
DTMIN	0.01
DTMAX	0.12
K_G	1
G_2	0.5
G_V	0.5
G_G	0.25
G_P	0.25

TABLE D-II
F50-O AVERAGE CORA SCORES FOR X, Z, AND RY DISPLACEMENT GROUPS.

X Avg.	Corridor Score	Phase Score	Size Score	Progression Score	Correlation Score	Total Score
Stock – Gravity	0.439	0.866	0.716	0.904	0.847	0.643
Stock -BPM	0.281	0.883	0.688	0.868	0.827	0.554
Ogden -Gravity	0.487	0.996	0.828	0.980	0.946	0.717
Ogden - BPM	0.461	0.996	0.816	0.978	0.942	0.701
Average	0.417	0.935	0.762	0.932	0.890	0.654
Z Avg.	Corridor Score	Phase Score	Size Score	Progression Score	Correlation Score	Total Score
Stock – Gravity	0.183	0.494	0.693	0.284	0.439	0.311
Stock -BPM	0.395	0.810	0.761	0.631	0.708	0.552
Ogden -Gravity	0.275	0.827	0.792	0.458	0.634	0.454
Ogden - BPM	0.391	0.866	0.817	0.556	0.699	0.545
Average	0.311	0.749	0.765	0.482	0.620	0.465
RY Avg.	Corridor Score	Phase Score	Size Score	Progression Score	Correlation Score	Total Score
Stock – Gravity	0.568	1.000	0.911	0.819	0.887	0.728
Stock -BPM	0.611	1.000	0.887	0.877	0.910	0.760
Ogden -Gravity	0.553	1.000	0.788	0.867	0.881	0.717
Ogden - BPM	0.566	1.000	0.794	0.878	0.887	0.727
Average	0.575	1.000	0.845	0.860	0.891	0.733

TABLE D-III
F50-OS AVERAGE CORA SCORES FOR X, Z, AND RY DISPLACEMENT GROUPS.

X Avg.	Corridor Score	Phase Score	Size Score	Progression Score	Correlation Score	Total Score
Stock – Gravity	0.346	0.952	0.751	0.925	0.888	0.617
Stock -BPM	0.336	0.931	0.764	0.928	0.888	0.612
Ogden -Gravity	0.375	0.991	0.756	0.963	0.918	0.647
Ogden - BPM	0.356	0.996	0.775	0.972	0.929	0.642
Average	0.353	0.968	0.762	0.947	0.906	0.629
Z Avg.	Corridor Score	Phase Score	Size Score	Progression Score	Correlation Score	Total Score
Stock – Gravity	0.074	0.429	0.303	0.227	0.297	0.185
Stock -BPM	0.106	0.567	0.421	0.329	0.411	0.259
Ogden -Gravity	0.071	0.489	0.439	0.282	0.373	0.222
Ogden - BPM	0.125	0.636	0.532	0.377	0.481	0.303
Average	0.094	0.530	0.424	0.304	0.390	0.242
RY Avg.	Corridor Score	Phase Score	Size Score	Progression Score	Correlation Score	Total Score
Stock – Gravity	0.299	0.857	0.598	0.814	0.771	0.535
Stock -BPM	0.321	0.857	0.581	0.817	0.768	0.544
Ogden -Gravity	0.274	0.926	0.535	0.804	0.767	0.521
Ogden - BPM	0.290	0.987	0.537	0.810	0.786	0.538
Average	0.296	0.907	0.563	0.811	0.773	0.535

TABLE D-IV
M50-O AVERAGE CORA SCORES FOR X, Z, AND RY DISPLACEMENT GROUPS.

X Avg.	Corridor Score	Phase Score	Size Score	Progression Score	Correlation Score	Total Score
Stock – Gravity	0.597	0.965	0.834	0.982	0.941	0.769
Stock -BPM	0.535	1.000	0.835	0.980	0.949	0.742
Ogden -Gravity	0.645	1.000	0.860	0.990	0.960	0.803
Ogden - BPM	0.543	1.000	0.848	0.987	0.955	0.749
Average	0.580	0.991	0.844	0.985	0.951	0.766
Z Avg.	**Corridor Score**	**Phase Score**	**Size Score**	**Progression Score**	**Correlation Score**	**Total Score**
Stock – Gravity	0.160	0.649	0.447	0.202	0.375	0.267
Stock -BPM	0.315	0.801	0.636	0.435	0.576	0.446
Ogden -Gravity	0.188	0.952	0.498	0.390	0.558	0.373
Ogden - BPM	0.405	0.935	0.675	0.585	0.695	0.550
Average	0.267	0.834	0.564	0.403	0.551	0.409
RY Avg.	**Corridor Score**	**Phase Score**	**Size Score**	**Progression Score**	**Correlation Score**	**Total Score**
Stock – Gravity	0.292	0.952	0.740	0.800	0.823	0.558
Stock -BPM	0.316	1.000	0.647	0.843	0.833	0.575
Ogden -Gravity	0.481	1.000	0.740	0.808	0.839	0.660
Ogden - BPM	0.458	1.000	0.711	0.870	0.863	0.661
Average	0.387	0.988	0.710	0.830	0.840	0.613

TABLE D-V
M50S-O AVERAGE CORA SCORES FOR X, Z, AND RY DISPLACEMENT GROUPS.

X Avg.	Corridor Score	Phase Score	Size Score	Progression Score	Correlation Score	Total Score
Stock – Gravity	0.439	0.909	0.808	0.954	0.906	0.673
Stock -BPM	0.411	0.918	0.820	0.963	0.916	0.664
Ogden -Gravity	0.460	0.965	0.797	0.975	0.928	0.694
Ogden - BPM	0.444	0.974	0.809	0.982	0.936	0.690
Average	0.438	0.942	0.808	0.968	0.922	0.680
Z Avg.	**Corridor Score**	**Phase Score**	**Size Score**	**Progression Score**	**Correlation Score**	**Total Score**
Stock – Gravity	0.128	0.753	0.388	0.188	0.380	0.254
Stock -BPM	0.205	0.801	0.407	0.393	0.498	0.352
Ogden -Gravity	0.155	0.779	0.502	0.260	0.450	0.303
Ogden - BPM	0.232	0.766	0.521	0.410	0.527	0.379
Average	0.180	0.775	0.455	0.313	0.464	0.322
RY Avg.	**Corridor Score**	**Phase Score**	**Size Score**	**Progression Score**	**Correlation Score**	**Total Score**
Stock – Gravity	0.320	0.857	0.654	0.803	0.779	0.550
Stock -BPM	0.330	0.874	0.596	0.809	0.772	0.551
Ogden -Gravity	0.255	0.970	0.577	0.800	0.787	0.521
Ogden - BPM	0.260	1.000	0.535	0.821	0.794	0.527
Average	0.291	0.925	0.590	0.808	0.783	0.537

TABLE D-VI
CORA SCORES FOR THE F50-O SIMULATION USING STOCK MATERIALS AND GRAVITY SETTLING METHODS.

Channel Name	Corridor Score	Phase Score	Size Score	Progression Score	Correlation Score	Total Score
Head X Displacement	0.535	1.000	0.862	0.997	0.964	0.749
Head Z Displacement	0.095	0.303	0.758	0.726	0.628	0.362
Head RY Displacement	0.198	1.000	0.746	0.940	0.906	0.552
T1 X Displacement	0.328	1.000	0.784	0.986	0.939	0.634
T1 Z Displacement	0.089	0.000	0.365	0.168	0.175	0.132
T1 RY Displacement	0.611	1.000	0.993	0.936	0.966	0.789
T8 X Displacement	0.426	1.000	0.723	0.969	0.916	0.671
T8 Z Displacement	0.279	0.424	0.921	0.412	0.542	0.411
T8 RY Displacement	0.729	1.000	0.962	0.980	0.980	0.855
T11 X Displacement	0.362	0.788	0.671	0.963	0.846	0.604
T11 Z Displacement	0.267	0.848	0.885	0.352	0.609	0.438
T11 RY Displacement	0.743	1.000	0.999	0.989	0.994	0.869
L1 X Displacement	0.389	0.606	0.649	0.903	0.766	0.577
L1 Z Displacement	0.162	0.727	0.963	0.172	0.509	0.335
L1 RY Displacement	0.741	1.000	0.961	0.970	0.975	0.858
L3 X Displacement	0.435	0.667	0.740	0.739	0.721	0.578
L3 Z Displacement	0.291	0.788	0.470	0.095	0.362	0.326
L3 RY Displacement	0.577	1.000	0.949	0.782	0.878	0.728
Pelvis (PSIS) X Displacement	0.596	1.000	0.583	0.769	0.780	0.688
Pelvis (PSIS) Z Displacement	0.099	0.364	0.489	0.066	0.246	0.173
Pelvis (PSIS) RY Displacement	0.377	1.000	0.770	0.135	0.510	0.444

TABLE D-VII
CORA SCORES FOR THE F50-O SIMULATION USING STOCK MATERIALS AND BPM SETTLING METHODS.

Channel Name	Corridor Score	Phase Score	Size Score	Progression Score	Correlation Score	Total Score
Head X Displacement	0.515	1	0.86	0.999	0.964	0.74
Head Z Displacement	0.077	0.424	0.826	0.751	0.688	0.383
Head RY Displacement	0.259	1	0.779	0.932	0.911	0.585
T1 X Displacement	0.332	1	0.779	0.989	0.939	0.635
T1 Z Displacement	0.095	0.788	0.358	0.54	0.556	0.326
T1 RY Displacement	0.676	1	1	0.934	0.967	0.822
T8 X Displacement	0.144	1	0.697	0.981	0.915	0.53
T8 Z Displacement	0.496	0.909	0.949	0.639	0.784	0.64
T8 RY Displacement	0.615	1	0.919	0.978	0.969	0.792
T11 X Displacement	0.123	0.909	0.615	0.964	0.863	0.493
T11 Z Displacement	0.506	0.848	0.903	0.743	0.809	0.658
T11 RY Displacement	0.749	1	0.925	0.989	0.976	0.863
L1 X Displacement	0.085	0.667	0.547	0.899	0.753	0.419
L1 Z Displacement	0.395	0.727	0.88	0.591	0.697	0.546
L1 RY Displacement	0.801	1	0.849	0.979	0.952	0.876
L3 X Displacement	0.083	0.606	0.584	0.696	0.645	0.364
L3 Z Displacement	0.572	0.97	0.618	0.561	0.677	0.625
L3 RY Displacement	0.668	1	0.896	0.837	0.893	0.78
Pelvis (PSIS) X Displacement	0.688	1	0.733	0.546	0.707	0.697
Pelvis (PSIS) Z Displacement	0.623	1	0.789	0.595	0.745	0.684
Pelvis (PSIS) RY Displacement	0.509	1	0.838	0.487	0.703	0.606

TABLE D-VIII
CORA SCORES FOR THE F50-O SIMULATION USING OGDEN MATERIALS AND GRAVITY SETTLING METHODS.

Channel Name	Corridor Score	Phase Score	Size Score	Progression Score	Correlation Score	Total Score
Head X Displacement	0.299	1	0.79	0.999	0.947	0.623
Head Z Displacement	0.15	1	0.675	0.843	0.84	0.495
Head RY Displacement	0.446	1	0.855	0.956	0.942	0.694
T1 X Displacement	0.601	1	0.951	0.995	0.985	0.793
T1 Z Displacement	0.156	0.364	0.954	0.171	0.415	0.285
T1 RY Displacement	0.492	1	0.714	0.908	0.882	0.687
T8 X Displacement	0.773	1	0.926	0.993	0.978	0.875
T8 Z Displacement	0.26	0.909	0.792	0.611	0.731	0.496
T8 RY Displacement	0.471	1	0.76	0.946	0.913	0.692
T11 X Displacement	0.453	1	0.803	0.991	0.946	0.7
T11 Z Displacement	0.442	0.848	0.835	0.665	0.753	0.598
T11 RY Displacement	0.574	1	0.872	0.978	0.957	0.765
L1 X Displacement	0.26	1	0.692	0.984	0.915	0.588
L1 Z Displacement	0.171	0.727	0.862	0.443	0.619	0.395
L1 RY Displacement	0.753	1	0.882	0.988	0.965	0.859
L3 X Displacement	0.215	0.97	0.661	0.963	0.889	0.552
L3 Z Displacement	0.484	0.97	0.78	0.322	0.599	0.541
L3 RY Displacement	0.657	1	0.964	0.862	0.922	0.789
Pelvis (PSIS) X Displacement	0.81	1	0.972	0.936	0.961	0.885
Pelvis (PSIS) Z Displacement	0.258	0.97	0.642	0.152	0.479	0.368
Pelvis (PSIS) RY Displacement	0.478	1	0.472	0.431	0.583	0.531

TABLE D-IX
CORA SCORES FOR THE F50-O SIMULATION USING OGDEN MATERIALS AND BPM SETTLING METHODS.

Channel Name	Corridor Score	Phase Score	Size Score	Progression Score	Correlation Score	Total Score
Head X Displacement	0.301	1	0.791	0.999	0.947	0.624
Head Z Displacement	0.207	1	0.761	0.864	0.872	0.54
Head RY Displacement	0.498	1	0.868	0.954	0.944	0.721
T1 X Displacement	0.608	1	0.961	0.995	0.988	0.798
T1 Z Displacement	0.308	0.606	0.999	0.33	0.566	0.437
T1 RY Displacement	0.511	1	0.731	0.905	0.885	0.698
T8 X Displacement	0.689	1	0.915	0.991	0.974	0.832
T8 Z Displacement	0.453	0.909	0.858	0.666	0.775	0.614
T8 RY Displacement	0.466	1	0.767	0.939	0.911	0.689
T11 X Displacement	0.436	1	0.792	0.988	0.942	0.689
T11 Z Displacement	0.527	0.848	0.899	0.737	0.805	0.666
T11 RY Displacement	0.558	1	0.879	0.976	0.958	0.758
L1 X Displacement	0.237	1	0.676	0.982	0.91	0.574
L1 Z Displacement	0.329	0.727	0.907	0.54	0.679	0.504
L1 RY Displacement	0.755	1	0.886	0.991	0.967	0.861
L3 X Displacement	0.176	0.97	0.63	0.963	0.881	0.529
L3 Z Displacement	0.551	0.97	0.789	0.45	0.664	0.608
L3 RY Displacement	0.678	1	0.967	0.873	0.928	0.803
Pelvis (PSIS) X Displacement	0.78	1	0.944	0.928	0.95	0.865
Pelvis (PSIS) Z Displacement	0.361	1	0.506	0.304	0.528	0.445
Pelvis (PSIS) RY Displacement	0.499	1	0.461	0.505	0.618	0.558

TABLE D-X
CORA SCORES FOR THE F50-OS SIMULATION USING STOCK MATERIALS AND GRAVITY SETTLING METHODS.

Channel Name	Corridor Score	Phase Score	Size Score	Progression Score	Correlation Score	Total Score
Head X Displacement	0.284	1	0.661	0.989	0.91	0.597
Head Z Displacement	0.044	1	0.329	0.943	0.804	0.424
Head RY Displacement	0.544	1	0.877	0.971	0.955	0.75
T1 X Displacement	0.181	1	0.67	0.99	0.912	0.547
T1 Z Displacement	0.056	0	0.196	0	0.049	0.053
T1 RY Displacement	0.263	1	0.47	0.982	0.858	0.561
T8 X Displacement	0.374	1	0.635	0.949	0.883	0.628
T8 Z Displacement	0.143	0.424	0.268	0.296	0.321	0.232
T8 RY Displacement	0.181	1	0.434	0.922	0.82	0.501
T11 X Displacement	0.333	1	0.795	0.922	0.91	0.621
T11 Z Displacement	0.09	0.848	0.366	0.309	0.458	0.274
T11 RY Displacement	0.074	1	0.541	0.968	0.869	0.472
L1 X Displacement	0.351	0.97	0.96	0.937	0.951	0.651
L1 Z Displacement	0.05	0.727	0.389	0.04	0.299	0.174
L1 RY Displacement	0.238	1	0.593	0.975	0.886	0.562
L3 X Displacement	0.374	0.97	0.79	0.97	0.925	0.65
L3 Z Displacement	0.087	0	0.376	0.002	0.095	0.091
L3 RY Displacement	0.551	1	0.778	0.881	0.885	0.718
Pelvis (PSIS) X Displacement	0.526	0.727	0.747	0.719	0.728	0.627
Pelvis (PSIS) Z Displacement	0.047	0	0.201	0.002	0.051	0.049
Pelvis (PSIS) RY Displacement	0.242	0	0.49	0	0.122	0.182

TABLE D-XI
CORA SCORES FOR THE F50-OS SIMULATION USING STOCK MATERIALS AND BPM SETTLING METHODS.

Channel Name	Corridor Score	Phase Score	Size Score	Progression Score	Correlation Score	Total Score
Head X Displacement	0.293	1	0.663	0.988	0.91	0.601
Head Z Displacement	0.045	1	0.389	0.956	0.825	0.435
Head RY Displacement	0.604	1	0.909	0.975	0.965	0.785
T1 X Displacement	0.187	1	0.681	0.989	0.914	0.551
T1 Z Displacement	0.068	0	0.313	0	0.078	0.073
T1 RY Displacement	0.259	1	0.478	0.979	0.859	0.559
T8 X Displacement	0.417	1	0.649	0.938	0.881	0.649
T8 Z Displacement	0.154	0.909	0.306	0.529	0.568	0.361
T8 RY Displacement	0.176	1	0.44	0.909	0.815	0.495
T11 X Displacement	0.314	0.909	0.815	0.906	0.884	0.599
T11 Z Displacement	0.099	0.848	0.448	0.58	0.614	0.357
T11 RY Displacement	0.07	1	0.542	0.974	0.873	0.471
L1 X Displacement	0.153	0.848	0.909	0.927	0.903	0.528
L1 Z Displacement	0.103	0.727	0.36	0.229	0.386	0.244
L1 RY Displacement	0.237	1	0.58	0.981	0.886	0.561
L3 X Displacement	0.36	0.97	0.71	0.977	0.908	0.634
L3 Z Displacement	0.101	0.485	0.708	0.007	0.302	0.201
L3 RY Displacement	0.597	1	0.855	0.898	0.913	0.755
Pelvis (PSIS) X Displacement	0.628	0.788	0.919	0.771	0.812	0.72
Pelvis (PSIS) Z Displacement	0.174	0	0.421	0.002	0.106	0.14
Pelvis (PSIS) RY Displacement	0.303	0	0.263	0	0.066	0.184

TABLE D-XII
CORA SCORES FOR THE F50-OS SIMULATION USING OGDEN MATERIALS AND GRAVITY SETTLING METHODS.

Channel Name	Corridor Score	Phase Score	Size Score	Progression Score	Correlation Score	Total Score
Head X Displacement	0.145	1	0.667	0.997	0.915	0.53
Head Z Displacement	0.044	1	0.269	0.93	0.782	0.413
Head RY Displacement	0.361	1	0.738	0.971	0.92	0.64
T1 X Displacement	0.136	1	0.687	0.995	0.919	0.527
T1 Z Displacement	0.049	0	0.205	0	0.051	0.05
T1 RY Displacement	0.224	1	0.423	0.973	0.843	0.533
T8 X Displacement	0.382	1	0.695	0.968	0.908	0.645
T8 Z Displacement	0.134	0.424	0.452	0.417	0.428	0.281
T8 RY Displacement	0.176	1	0.393	0.906	0.801	0.489
T11 X Displacement	0.287	1	0.918	0.95	0.954	0.62
T11 Z Displacement	0.09	0.848	0.605	0.471	0.599	0.344
T11 RY Displacement	0.063	1	0.52	0.968	0.864	0.464
L1 X Displacement	0.488	0.97	0.821	0.969	0.932	0.71
L1 Z Displacement	0.042	0.727	0.586	0.141	0.399	0.22
L1 RY Displacement	0.262	1	0.592	0.98	0.888	0.575
L3 X Displacement	0.44	1	0.707	0.992	0.923	0.681
L3 Z Displacement	0.095	0.424	0.661	0.01	0.276	0.185
L3 RY Displacement	0.558	1	0.81	0.825	0.865	0.712
Pelvis (PSIS) X Displacement	0.75	0.97	0.799	0.868	0.876	0.813
Pelvis (PSIS) Z Displacement	0.043	0	0.295	0.003	0.075	0.059
Pelvis (PSIS) RY Displacement	0.273	0.485	0.271	0.001	0.189	0.231

TABLE D-XIII
CORA SCORES FOR THE F50-OS SIMULATION USING OGDEN MATERIALS AND BPM SETTLING METHODS.

Channel Name	Corridor Score	Phase Score	Size Score	Progression Score	Correlation Score	Total Score
Head X Displacement	0.149	1	0.666	0.996	0.915	0.532
Head Z Displacement	0.044	1	0.312	0.939	0.797	0.421
Head RY Displacement	0.354	1	0.751	0.972	0.924	0.639
T1 X Displacement	0.133	1	0.697	0.994	0.921	0.527
T1 Z Displacement	0.053	0	0.33	0	0.083	0.068
T1 RY Displacement	0.222	1	0.435	0.966	0.842	0.532
T8 X Displacement	0.387	1	0.715	0.958	0.908	0.648
T8 Z Displacement	0.144	0.909	0.489	0.578	0.638	0.391
T8 RY Displacement	0.171	1	0.404	0.897	0.799	0.485
T11 X Displacement	0.314	1	0.945	0.937	0.954	0.634
T11 Z Displacement	0.264	0.848	0.712	0.666	0.723	0.493
T11 RY Displacement	0.108	1	0.516	0.981	0.87	0.489
L1 X Displacement	0.368	0.97	0.777	0.967	0.92	0.644
L1 Z Displacement	0.069	0.727	0.583	0.392	0.524	0.296
L1 RY Displacement	0.229	1	0.561	0.975	0.878	0.553
L3 X Displacement	0.293	1	0.646	0.992	0.908	0.6
L3 Z Displacement	0.106	0.97	0.612	0.064	0.428	0.267
L3 RY Displacement	0.603	1	0.976	0.86	0.924	0.763
Pelvis (PSIS) X Displacement	0.845	1	0.981	0.958	0.974	0.91
Pelvis (PSIS) Z Displacement	0.193	0	0.687	0.003	0.173	0.183
Pelvis (PSIS) RY Displacement	0.345	0.909	0.119	0.017	0.266	0.305

TABLE D-XIV
CORA SCORES FOR THE M50-O SIMULATION USING STOCK MATERIALS AND GRAVITY SETTLING METHODS.

Channel Name	Corridor Score	Phase Score	Size Score	Progression Score	Correlation Score	Total Score
Head X Displacement	0.332	1	0.886	0.995	0.969	0.651
Head Z Displacement	0.173	1	0.101	0.137	0.344	0.258
Head RY Displacement	0.565	1	0.967	0.959	0.971	0.768
T1 X Displacement	0.582	1	0.79	0.992	0.943	0.763
T1 Z Displacement	0.026	0	0.316	0	0.079	0.052
T1 RY Displacement	0.461	1	0.661	0.985	0.908	0.684
T8 X Displacement	0.689	1	0.818	0.989	0.949	0.819
T8 Z Displacement	0.054	1	0.424	0.384	0.548	0.301
T8 RY Displacement	0.127	1	0.479	0.963	0.851	0.489
T11 X Displacement	0.919	1	0.949	0.987	0.981	0.95
T11 Z Displacement	0.098	0.97	0.528	0.314	0.531	0.314
T11 RY Displacement	0.087	1	0.541	0.976	0.873	0.48
L1 X Displacement	0.506	1	0.98	0.982	0.986	0.746
L1 Z Displacement	0.079	0.727	0.847	0.141	0.464	0.271
L1 RY Displacement	0.313	1	0.737	0.958	0.913	0.613
L3 X Displacement	0.953	0.97	0.921	0.995	0.97	0.962
L3 Z Displacement	0.422	0.485	0.692	0.081	0.335	0.378
L3 RY Displacement	0.376	1	0.808	0.752	0.828	0.602
Pelvis (PSIS) X Displacement	0.199	0.788	0.493	0.932	0.786	0.493
Pelvis (PSIS) Z Displacement	0.266	0.364	0.221	0.359	0.326	0.296
Pelvis (PSIS) RY Displacement	0.116	0.667	0.99	0.006	0.417	0.267

TABLE D-XV
CORA SCORES FOR THE M50-O SIMULATION USING STOCK MATERIALS AND BPM SETTLING METHODS.

Channel Name	Corridor Score	Phase Score	Size Score	Progression Score	Correlation Score	Total Score
Head X Displacement	0.287	1	0.899	0.995	0.972	0.63
Head Z Displacement	0.175	1	0.145	0.191	0.382	0.279
Head RY Displacement	0.594	1	0.984	0.959	0.976	0.785
T1 X Displacement	0.46	1	0.802	0.99	0.945	0.702
T1 Z Displacement	0.027	0.606	0.102	0.129	0.241	0.134
T1 RY Displacement	0.466	1	0.671	0.992	0.913	0.69
T8 X Displacement	0.742	1	0.866	0.977	0.955	0.848
T8 Z Displacement	0.081	1	0.649	0.769	0.797	0.439
T8 RY Displacement	0.144	1	0.45	0.939	0.832	0.488
T11 X Displacement	0.727	1	0.932	0.964	0.965	0.846
T11 Z Displacement	0.373	1	0.765	0.72	0.801	0.587
T11 RY Displacement	0.086	1	0.487	0.975	0.859	0.472
L1 X Displacement	0.158	1	0.789	0.963	0.929	0.543
L1 Z Displacement	0.355	1	0.992	0.601	0.798	0.577
L1 RY Displacement	0.28	1	0.603	0.968	0.885	0.582
L3 X Displacement	0.892	1	0.77	0.995	0.94	0.916
L3 Z Displacement	0.746	1	0.85	0.615	0.77	0.758
L3 RY Displacement	0.343	1	0.581	0.836	0.813	0.578
Pelvis (PSIS) X Displacement	0.483	1	0.79	0.979	0.937	0.71
Pelvis (PSIS) Z Displacement	0.447	0	0.947	0.018	0.246	0.346
Pelvis (PSIS) RY Displacement	0.302	1	0.755	0.23	0.554	0.428

TABLE D-XVI
CORA SCORES FOR THE M50-O SIMULATION USING OGDEN MATERIALS AND GRAVITY SETTLING METHODS.

Channel Name	Corridor Score	Phase Score	Size Score	Progression Score	Correlation Score	Total Score
Head X Displacement	0.557	1	0.957	0.999	0.989	0.773
Head Z Displacement	0.162	1	0.143	0.141	0.357	0.259
Head RY Displacement	0.603	1	0.985	0.969	0.981	0.792
T1 X Displacement	0.783	1	0.985	0.999	0.996	0.889
T1 Z Displacement	0.026	1	0.312	0.364	0.51	0.268
T1 RY Displacement	0.688	1	0.803	0.993	0.947	0.818
T8 X Displacement	0.902	1	0.951	0.999	0.987	0.945
T8 Z Displacement	0.058	1	0.548	0.698	0.736	0.397
T8 RY Displacement	0.393	1	0.65	0.891	0.858	0.625
T11 X Displacement	0.833	1	0.812	0.996	0.951	0.892
T11 Z Displacement	0.096	1	0.54	0.577	0.673	0.385
T11 RY Displacement	0.282	1	0.685	0.93	0.886	0.584
L1 X Displacement	0.185	1	0.745	0.985	0.929	0.557
L1 Z Displacement	0.078	1	0.666	0.343	0.588	0.333
L1 RY Displacement	0.51	1	0.846	0.974	0.948	0.729
L3 X Displacement	0.886	1	0.806	0.986	0.944	0.915
L3 Z Displacement	0.474	1	0.747	0.221	0.547	0.511
L3 RY Displacement	0.581	1	0.839	0.82	0.87	0.726
Pelvis (PSIS) X Displacement	0.37	1	0.76	0.965	0.922	0.646
Pelvis (PSIS) Z Displacement	0.424	0.667	0.531	0.387	0.493	0.459
Pelvis (PSIS) RY Displacement	0.309	1	0.372	0.082	0.384	0.346

TABLE D-XVII
CORA SCORES FOR THE M50-O SIMULATION USING OGDEN MATERIALS AND BPM SETTLING METHODS.

Channel Name	Corridor Score	Phase Score	Size Score	Progression Score	Correlation Score	Total Score
Head X Displacement	0.544	1	0.968	0.999	0.991	0.767
Head Z Displacement	0.165	1	0.195	0.188	0.393	0.279
Head RY Displacement	0.602	1	0.984	0.967	0.98	0.791
T1 X Displacement	0.642	1	0.994	0.999	0.998	0.82
T1 Z Displacement	0.241	1	0.542	0.755	0.763	0.502
T1 RY Displacement	0.706	1	0.803	0.993	0.947	0.827
T8 X Displacement	0.878	1	0.914	0.998	0.977	0.928
T8 Z Displacement	0.25	1	0.763	0.868	0.875	0.562
T8 RY Displacement	0.357	1	0.617	0.882	0.845	0.601
T11 X Displacement	0.515	1	0.749	0.99	0.932	0.724
T11 Z Displacement	0.413	1	0.759	0.806	0.843	0.628
T11 RY Displacement	0.212	1	0.642	0.934	0.878	0.545
L1 X Displacement	0.082	1	0.654	0.977	0.902	0.492
L1 Z Displacement	0.385	1	0.923	0.699	0.83	0.607
L1 RY Displacement	0.395	1	0.767	0.977	0.93	0.662
L3 X Displacement	0.673	1	0.669	0.974	0.904	0.788
L3 Z Displacement	0.913	1	0.926	0.772	0.867	0.89
L3 RY Displacement	0.576	1	0.707	0.84	0.847	0.711
Pelvis (PSIS) X Displacement	0.47	1	0.987	0.97	0.982	0.726
Pelvis (PSIS) Z Displacement	0.466	0.545	0.616	0.01	0.295	0.381
Pelvis (PSIS) RY Displacement	0.362	1	0.454	0.501	0.614	0.488

TABLE D-XVIII
CORA SCORES FOR THE M50-OS SIMULATION USING STOCK MATERIALS AND GRAVITY SETTLING METHODS.

Channel Name	Corridor Score	Phase Score	Size Score	Progression Score	Correlation Score	Total Score
Head X Displacement	0.432	1	0.868	0.997	0.965	0.699
Head Z Displacement	0.141	1	0.09	0.149	0.347	0.244
Head RY Displacement	0.836	1	0.936	0.99	0.979	0.907
T1 X Displacement	0.249	1	0.728	0.997	0.931	0.59
T1 Z Displacement	0.026	0	0.667	0	0.167	0.096
T1 RY Displacement	0.489	1	0.681	0.998	0.919	0.704
T8 X Displacement	0.343	1	0.697	0.991	0.92	0.631
T8 Z Displacement	0.058	1	0.197	0.367	0.483	0.27
T8 RY Displacement	0.12	1	0.439	0.894	0.807	0.463
T11 X Displacement	0.68	1	0.85	0.982	0.953	0.817
T11 Z Displacement	0.099	1	0.238	0.208	0.414	0.256
T11 RY Displacement	0.044	1	0.428	0.901	0.807	0.426
L1 X Displacement	0.334	0.97	0.99	0.959	0.969	0.652
L1 Z Displacement	0.064	0.848	0.453	0.059	0.355	0.209
L1 RY Displacement	0.065	1	0.561	0.961	0.871	0.468
L3 X Displacement	0.925	0.848	0.992	0.973	0.947	0.936
L3 Z Displacement	0.291	0.424	0.849	0.008	0.322	0.307
L3 RY Displacement	0.619	1	0.94	0.879	0.924	0.772
Pelvis (PSIS) X Displacement	0.107	0.545	0.533	0.781	0.66	0.384
Pelvis (PSIS) Z Displacement	0.217	1	0.225	0.527	0.57	0.393
Pelvis (PSIS) RY Displacement	0.069	0	0.59	0	0.148	0.108

TABLE D-XIX
CORA SCORES FOR THE M50-OS SIMULATION USING STOCK MATERIALS AND BPM SETTLING METHODS.

Channel Name	Corridor Score	Phase Score	Size Score	Progression Score	Correlation Score	Total Score
Head X Displacement	0.373	1	0.89	0.997	0.971	0.672
Head Z Displacement	0.149	1	0.12	0.202	0.381	0.265
Head RY Displacement	0.822	1	0.936	0.99	0.979	0.901
T1 X Displacement	0.308	1	0.752	0.996	0.936	0.622
T1 Z Displacement	0.033	0	0.182	0	0.046	0.039
T1 RY Displacement	0.415	1	0.682	0.996	0.918	0.667
T8 X Displacement	0.488	1	0.74	0.984	0.927	0.707
T8 Z Displacement	0.064	1	0.306	0.784	0.718	0.391
T8 RY Displacement	0.146	1	0.434	0.877	0.797	0.472
T11 X Displacement	0.661	1	0.941	0.968	0.969	0.815
T11 Z Displacement	0.145	1	0.323	0.644	0.653	0.399
T11 RY Displacement	0.045	1	0.411	0.906	0.806	0.425
L1 X Displacement	0.176	0.909	0.863	0.949	0.917	0.547
L1 Z Displacement	0.065	1	0.467	0.433	0.583	0.324
L1 RY Displacement	0.068	1	0.52	0.977	0.868	0.468
L3 X Displacement	0.768	0.848	0.792	0.982	0.901	0.835
L3 Z Displacement	0.457	1	0.538	0.152	0.46	0.459
L3 RY Displacement	0.665	1	0.79	0.913	0.904	0.785
Pelvis (PSIS) X Displacement	0.106	0.667	0.764	0.863	0.789	0.448
Pelvis (PSIS) Z Displacement	0.522	0.606	0.91	0.535	0.646	0.584
Pelvis (PSIS) RY Displacement	0.151	0.121	0.401	0.001	0.131	0.141

TABLE D-XX
CORA SCORES FOR THE M50-OS SIMULATION USING OGDEN MATERIALS AND GRAVITY SETTLING METHODS.

Channel Name	Corridor Score	Phase Score	Size Score	Progression Score	Correlation Score	Total Score
Head X Displacement	0.43	1	0.841	0.997	0.959	0.694
Head Z Displacement	0.134	1	0.075	0.143	0.34	0.237
Head RY Displacement	0.625	1	0.967	0.978	0.981	0.803
T1 X Displacement	0.207	1	0.698	0.999	0.924	0.565
T1 Z Displacement	0.025	0	0.821	0	0.205	0.115
T1 RY Displacement	0.317	1	0.566	0.995	0.889	0.603
T8 X Displacement	0.406	1	0.702	0.99	0.921	0.663
T8 Z Displacement	0.055	1	0.308	0.541	0.597	0.326
T8 RY Displacement	0.109	1	0.36	0.882	0.781	0.445
T11 X Displacement	0.77	1	0.9	0.979	0.965	0.867
T11 Z Displacement	0.098	1	0.396	0.447	0.572	0.335
T11 RY Displacement	0.044	1	0.391	0.909	0.802	0.423
L1 X Displacement	0.274	1	0.909	0.962	0.958	0.616
L1 Z Displacement	0.064	1	0.64	0.242	0.531	0.297
L1 RY Displacement	0.07	1	0.51	0.968	0.862	0.466
L3 X Displacement	0.939	0.909	0.887	0.988	0.943	0.941
L3 Z Displacement	0.355	0.848	0.936	0.092	0.492	0.424
L3 RY Displacement	0.543	1	0.724	0.861	0.862	0.702
Pelvis (PSIS) X Displacement	0.193	0.848	0.639	0.91	0.827	0.51
Pelvis (PSIS) Z Displacement	0.353	0.606	0.342	0.353	0.414	0.384
Pelvis (PSIS) RY Displacement	0.08	0.788	0.52	0.01	0.332	0.206

TABLE D-XXI
CORA SCORES FOR THE M50-OS SIMULATION USING OGDEN MATERIALS AND BPM SETTLING METHODS.

Channel Name	Corridor Score	Phase Score	Size Score	Progression Score	Correlation Score	Total Score
Head X Displacement	0.417	1	0.857	0.997	0.963	0.69
Head Z Displacement	0.139	1	0.097	0.175	0.362	0.25
Head RY Displacement	0.62	1	0.943	0.978	0.975	0.797
T1 X Displacement	0.233	1	0.714	0.998	0.928	0.58
T1 Z Displacement	0.026	0	0.29	0	0.072	0.049
T1 RY Displacement	0.228	1	0.568	0.992	0.888	0.558
T8 X Displacement	0.478	1	0.736	0.986	0.927	0.702
T8 Z Displacement	0.057	1	0.433	0.821	0.769	0.413
T8 RY Displacement	0.119	1	0.359	0.872	0.776	0.447
T11 X Displacement	0.705	1	0.975	0.971	0.979	0.842
T11 Z Displacement	0.142	1	0.524	0.747	0.755	0.448
T11 RY Displacement	0.045	1	0.378	0.916	0.802	0.424
L1 X Displacement	0.182	0.909	0.802	0.958	0.907	0.545
L1 Z Displacement	0.188	1	0.781	0.607	0.749	0.468
L1 RY Displacement	0.069	1	0.476	0.982	0.86	0.465
L3 X Displacement	0.752	0.909	0.73	0.994	0.906	0.829
L3 Z Displacement	0.629	1	0.888	0.474	0.709	0.669
L3 RY Displacement	0.481	1	0.621	0.886	0.848	0.665
Pelvis (PSIS) X Displacement	0.341	1	0.846	0.967	0.945	0.643
Pelvis (PSIS) Z Displacement	0.444	0.364	0.633	0.042	0.27	0.357
Pelvis (PSIS) RY Displacement	0.254	1	0.401	0.12	0.41	0.332